Highly Conjugated Imidazoline Porous Organic Polymer (POP) for Green Photocatalytic Degradation of Toxic Mustard Gas

A Thesis

Submitted in Partial Fulfilment of the Requirements for the Degree of

Master of Science (M. Sc.)

By

Vartika Jaiswal

Reg. ID: 20226210

Research Supervisor

Prof. Sujit K. Ghosh

Indian Institute of Science Education and Research (IISER), Pune

2024

Certificate

This is to certify that this dissertation entitled '***Highly Conjugated Imidazole Porous Organic Polymer (POP) for Green Photocatalytic Degradation of Toxic Mustard Gas'*** towards the partial fulfilment of the M.Sc. degree programme at the Indian Institute of Science Education and Research (IISER), Pune represents study/work carried out by *Ms. Vartika Jaiswal* at Indian Institute of Science Education and Research under the supervision of Dr. Sujit K. Ghosh, Professor, Department of Chemistry, during the academic year 2023-2024.

Prof. Sujit K. Ghosh
Research Supervisor
Email: sghosh@iiserpune.ac.in
Contact No.: +91(20)25908076

Committee:

Prof. Sujit K. Ghosh
Dr. Debangsu Sil

Dedicated to

Maa

Declaration

I hereby declare that the matter embodied in the report entitled '***Highly Conjugated Imidazole Porous Organic Polymer (POP) for Green Photocatalytic Degradation of Toxic Mustard Gas'*** are the results of the work carried out by me at the Department of Chemistry, Indian Institute of Science Education and Research (IISER) Pune, under the supervision of Prof. Sujit K. Ghosh, and the same has not been submitted elsewhere for any other degree. Wherever others have contributed, every effort is made to indicate this clearly, with due reference to the literature and acknowledgement of collaborative research and discussions.

Vartika Jaiswal

Vartika Jaiswal

Reg. ID: 20226210

Contents

Acknowledgment

I would like to take this opportunity to express my sincerest gratitude to my master's thesis supervisor **Prof. Sujit K. Ghosh** for his unwavering support and guidance.

I would also like to thank former director of IISER Pune, Prof. J. B. Udgaonkar and current director Prof. Sunil S. Bhagwat, and current chair of the department of chemistry, Prof. Nirmalya Ballav for providing such great research facilities. I would also like to thank my thesis advisory committee member, **Dr. Debangsu Sil**, for his valuable input and encouragement regarding my work.

My research experience was enhanced by members of **'Microporous Materials Lab'** group (both current and former). I would like to thank them (Dr. Sumanta Let, Dr. Debanjan Mahato, Dr. Writakshi Mandal, Dr. Sahel Fajal, Gourab K. Dam, Dipanjan Majumdar, Kishalay Biswas, Dibyaranjan Sahoo, Anirban Roy and Dipayan Ghosh) for all their contributions at varying stages of my research journey. Of them I would like to express my gratitude towards **Sumanta da** who helped me understand the basics of the field. With his guidance I was able to gain fundamental knowledge and garner more interest in research work.

I would like to convey my deepest acknowledgement to my senior **Gourab da**. I have been working with Gourab Da for the entirety of my research project and he has supported me and helped me leaps and bounds to explore my research interests and taught me a lot of valuable lessons. He has gone heaps and beyond to ensure that I can learn and get as much experience as possible. It was Gourab da's unwavering support and constant guidance that allowed me to hone my abilities as a researcher and develop a keen interest in research work.

I would also like to thank my seniors **Kishalay da**, **Dibyaranjan da** and **Anirban da** who made my time in the lab fun and helped me whenever I had any problems. They have helped me get familiar with the lab and guided me through ups and downs that I faced and I'm extremely grateful for their support.

Lastly, I would like to acknowledge the support and encouragement I received from my family and friends who made this incredible journey possible.

- Vartika Jaiswal

List of figures

List of tables

Abstract: Effective detoxification of CWA Mustard Gas (HD) via selective partial oxidation is the most effective but challenging method because the overoxidized sulfone product is toxic and the choice of solvent system. All organic and heterogenous photoactive porous organic polymers are more environmentally friendly and sustainable. Imidazoline-based POP, a new material class, consists of electron-rich and electron-deficient units in donor−acceptor junction and has mild oxidizing power and ROS generation ability. In this current work, IPPOP-4, a new Imidazoline POP, was synthesized, characterized, and found to be photoactive. Towards detoxification of HD simulant 2-chloroethyl ethylsulfide (CEES), IPPOP-4 showed excellent performance with ultrafast kinetics of $t_{1/2}$ = 4.7 min in O_2 and $t_{1/2}$ = 5.8 min in air atmosphere, respectively, in MeOH as a suitable solvent system. Experimental data was presented that validates the crucial stage of the catalytic process that results in a plausible mechanism in the different solvent systems. Additionally, the versatile photocatalytic oxidative nature of the IPPOP-4 was established from its competence in the sulfide oxidation and aromatic aldehyde oxidation reaction with wide substrate scope. Furthermore, recyclability of the photocatalyst (upto 10 cycles) validates the conceptual feasibility of the photocatalyst.

1. Introduction

The chemical warfare agents (CWAs) have been a serious threat to human civilization since World War I (WW-I) and remains till date due to their cost-effective production and stockpiling.[1] Sulfur Mustard (bis(2-chloroethyl)sulfide); also known as HD, one of the CWAs, which is notorious as a blistering agent, causes severe damage to skin, eyes and respiratory system. Additionally, oxidative stress and antioxidant depletion brought on by HD exposure might result in DNA alkylation and cell death.[2] Among trivial detoxification methods, hydrolysis[3] and dehydrohalogenation[4] are limited by slow kinetics because of very low solubility of HD in aqueous system. The most encouraging route to detoxify HD is selective partial oxidation to nontoxic sulfoxide because overoxidized sulfone is also toxic.[5] In this point, singlet oxygen ($^1O_2$) has been a well-established, mild oxidizing agent for the selective partial oxidation of CEES, avoiding the overoxidised toxic sulfone product.[6]

$^1O_2$ is a type II reactive oxygen species (ROS) that is produced when light irradiation on a photosensitizer (PS) causes energy transfer from the excited triplet state of the PS to molecular oxygen in the ground state.[7] Since Farha et al. originally showed that $^1O_2$ catalyzed by PCN-222/MOF-545, a porphyrin-based metal-organic framework (MOF) selectively oxidized sulfur mustard simulant, other investigations based on photosensitized $^1O_2$ have been reported.[6, 8] The majority of PSs include well-known photosensitive moieties that are typically linked to heavy-metal effects, such as pyrene, porphyrin,[9] or 4,4-difluoro-4-bora-3a,4a-diaza-s-indacene (BODIPY)[10] containing MOFs and Covalent organic framework (COF).[11] In practical terms, sulfur mustard photo-oxidation in ambient conditions might be more appropriate; nonetheless, most research has been done in an O_2 atmosphere with lasers or lamps as the light source. Therefore, developing new PS types with high ROS production efficiency is critical for the selective catalytic detoxification of sulfur mustards in environments like surrounding air**.**

Porous organic polymers (POPs) have recently gained attention in the science community due to their ease of synthesis, long-term stability, and versatile application in various sectors like water remediation,[12] catalysis,[13] CO_2 capture,[14] energy storage,[15] H_2 evolution[16] etc. Also, their modular and fully conjugated structure, inherent porosity, and heterogenous nature make them attractive platforms for photocatalytic reactions. In this context, imidazoline moiety containing highly conjugated POPs is the new class of photosensitizer, which is known for its high $^1O_2$ generation capability.[5, 17]

In this work, we developed a new novel conjugated imidazoline porous organic polymer, IPPOP-4, using 4',5'-bis(4-formylphenyl)-[1,1':2',1''-terphenyl]-4,4''-dicarbaldehyde and NH_4Cl. IPPOP-4 acts as an efficient photosensitizer for singlet oxygen generation in ambient conditions. IPPOP-4, a metal-free photocatalyst, demonstrated remarkably fast kinetics toward the HD simulant 2-chloroethyl ethyl sulfide (CEES) detoxification upon blue LED irradiation in air atmosphere, with a half-life ($t_{1/2}$; 50% conversion) of 5.7 min. Compared to other previously published Metal-Organic Framework (MOF), Covalent Organic Framework (COF), and Conjugated Microporous Polymer (CMP)-based photocatalysts, this $t_{1/2}$ is significantly lower. Additionally, we performed industrially relevant sulfide oxidation (important in the petrochemical industry) and aldehyde oxidation to carboxylic acid in ambient conditions. This study highlights very efficient photocatalytic properties of an imidazoline POP towards HD simulant detoxification under ambient conditions.

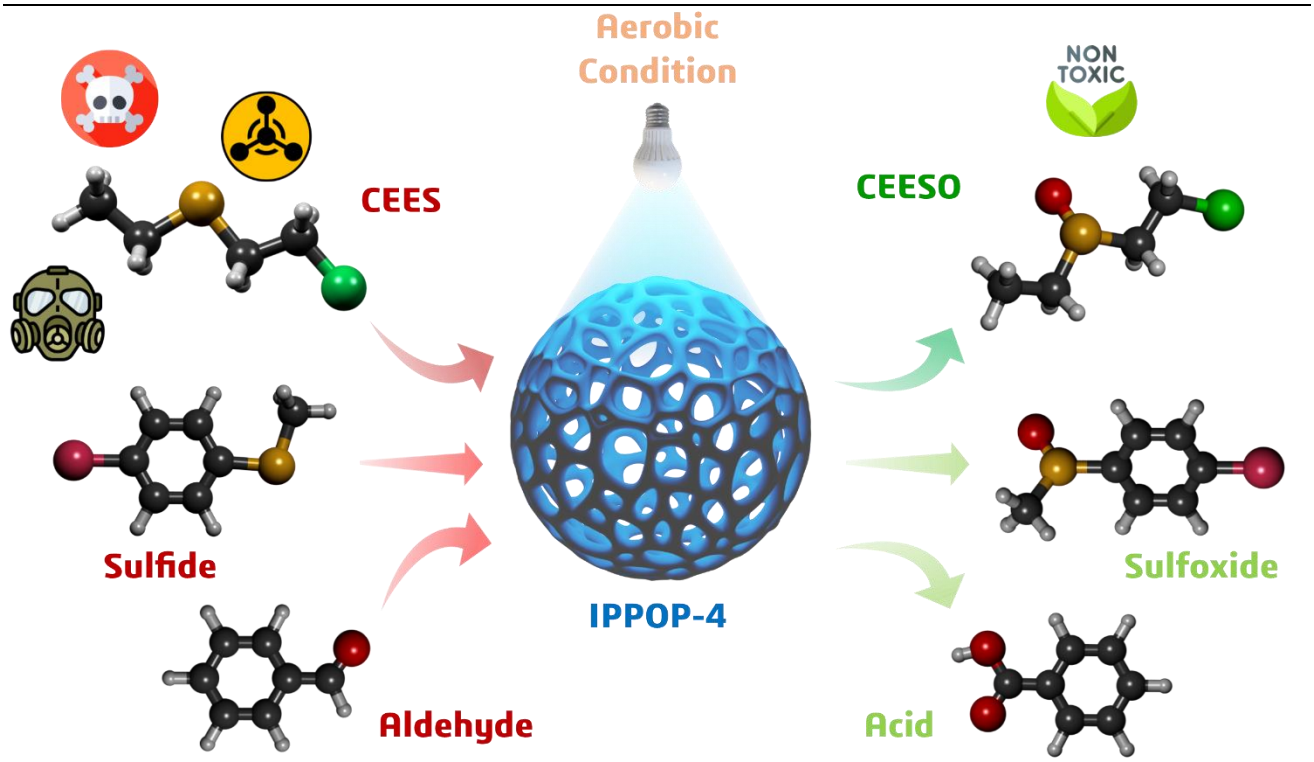

Scheme 1: Photocatalytic Activity of IPPOP-4

2. Methods:

2.1. Experimental Section

2.1.1. Materials: All the reagents, starting materials and solvents were commercially purchased from BLD Pharma, Sigma-Aldrich, TCI Chemicals, Alfa asar, Spectrochem, Rankem Chemicals depending on their availability and used without

further purification. 2-Chloroethyl ethyl sulfide is toxic in nature and proper protective gear (masks, gloves) is always to be used.

2.1.2. Synthesis of IPPOP-4: IPPOP-4 system was synthesized from cost-effective starting materials through a one-pot reaction with slightly modified reported protocol. A 20 mL Teflon Lined stainless steel Autoclave was charged with 4',5'-bis(4-formylphenyl)-[1,1':2',1''-terphenyl]-4,4''-dicarbaldehyde (1 mM) and ammonium chloride (8.1 mM) and 10 mL DMF. The mixture in the autoclave was then allowed to heat at 150°C for 48 h. The pale-yellow precipitate was collected, filtered, and washed repeatedly with water, methanol, acetone, and chloroform. The resulting powder was dried at 80°C under a vacuum overnight.

2.1.3. Physical Measurements: Solid-state ^{13}C cross-polarization magic-angle-spinning (CP-MAS) spectra were acquired on a Bruker 500 MHz NMR spectrometer with a CP-MAS probe. Carbon chemical shifts are expressed in parts per million (δ scale). The ^{13}C chemical shifts were externally referenced to tetramethylsilane (δ = 0.0 ppm). The FT-IR Spectra were acquired by using Bruker Alpha-II ECO-ATR spectrophotometer using solid sample in 550-4000 cm^{-1} range. Thermogravimetric analyses were performed using Perkin-Elmer STA 6000 TGA analyzer by heating the samples from 30 to 800°C under N_2 atmosphere with a heating rate of 10°C min^{-1}. For high-resolution TEM analysis, all the samples were dispersed in isopropanol (0.5 mg/mL) and sonicated for 15 minutes. Then, the samples were left undisturbed for 2 minutes, and the upper part of the solution was taken for preparing TEM samples on a lacey carbon-coated copper grid (Electron Microscopy Science). TEM imaging was performed on the HRTEM (JEM-2200FS, JEOL) operating at acceleration voltage of 200 kV. N_2 and CO_2 gas adsorption measurements were performed using BelSorp-Max instrument (Bel-Japan). Prior to adsorption measurements, the activated samples were heated at 120°C under vacuum for 12 hours using BelPrepvacII. As-obtained powder samples was stuck to conductive paste and then measured by X-ray photoelectron spectroscopy using K-Alpha+ model (Thermo Fischer Scientific, UK) with Al Kα source. All ^1H spectra were recorded on Bruker 400 MHz spectrometer. The chemical shifts (δ) in ppm were referenced to the residual signal of deuterium solvents (^1H NMR in $CDCl_3$, ^1H NMR in $CDCl_3$ and DMSO-d^6 equivalent mixture). The multiplicities of the peaks are s (singlet), d (doublet), t (triplet), q (quartet), dd (doublet of doublet), m (multiplet). DRS spectra and corresponding absorbance spectra was collected on

a Shimadzu UV-3600i UV/Visible/NIR Spectrophotometer with solid sample. Fluorescence emission spectra and PLE was collected on a HORIBA Fluromax+ solid sample and water dispersed samples. **(**EPR) spectroscopy was carried out on a Bruker EMX plus spectrometer.

2.1.4. Photocatalytic CEES degradation experiment by IPPOP-4: 10 mg of IPPOP-4 was dispersed in 4 mL of solvent (MeCN, MeOH) placed in a glass 10 mL Schlenk tubes and bubbled with O_2. After that, 23 µL of CEES was added to the reaction tube. Then, the tube was irradiated with Blue LED. The ^{1}H NMR was collected after a certain time interval. Photocatalytic study under atmospheric conditions is carried out with air instead of oxygen at the beginning of the reaction.

2.1.5. Recyclability Test: After the photocatalytic reaction, conducted under blue LED illumination, the catalyst was separated by centrifugation and washed thrice with CH_3OH (10 mL). The supernatant was carefully removed, and the powder was dried under a vacuum. After washing, centrifugation, and vacuum-drying, 4 mL of suitable solvent was added to the IPPOP-4, and the mixture was transferred to Schlenk tube. Fresh CEES (23 µL) was added to the mixture, and the resultant mixture was directly used for the next catalytic cycle.

2.1.6. Photocatalytic aromatic sulfide oxidation by IPPOP-4: 5 mg of IPPOP-4 was dispersed in 4 mL of solvent placed in a glass vial. After that, 0.2 mM of aromatic sulfide was added to the reaction vial. Then, the tube was irradiated with Blue LED under air. The ^{1}H NMR was collected for the calculation of the conversion rate.

2.1.7. Recyclability Test: After the photocatalytic reaction conducted under blue LED illumination, the catalyst was separated by centrifugation and washed thrice with CH_3OH (10 mL). The supernatant was carefully removed, and the powder was dried under a vacuum. After washing, centrifugation, and vacuum-drying, 4 mL of solvent was added to the IPPOP-4, and the mixture was transferred to a glass vial. Fresh aromatic sulfide (0.2 mM) was added to the mixture, and the resultant mixture was directly used for the next catalytic cycle.

2.1.8. Photocatalytic aromatic aldehyde oxidation by IPPOP-4: 5 mg of IPPOP-4 was dispersed in 4 mL of solvent placed in a glass vial. After that, 0.2 mM of aromatic aldehyde was added to the reaction vial. Then, the tube was irradiated with Blue LED under air. The ^{1}H NMR was collected for the calculation of the conversion rate.

2.1.9. Recyclability Test: After the photocatalytic reaction conducted under blue LED illumination, the catalyst was separated by centrifugation and washed thrice with CH_3OH (10 mL). The supernatant was carefully removed, and the powder was dried under a vacuum. After washing, centrifugation, and vacuum-drying, 4 mL of solvent was added to the IPPOP-4, and the mixture was transferred to a glass vial. Fresh aromatic aldehyde (0.2 mM) was added to the mixture, and the resultant mixture was directly used for the next catalytic cycle.

3. Result and Discussion

3.1. Structural Characterization:

Following the successful synthesis of the imidazolium functionalized polymeric network IPPOP-4, a diverse array of sophisticated analytical methods was employed to characterize and confirm the synthesis of the polymer, including solid-state ^{13}C cross polarization magic-angle-spinning Nuclear Magnetic Resonance (^{13}CP-MAS NMR), Fourier transform infrared (FTIR), thermogravimetric analysis (TGA), transmission electron microscopy (TEM), X-ray photoelectron spectroscopy (XPS), low-temperature nitrogen (N_2) and carbon dioxide (CO_2) gas sorption measurements, zeta potential etc. ^{13}C CP-MAS NMR spectroscopy confirmed the formation of an imidazolium cationic framework after a complete cyclization reaction. The peak at ~166 pm confirmed the -C=N linkage from the imidazolium ring, while peaks at ~43, ~67, and ~77 ppm were attributed to the other carbon atoms in the imidazolium moiety. Peaks in the ~129-140 ppm range were assigned to the aromatic carbons from the benzene ring in the polymeric network (Figure-1b). The FT-IR spectra revealed peaks at ~3402 cm^{-1} and ~1665 cm^{-1} ascribing to -N-H and -C=N stretching frequencies from the imidazolium moiety, and also a decrease in the peak intensity was observed at ~1701 cm^{-1} corresponding to the -C=O functional group (Figure-1c) as compared to the monomer precursor attests to the successful formation of the imidazolium polymeric network. TGA was carried out to assess the robustness and thermal stability of the polymer. A slight initial loss of ~5% was observed, attributed to the entrapped solvents inside the pores of the pristine polymer. However, no significant gradual weight loss was found till ~250ºC, suggesting the good thermal stability of the polymeric network, and thereafter, a gradual weight loss was observed beyond 250ºC due to the collapse of the polymeric framework of IPPOP-4 (Figure-1d). TEM imaging of

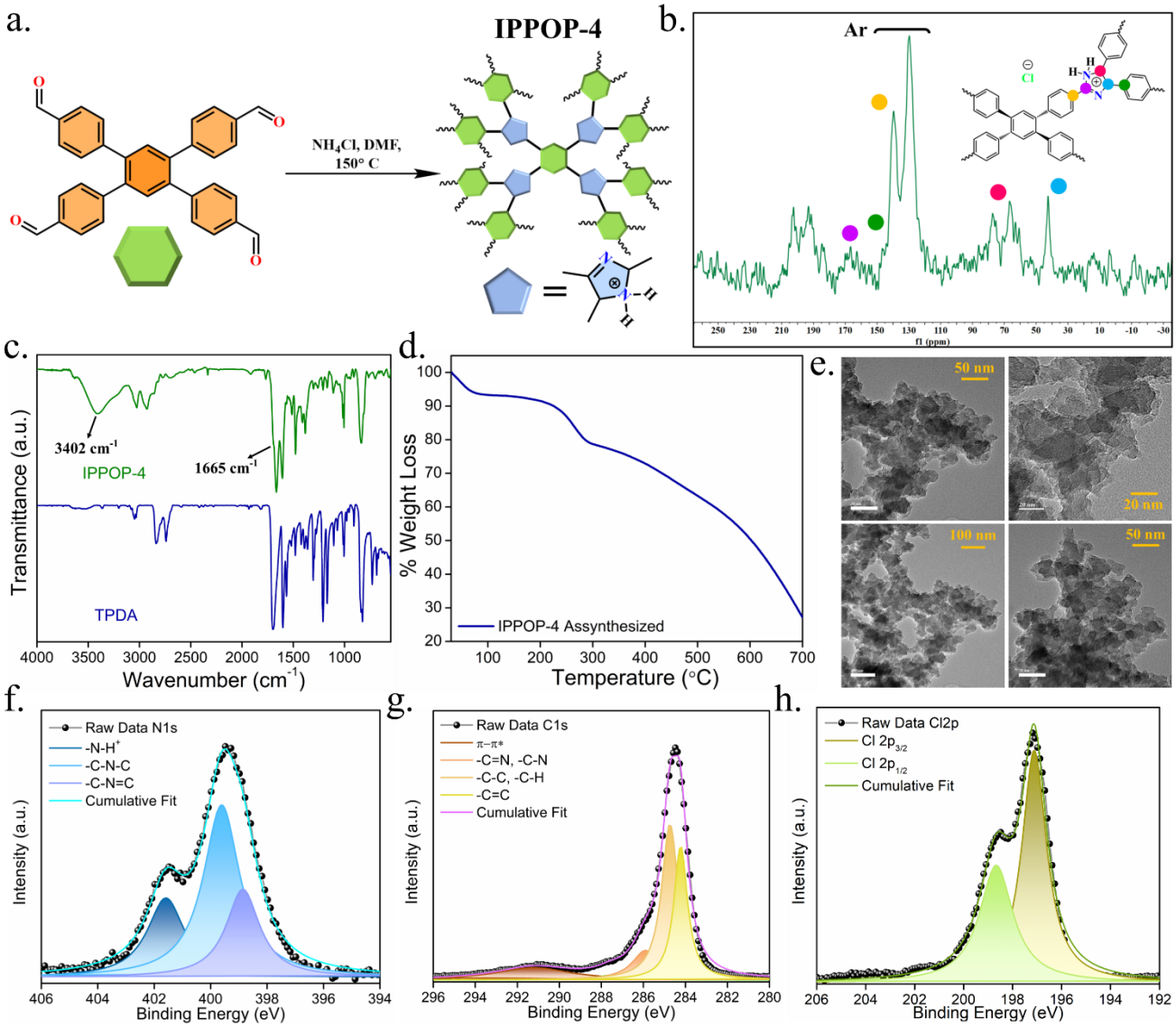

Figure 1: a. Synthetic scheme of IPPOP-4, b. ^{13}C CP-MAS NMR of IPPOP-4, c. FT-IR spectra, d. TGA profile, e. HRTEM images of IPPOP-4, deconvulted XPS spectra of IPPOP-4, f. N1s, g. C 1s, and h. Cl 2p

IPPOP-4 showed irregular morphology with layered structures (Figure-1e, A1). The elemental analysis and the corresponding spectroscopy (EDS) revealed the homogeneous distribution of all the compositional elements of Carbon (C), Nitrogen (N) and Chlorine (Cl) on the surface of the polymeric network of IPPOP-4 (Appendix A2). Further, the XPS spectra confirmed the presence of the compositional elements and their chemical state. Three main peaks at ~283.4 eV, ~389.9 eV, and ~198.2 eV were found in the XPS survey scan (Figure-A3), which are characteristic and correspond to Carbon (C 1s), Nitrogen (N 1s), and Chlorine (Cl 2p), respectively. High-resolution deconvoluted N1s spectra fitted into three peaks with binding energies at ~401.6 eV, ~399.6 eV, and ~398.8 eV corresponding to cationic N from the

imidazolium ring (N^+-H), pyrrolic N (C-N-C) and imine bond (C=N-C) respectively (Figure-1f). Deconvoluted C 1s spectra were fitted into four peaks at ~284.2 eV, ~284.7 eV, ~285.5 eV, and ~291.2 eV attributed to aromatic -C=C bond, -C-C and C-H, for the imine bond and the cationic N and C bond (C=N, C-N^+) and from the π-π* interaction between the layers (Figure-1g). Cl 2p spectra were deconvoluted into two peaks at ~197 eV and ~198.6 eV assigned for Cl $2p_{3/2}$ and Cl $2p_{1/2}$, respectively (Figure-1h). Moreover, N_2 adsorption-desorption isotherm at 77K does not demonstrate any appreciable uptake of nitrogen gas, indicating that counter chloride (Cl^-) anions in the cationic network obstruct the internal pores (Appendix A4). Brunauer-Emmett-Teller (BET) surface area was found to be 163 m^2g^{-1} from N_2 adsorption. However, the porous nature of the IPPOP-4 is suggested by CO_2 adsorption at 195 K (Appendix A5). Additionally, Zeta potential showed +39 mV of the surface charge, indicating the cationic nature of the IPPOP-4 polymeric network (Appendix A6). Also, we tested the chemical stability of IPPOP-4 in the presence of 1M HCl and 1M NaOH, and it was found that IPPOP-4 is very stable in this condition (Appendix A7). These observations and results from different characterization techniques strongly suggest the successful formation of the cationic polymeric network with imidazolium moiety in IPPOP-4.

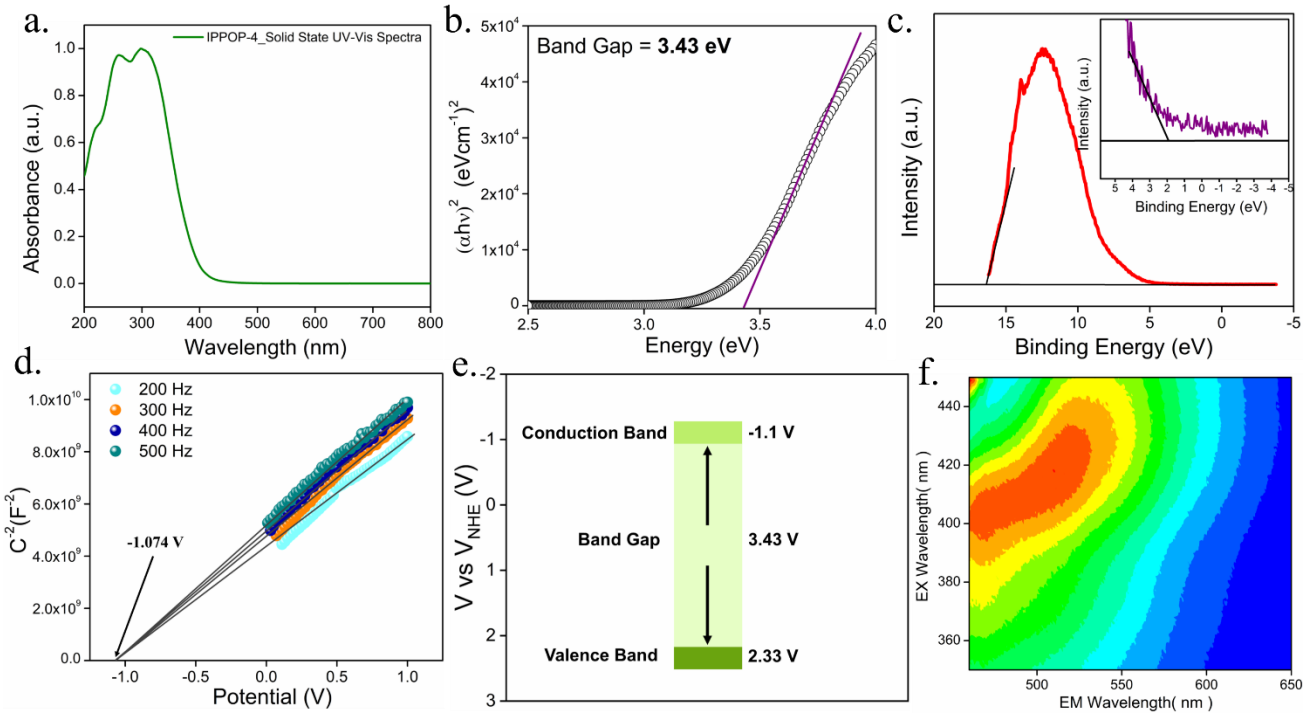

Figure 2: a. Solid state UV-Vis spectra, b. Tauc's plot, c. Ultra-violet photoelectron spectra, d. Mott-Schottky plot, e. Band gap of IPPOP-4, and f. PLE spectra of IPPOP-4 in MECN.

After successful synthesis and characterization, in the same lane, the photophysical properties and band gap calculation were analyzed to confirm the photocatalytic behavior of

IPPOP-4. From the Solid state UV-vis spectrum (DRS), the IPPOP-4 was found to harvest light from the 200 to 400 nm range with maximum absorbance (λmax) at 298 nm (Figure- 2a). Tauc's plot analysis indicated that the optical of IPPOP-4 was estimated to be 3.43 eV (Figure- 2b). The valence band (VB) was calculated from Ultraviolet Photo-electron Spectroscopy (UPS) to be 2.3 V (Figure- 2c). Thus, the conduction band (CB) was calculated to be -1.1 V, which was well matched with the value of -1.07 V obtained from the Mott-Schottky Plot (Figure-2d). Based on these values, we estimated the band structure of IPPOP-4 (Figure-2e).

The solid-state photoluminescence spectrum for IPPOP-4 showed maximum emission at 543 nm when excited with a wavelength of 460 nm of light (Appendix A8). It was also found that with increasing the excitation wavelength, emission maxima showed a red-shift in its wavelength (Appendix A8), which was also found in the PLE spectrum from a dispersed phase in acetonitrile (Figure- 2f). Time-resolved Photoluminescence spectra (TRPL) were recorded to ascertain the lifetime of the polymer, and it was found to be 1.25 ns (Appendix A9). Additionally, the photoactivity of IPPOP-4 was found in the Electron paramagnetic resonance (EPR) spectroscopy. No signal was found in the dark condition, but when data was collected in the presence of blue light irradiation, the singlet EPR signal was found (Appendix A10), which again confirmed the photoactivity of IPPOP-4.

3.2. Photocatalytic Degradation of Mustard Gas Simulant:

After successful synthesis and characterization, we go for the photocatalytic activity of the IPPOP-4. Imidazoline polymeric network is well known for its ROS ($^1O_2$, $^{\bullet}O_2^{-\cdot}$) generation ability in the presence of light (Appendix A11). The photocatalytic activity of IPPOP-4 towards degradation of Mustard Gas simulant (MGS), 2-chloroethyl ethyl sulfide (CEES) to 2-chloroethyl ethyl sulfoxide (CEESO) was investigated under different atmospheric conditions and solvent systems. The conversion and selectivity for the conversion of CEES were calculated from ^{1}H NMR. To evaluate the optimized condition of the photocatalytic degradation of CEES, we examined the reaction in different solvent systems under atmospheric conditions (Appendix A12). IPPOP-4 showed an excellent 83% conversion of CEES to CEESO in methanol within 15 min. Also, 78% of conversion could be achieved in acetonitrile, but in the case of THF and $CHCl_3$, only 33% (Appendix A13) and 13.8% (Appendix A14) of conversion were noticed, respectively (Appendix A15). From the optimization result, further studies were performed in methanol (MeOH) and acetonitrile

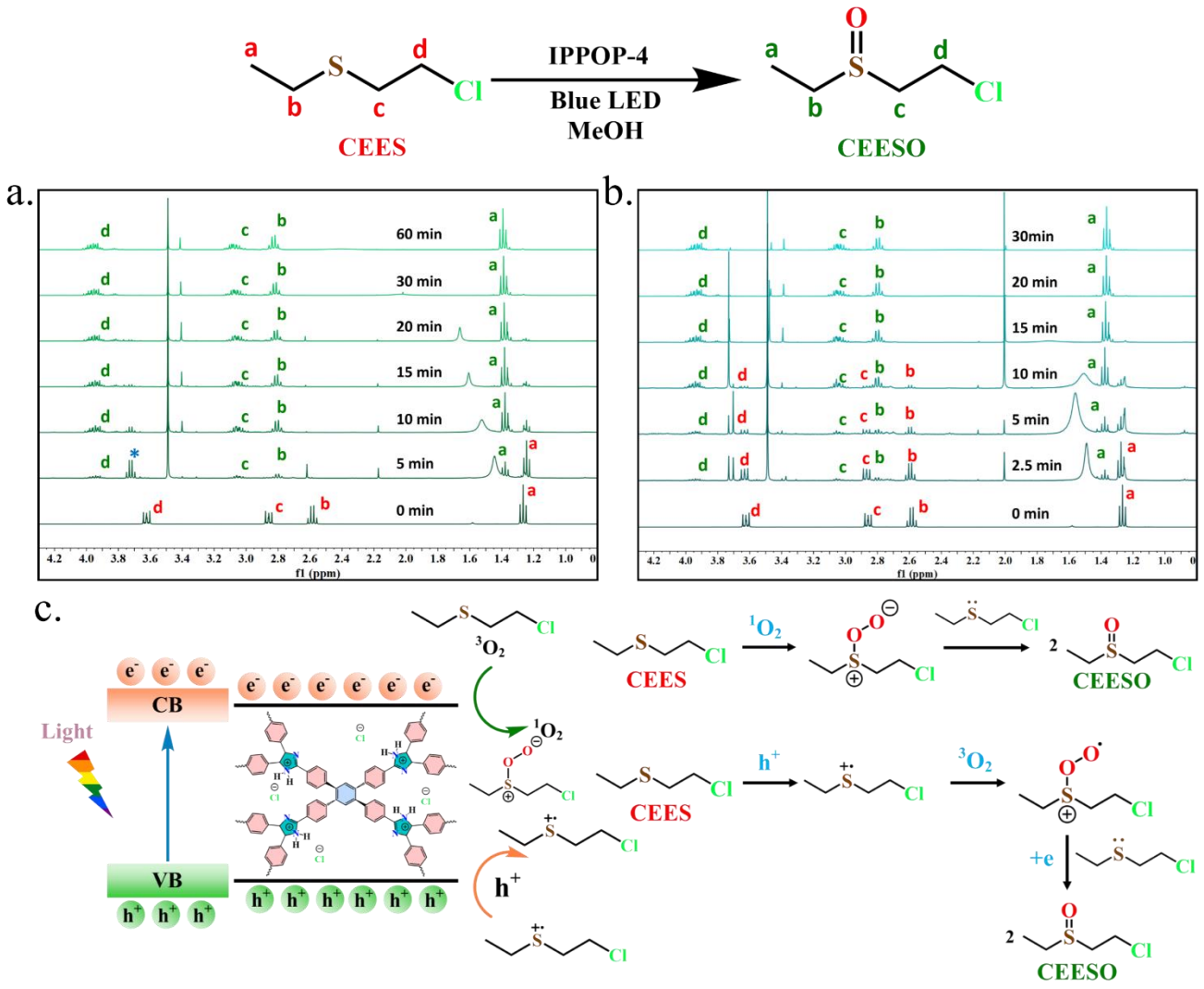

Figure 3: a. Time dependent ^{1}H NMR of photocatalytic degradation of CEES in MeOH in a. Air, b. O_2, and c. Plausible mechanism of CEES degradation by IPPOP-4.

(MeCN). From the time dependent ^{1}H NMR, the disappearance of peaks at 1.27, 2.58, 2.86 and 3.62 ppm of CEES and the rise of the peaks at 1.36, 2.81, 3.04 and 3.92 ppm of CEESO was noticed. IPPOP-4 can convert CEES to CEESO completely within 60 min in air (Figure- 3a, A16), but in the presence of O_2, the full conversion time reduced to 20 min (Figure- 3b, A18) in MeOH with no over oxidized toxic sulfone derivative (e.g., 2-chloroethyl ethyl sulfone ($CEESO_2$)) (Appendix A17, A19) thereby demonstrating the highly selective partial oxidation ability of IPPOP-4. The kinetic plot (Appendix A20) indicated that the $t_{1/2}$ of CEES oxidation reaction is 5.7 min in air and 4.9 min in O_2, which is lower than those of previously reported materials[18] (e.g. PCN-222, $t_{1/2}$= 26 min;[6a] NU-1000, $t_{1/2}$=6 min;[18a] Por-MOFs, $t_{1/2}$= 14 min;18b CMPs (e.g. CzBSe-CMP[18c] and Fc-based CMPs[18d]). But when MeCN was used as a solvent, the over-oxidised product formation was noticed. In air, the main product (CEESO) formation was observed till 30 min, then the over-oxidized product ($CEESO_2$) formation was observed with a rising peak at 1.42 ppm in ^{1}H NMR (Appendix A21) and vinyl oxidation product ethyl vinyl sulfoxide (EVSO) (Appendix A22, A23). In addition, when the reaction was in the O_2 atmosphere, the conversion to CEESO increased to 20 min of 93.2%, but then it started to decrease with the increase of the conversion to $CEESO_2$ over time (Appendix A24, A25) along with formation of EVSO (Appendix A26, A27, A28, A29). This observation makes MeOH a suitable solvent, and over-oxidized product formation in the case of MeCN could be due to the solvent effect in the conversion (Appendix A30).[11b]

To find the mechanistic pathway of the photocatalytic mustard gas detoxification by IPPOP-4, we performed several control experiments with the different chemical scavengers. Sodium azide (NaN_3), 1,4 Diazabicyclo[2.2.2]octane (DABCO), tert-butyl alcohol (TBA), p-benzoquinone (BQ), potassium iodide (KI) and silver nitrate ($AgNO_3$) was used to selectively eliminate Singlet Oxygen ($^1O_2$), hydroxide radical ($^{\bullet}OH$), superoxide radical ($^{\bullet}O_2^-$), hole (h^+) and electron (e^-) respectively. In the presence of NaN_3, DABCO, and KI, the CEES oxidation rate was suppressed completely compared to another scavenging agent, suggesting that $^1O_2$ is the main ROS responsible for the photocatalytic CEES oxidation along with h^+ (Appendix A31). Using 9,10-dimethyl anthracene (DMA) as a fluorescent probe, we corroborated the formation of $^1O_2$ even more (Appendix A32). As the oxidation of DMA to endoperoxide progressed, the emission peaks rapidly decreased, indicating that $^1O_2$ generation had occurred, which indicates the higher ability to produce $^1O_2$ by IPPOP-4.

Based on all these results, we found that singlet oxygen ($^1O_2$) and hole (h^+) are responsible for the CEES oxidation process, and we tried to draw a plausible mechanistic pathway based on these results. In first case, CEES reacts with $^1O_2$ to generate persulfoxide intermediate, which can be stabilised by protic solvents via hydrogen bonding. Subsequently, the persulfoxide intermediate is captured by another CEES molecule via nucleophilic attack to provide the single sulfoxide product CEESO (Figure- 3c). In the case of h^+, in the first step, a cation radical was formed, and then interacting with oxygen, it generated sulfonium cation. After that, it reacts with another CEES molecule to provide the CEESO as a product.

Recyclability is one of the main parameters of heterogeneous catalysis used to test the long-term applicability of the material. Keeping that in mind we performed a recyclability test of MGS detoxification. It was found that IPPOP-4 can efficiently detoxify the MGS even after 10 cycles without any decrease in performance (Appendix 33).

3.3. Photocatalytic Sulfide Oxidation:

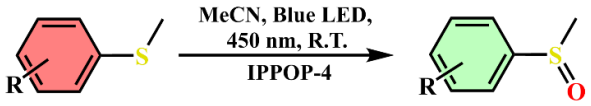

Entry	Substrate	Product	Time (h)	Conversion (%)	Selectivity (%)
1			2	100	100
2	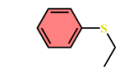		2	100	100
3		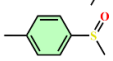	2	100	100
4		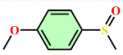	2	100	100
5	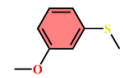	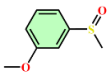	2	100	100
6	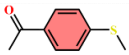	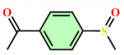	2	100	100
7	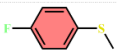	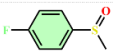	2	100	100
8	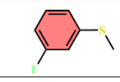		2	100	100

Entry	Substrate	Product	Time (h)	Conversion (%)	Selectivity (%)
9	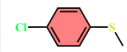	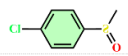	2	100	100
10	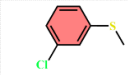	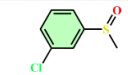	2	100	100
11	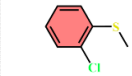	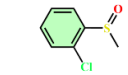	2	100	100
12	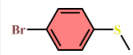	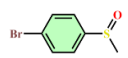	2	100	95
13	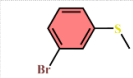	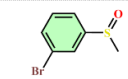	2	100	100
14	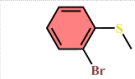	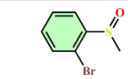	2	100	100
15	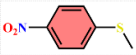	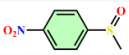	2	100	87
16	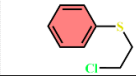	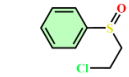	2	100	100

Table 1: Substrate scope of photocatalytic sulfide oxidation by IPPOP-4

Combusting sulfides in fuel oils produces Sulfur oxide (SO_X), a major source of air pollution.[19] One feasible alternative to separating SOx from combustion products is to oxidize them into sulfoxides, and sulfones can be used in the environmental and energy industries to reduce the sulfur content.[20, 21] These oxidative products are much

easier to extract than their corresponding sulfides. Moreover, the oxidation of sulfides is a fundamentally significant reaction in synthetic chemistry as the sulfoxides produced are utilized as vital bioactive ingredients in the pharmaceutical sectors and widely applied in the manufacture of medicine.[22]

This typical sulfide oxidation reaction was chosen to assess the further photocatalytic activity of the created IPPOP-4. 4-Bromothioanisole was chosen to find the optimized condition for the sulfide oxidation reaction. At first, we tested this reaction under different solvent systems by taking 5 mg of IPPOP-4 as a catalyst, 0.2 mM of the substrate in the presence of Air by irradiation of Blue LED (450 nm). We calculated the % conversion by ^{1}H NMR. We found ~ 95% conversion to 4-Bromophenyl methyl sulphoxide in MeCN within 2 hours, whereas in other different organic solvent like ethanol, methanol, THF, toluene, and chloroform, the conversion is 57%, 51%, 25%, 6.5%, and 50% respectively (Appendix A34, A35). After that, we performed a kinetics study of sulfide oxidation in MeCN; from the NMR titration data, it was found with an increase in time, the conversion to oxidized product 4-Bromophenylmethylsulphoxide increased. Within 1.5 hours, the conversion was found to be 52% and increased to 95% after 2 hours with 5% of over-oxidized product 4-Bromophenylmethylsulfone. This over-oxidized product increases to 12% after 4 hours (Appendix A36). By screening the optimal condition, we choose MeCN as the solvent and the aerobic condition for the sulfide oxidation reaction. After the optimization of the reaction condition, to examine the generality of the IPPOP-4 for photocatalysis, the substrate scope was investigated with different sulfide derivatives. Under the optimized reaction condition, sulfide derivatives with electron donating group of $-CH_3$ (thioanisole), $-CH_2CH_3$ (ethyl phenyl sulfide) (Table-1, Entry- 1, 2) attached with sulfur atom and thioanisole derivative electron donating group like $-4CH_3$, -4OMe, -3OMe (Table-1, Entry- 3, 4, 5) shows 100 % conversion with 100% selectivity towards the sulfoxide product. Thioanisole derivatives containing electron withdrawing group as $-4COCH_3$, -4F, -3F, -4Cl, -3Cl, -2Cl, -3Br, -2Br (Table-1, Entry- 6, 7, 8, 9, 10, 11, 13, 14) also shows the 100 % conversion with 100% selectivity towards the sulfoxide product. Only two thioanisole derivatives with electron-withdrawing groups of -4Br and $-4NO_2$ (Table-1, Entry- 12, 15) show a slightly lower selectivity towards sulfoxide products of 95% and 87%, respectively. Also, the oxidation of Chloroethyl phenyl sulfide (CEPS), one of the mustard's simulants, was tested, and it was found that IPPOP-4 efficiently oxidizes CEPS with 100% selectivity (Table-1, Entry- 16). These observations indicate the

versatility of IPPOP-4 towards photocatalytic sulfide oxidation irrespective of the presence of different electron-donating or electron-withdrawing groups.

Along this line, several control experiments with diverse chemical scavengers were performed to find out the reactive oxygen species (ROS) responsible for the oxidation reaction of sulfide. NaN_3 and DABCO were used as $^1O_2$ scavenger, TBA as $^{\bullet}OH$ scavenger, BQ as $^{\bullet}O_2^-$ scavenger, KI as h^+ and $AgNO_3$ as e^- scavenger respectively (Appendix A37). Remarkably, the sulfide oxidation quenches completely in the case of DABCO and to 9% in the case of NaN_3, which indicates that singlet oxygen ($^1O_2$) is the main reactive species. The decrease in conversion to 25%, 0%, and 47% was also noticed when BQ, KI, and $AgNO_3$ were used as scavengers, respectively, suggesting that the superoxide radicals, holes, and electrons were also responsible for the sulfide oxidation reaction. However, no suppression in conversion rate was noticed when TBA was used as a scavenger, indicating no hydroxyl radical role in the reaction.

Based on the following result, we draw the plausible mechanism of photocatalytic sulfide oxidation under aerobic conditions by IPPOP-4 (Appendix A38). Additionally, we performed a series of control experiments to evaluate the requirement of catalyst, light, and O_2, and we discovered that without these three parameters, the sulfide oxidation reaction did not show any conversion (Appendix A39). These findings imply that the heterogeneous catalyst IPPOP-4 effectively and very selectively photocatalyzes the sulfide oxidation process. Additionally, we performed the recyclability test for photocatalytic sulfide oxidation reaction, and it was found that after 10 cycles of reaction, IPPOP-4 can convert sulfide to sulfoxide without diminishing performance (Appendix A40).

3.4. Photocatalytic Aldehyde Oxidation:

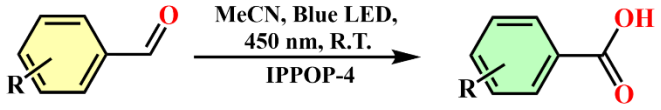

Entry	Substrate	Product	Yield (%)
1	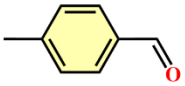	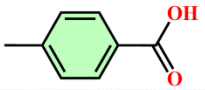	100
2	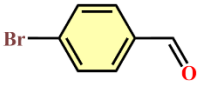	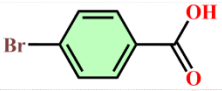	100
3	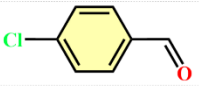	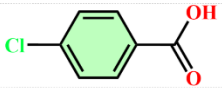	100
4	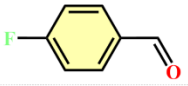	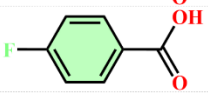	100
5	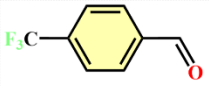	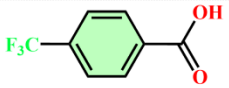	100
6	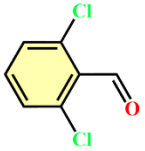	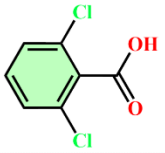	100
7	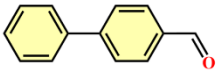	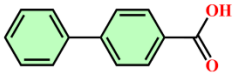	100
8	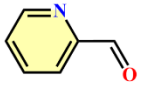	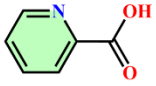	100

Table 2: Substrate scope of photocatalytic aldehyde oxidation by IPPOP-4

One of the easiest, straightforward methods for synthesizing useful, valuable carboxylic acids is the oxidation of industrially generated aldehydes.[23] Commercially available chemical oxidants such copper (II) salts, silver nitrate, $KMnO_4$, H_5IO_6, CrO_3, $KHSO_5$, $NaClO_2$, and so on are typically used to facilitate this process of oxidation; nevertheless, the use of such costly and hazardous reagents places a limit on green sustainable synthesis. Therefore, one of the main objectives is to create a highly effective process for catalytically converting aldehydes into carboxylic acids in a mild and environmentally friendly manner. In a typical reaction condition, 4-chlorobenzaldehyde was chosen to optimize the photocatalytic aldehyde oxidation reaction by IPPOP-4. The photocatalytic experiment was performed with different solvent systems with 0.2 mM of 4-chlorobenzaldehyde, 5 mg of IPPOP-4, 4 mL solvent, and irradiation of blue LED light to optimize the best reaction condition. ^1H NMR determined the yield of the product. The yield of 4-chlorobenzoic acid in different

organic solvents systems like methanol, ethanol, THF, toluene, MeCN, and $CHCl_3$ was found to be ~56%, ~8%, ~65%, ~77%, ~99%, and ~99% respectively within 4 hours (Appendix A41, A42). The best performance was shown in MeCN and $CHCl_3$, but MeCN was chosen for the further reaction because it is greener than $CHCl_3$.[24] After that, the substrate scope was tested with benzaldehyde substitutes. Despite of presence of different electron donating group like -4CH_3, -4Ph (Table-2, Entry- 1, 7) and electron withdrawing group like -4Br, -4Cl, -4F, -2,6-di-Cl, -4CF_3 (Table-2, Entry- 2, 3, 4, 5, 6), IPPOP-4 can efficiently oxidize aromatic aldehyde to aromatic acid. Additionally, for the heterocyclic compound, it was found that the yield of the product was ~100% (Table-2, Entry- 8), indicating the versatile nature of IPPOP-4 towards the photocatalytic oxidation of aromatic aldehydes.

Several experiments with different scavengers were performed to determine the responsible reactive oxygen species for the aldehyde oxidation reaction. When TBA, BQ, and $AgNO_3$ were used as scavenging agents for $^{\bullet}OH$, $^{\bullet}O_2^-$, and e^-, the conversion of aldehyde to acid was found to be ~25%, ~39%, and ~84%, respectively. However, in the case of NaN_3 and DABCO, which are scavenging agents for $^1O_2$, the conversion rate diminishes to 0%. Additionally, when KI was used as a scavenger of the h^+, the conversion also decreased to 0% (Appendix A43). These experiments suggest that $^1O_2$ and h^+ are the main reactive species responsible for photocatalytic aldehyde oxidation by IPPOP-4. We suggest the likely mechanism of photocatalytic aldehyde oxidation in aerobic conditions by IPPOP-4 based on the following data (Appendix A44).

In addition, we conducted several control experiments to assess the need for catalyst, light, and O_2. The aldehyde oxidation reaction to acid did not exhibit any conversion without these three conditions (Appendix A45). The recyclability test also showed that after 10 cycles, IPPOP-4 could efficiently convert aldehyde to acid (Appendix A46).

3.5. Post-Catalytic Characterization:

The stability of the polymeric network IPPOP-4 was further characterized after catalytic activity by FT-IR, TGA, solid-state UV-Vis spectra, and solid-state PL spectra. FT-IR spectra found no change in peak position or diminishing any peak (Appendix A47), whereas the TGA spectra were also unchanged after catalytic activity (Appendix A48). These two results confirm the structural stability of the IPPOP-4. Solid state UV-vis spectra (Appendix A49) and PL spectra (Appendix A50) were also found to be

unchanged after photocatalytic activity, suggesting that there was no change in the photophysical properties of IPPOP-4.

4. Conclusion:

In summary, we have described a readily manufactured imidazoline porous organic polymer (IPPOP-4) that exhibits strong heterogeneous photocatalytic activity. The highly conjugated IPPOP-4 with spatial distribution of imidazoline moeity effectively produce reactive oxygen species singlet oxygen ($^1O_2$). It can effeciently detoxify HD simulant 2-choloroethyl ethylsulfide (CEES) with ultrafast kinetics in both O_2 and air atmosphere. Also, here we demostrated the solvent effect for detoxification of CEES. Different mechanism was established based on the photocatalytic results on different solvent systems. Additionally, photocatalytic sulfide oxidation and aromatic aldehyde oxidation in air further proved the excellent photocatalytic activity of IPPOP-4. Heterogenosity and real world long term applicability was checked with recyclabilty test of 10 cycle.

5. Appendix

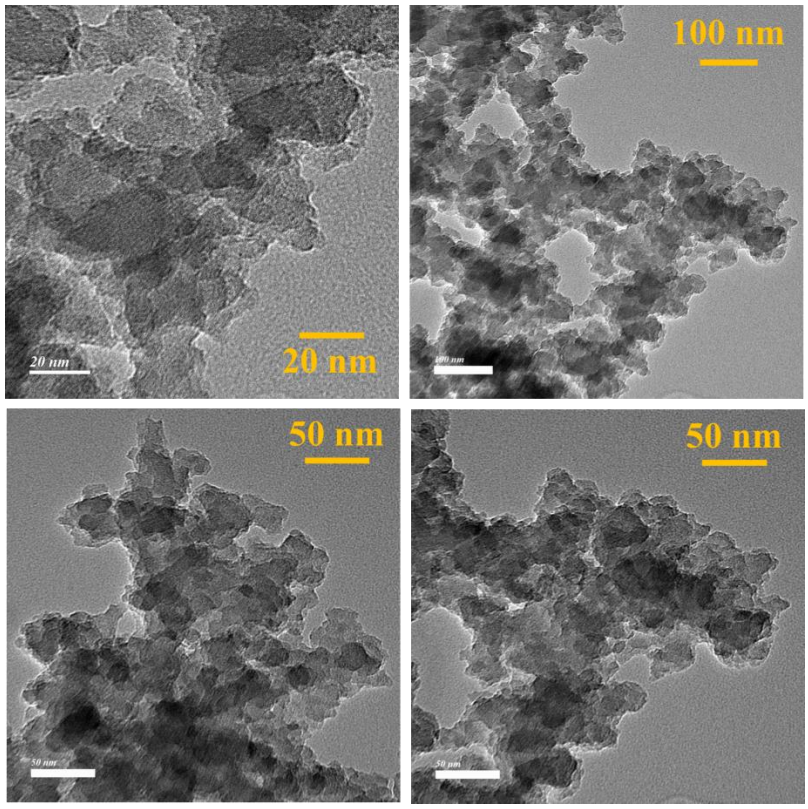

Appendix A1: HRTEM images of IPPOP-4

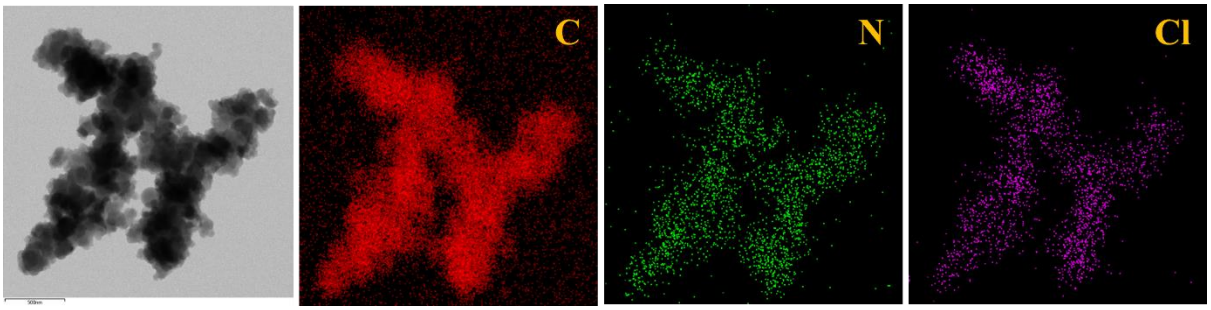

Appendix A2: EDS elemental distribution images of IPPOP-4

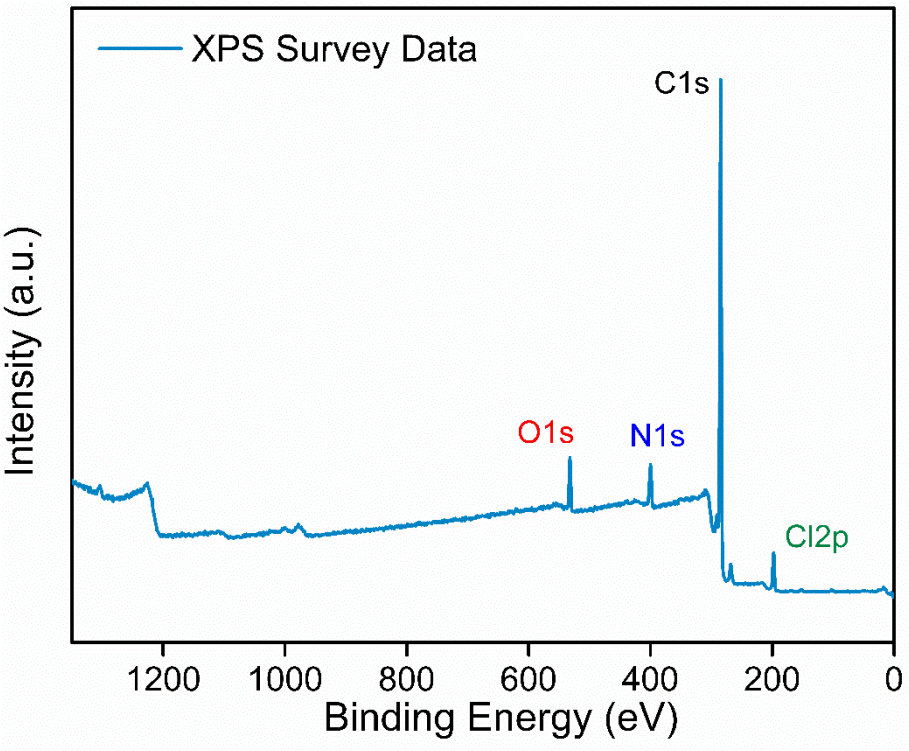

Appendix A3: XPS survey spectra of IPPOP-4

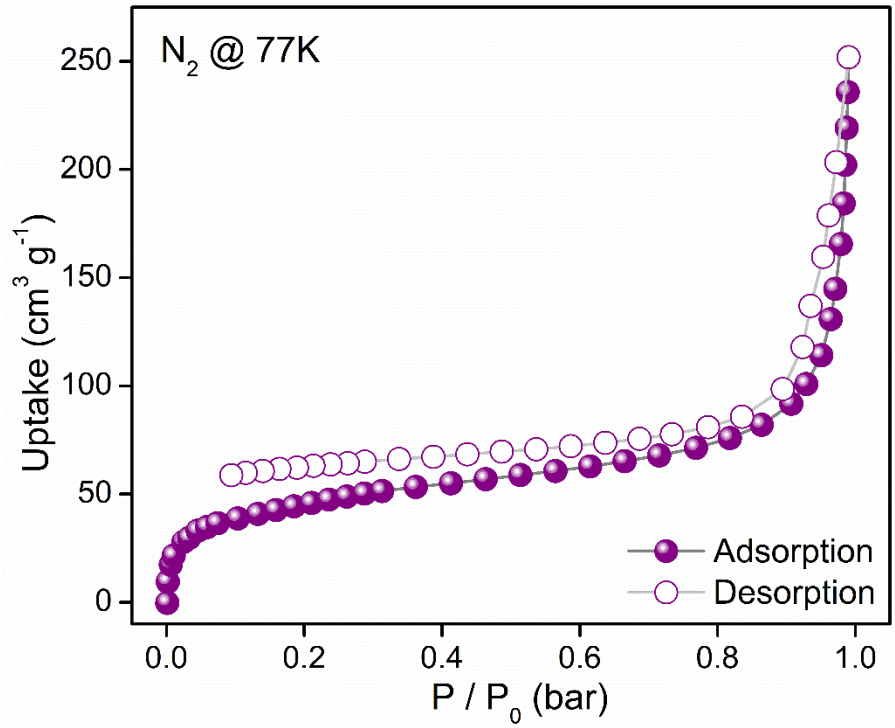

Appendix A4: Low temperature N_2 at 77 K gas adsorption isotherm of IPPOP-4

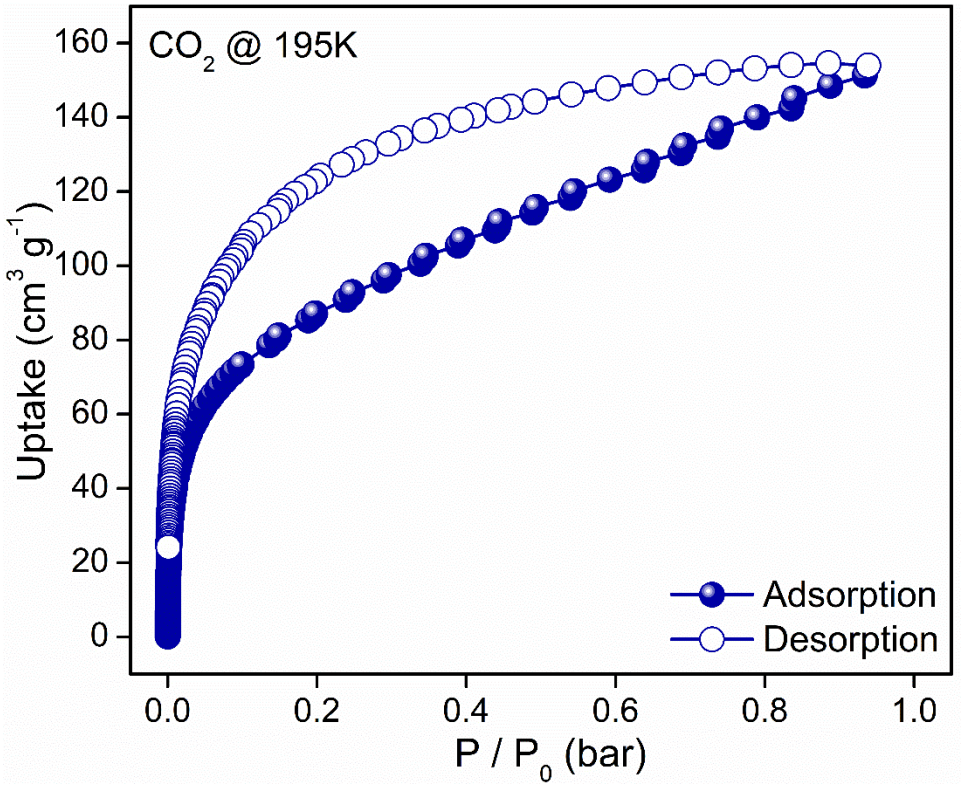

Appendix A5: Low temperature CO_2 at 195 K gas adsorption isotherm of IPPOP-4

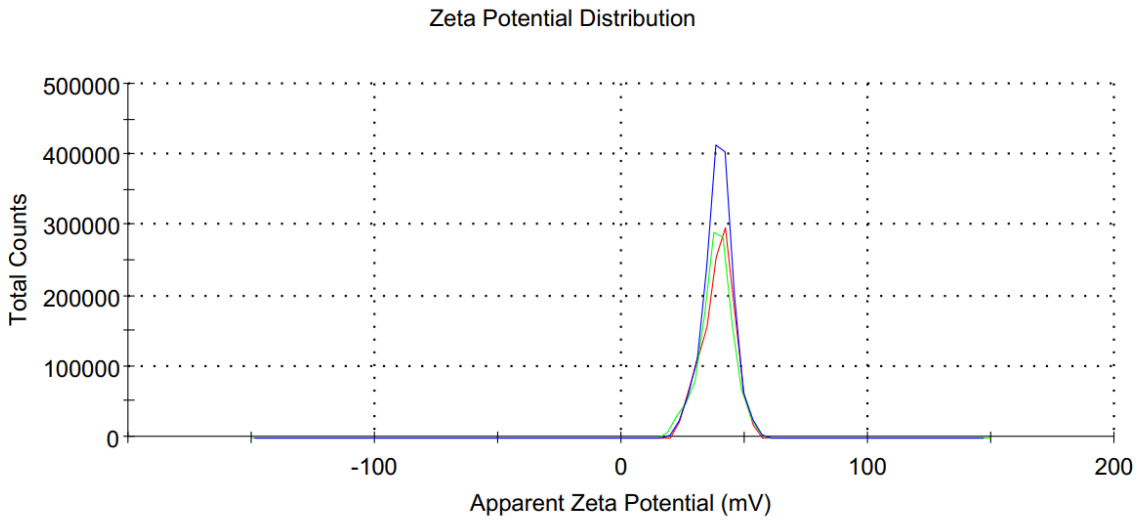

Appendix A6: Zeta potential of IPPOP-4

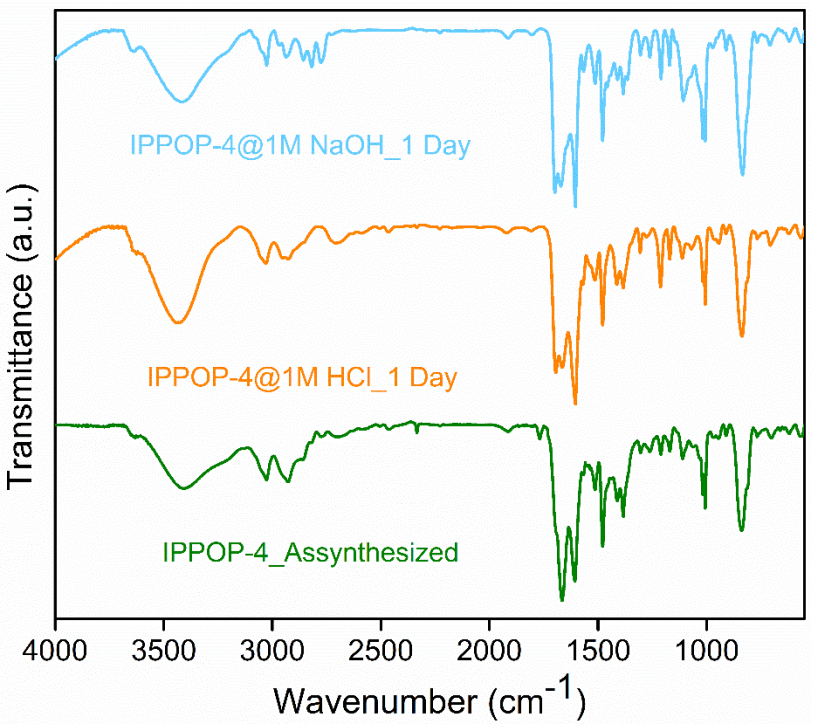

Appendix A7: Chemical Stability of IPPOP-4

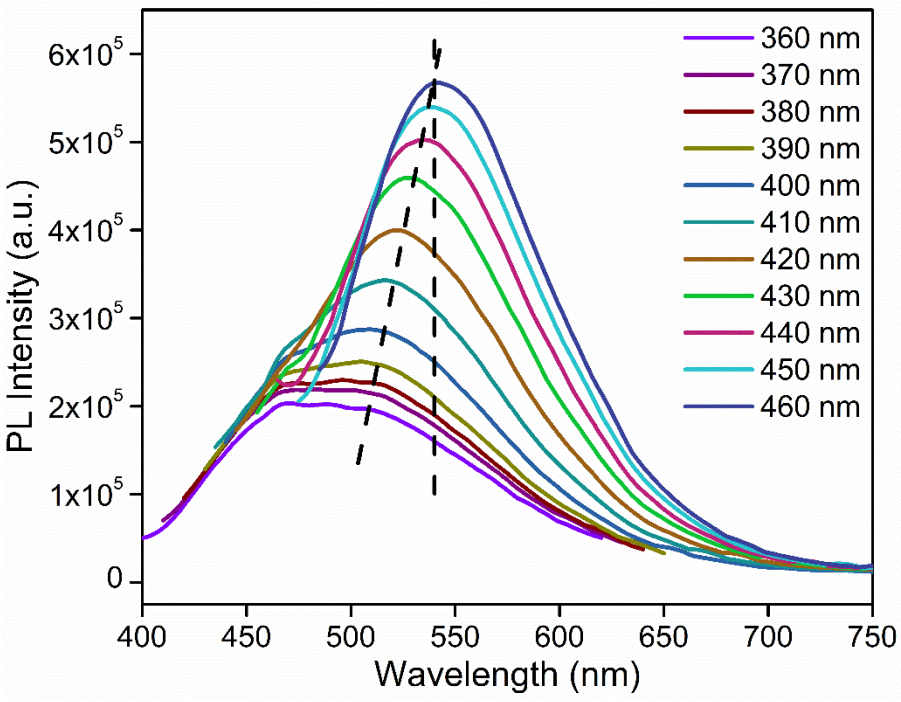

Appendix A8: Solid-state fluorescence spectra of IPPOP-4

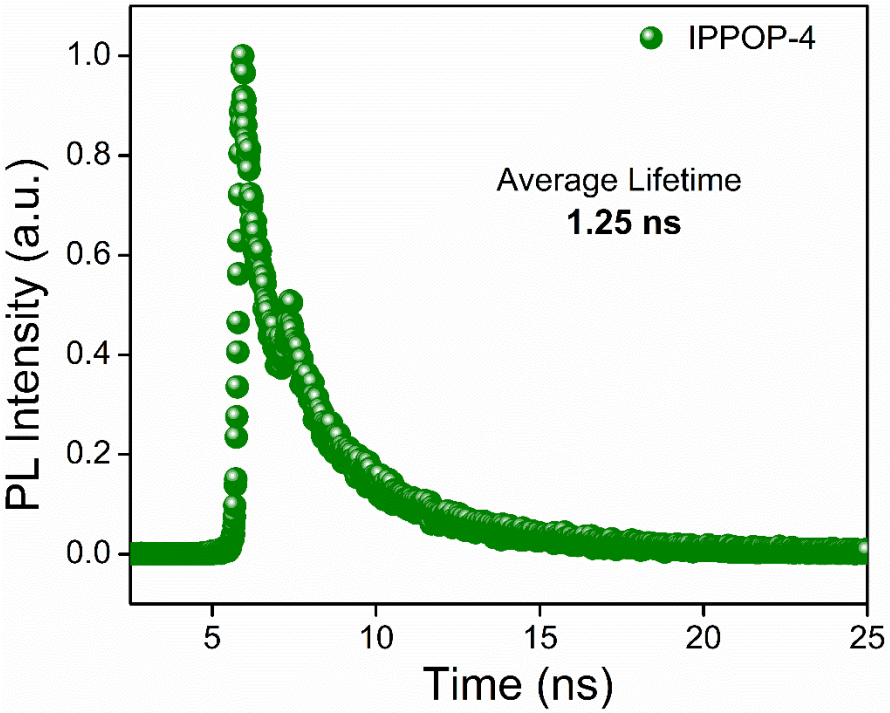

Appendix A9: Solid-state time-resolved photoluminescence spectra of IPPOP-4

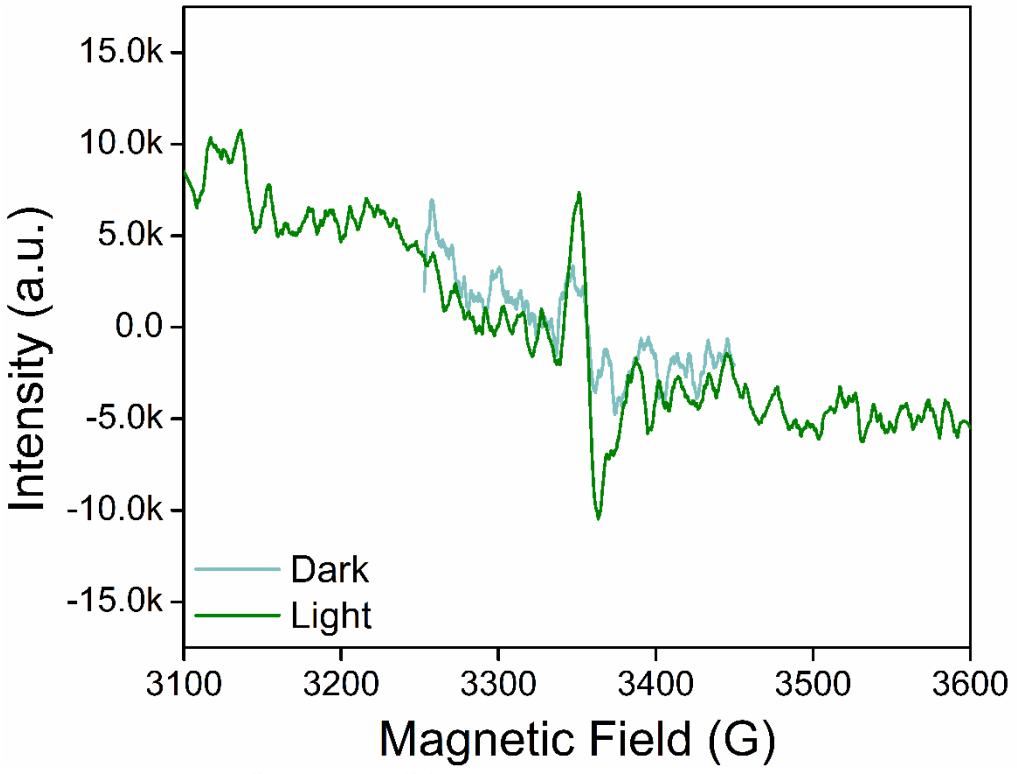

Appendix A10: Solid-state EPR spectra of IPPOP-4

5.1. Catalytic Studies:

As of right now, four ROS are recognized as major: hydrogen peroxide (H_2O_2), singlet oxygen ($^1O_2$), hydroxyl radical ($^{\bullet}OH$), and superoxide anion radical ($^{\bullet}O_2^-$). Previous results indicate that $^1O_2$ and $O_2^{\bullet-}$ can react with sulfide to produce CEESO in a selective manner.[S2] Utilizing $^{\bullet}OH$ radicals as oxidants may cause them to over oxidize, producing the hazardous sulfone compound $CEESO_2$.[S3] The primary source of additional ROS, including $^1O_2$, $^{\bullet}OH$, and $^{\bullet}O_2^-$, in the H_2O_2 oxidation pathway is its decomposition. Since H_2O_2 decomposition is not very efficient, effective oxygen transfer needs the employment of a promoter.[S4]

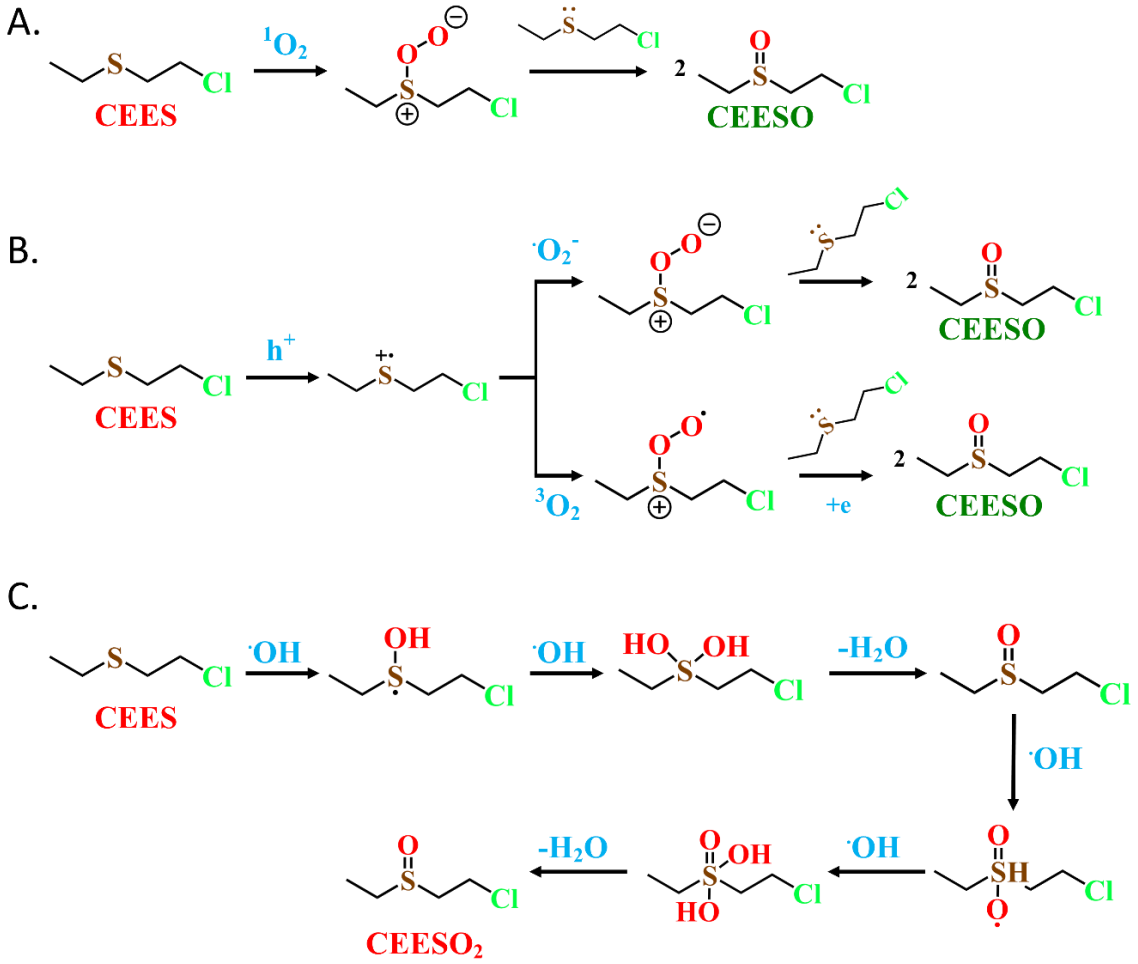

Appendix A11: Plausible reaction mechanism by different ROS.

These unpredictable activities lead to a complicated ROS being produced. Using H_2O_2 as a cocatalyst, several researchers have made some progress in recent years toward the highly selective sulfoxidation of HD simulants. During the catalytic process, additional substances were discovered, including over-oxidized $CEESO_2$,[S5] the dimeric sulfonium salt bisCEES,[S6] and the oxidation elimination product vinyl ethyl sulfoxide (VESO).[S7] H_2O_2 is therefore not the best option for the selective conversion of CEES to CEESO. Appendix A11 shows the mechanisms of the sulfoxidation reaction via $^1O_2$, $^{\bullet}O_2^-$, and $^{\bullet}OH$.

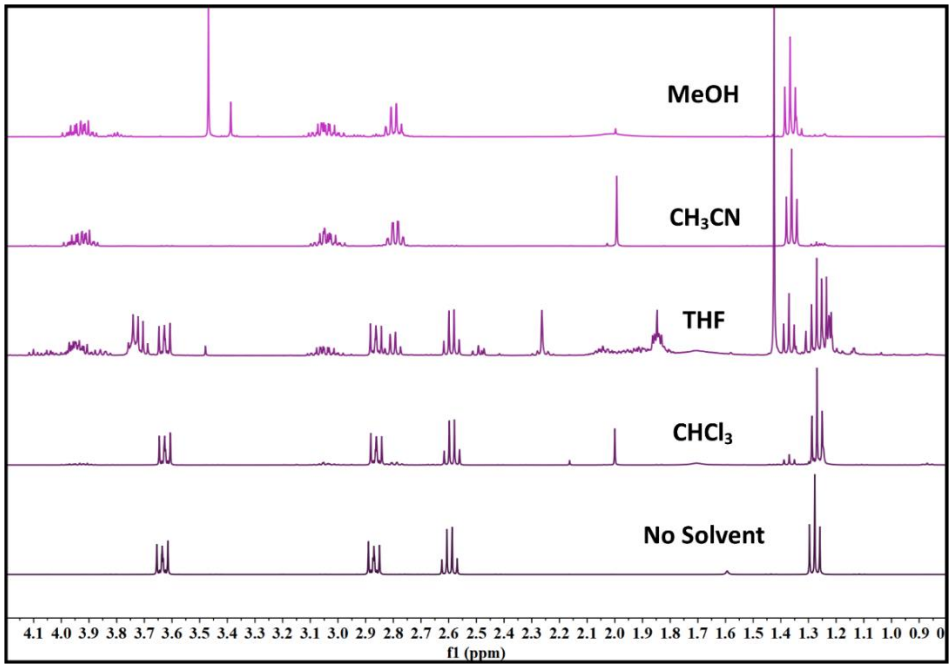

Appendix A12: ^{1}H NMR spectra before and after photooxidation reaction of CEES by IPPOP-4 catalyst in Air in different Solvent Systems

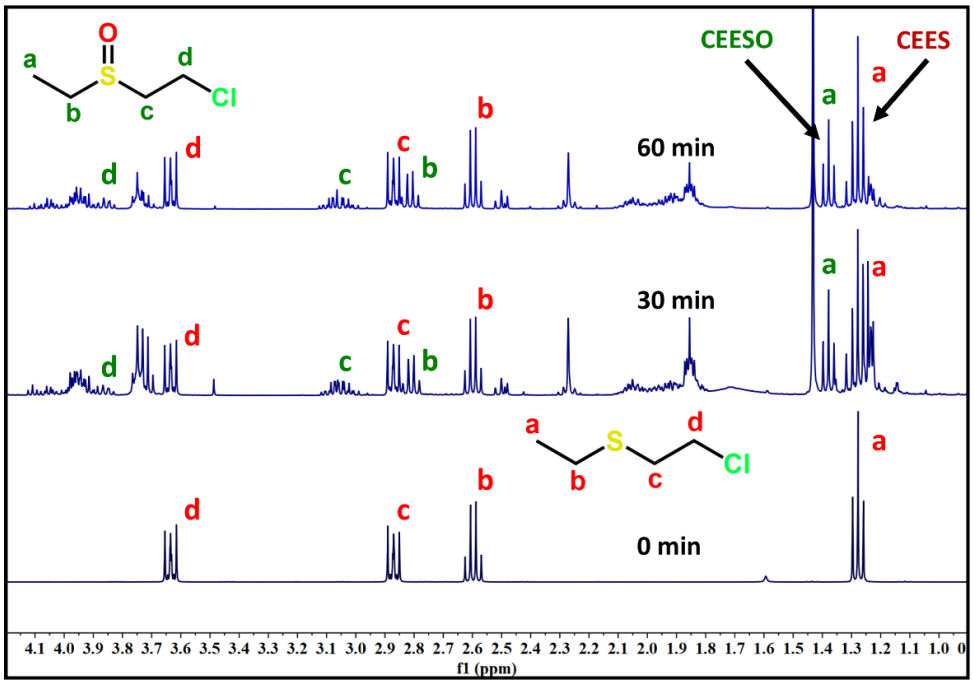

Appendix A13: ^{1}H NMR spectra before and after photooxidation reaction of CEES by IPPOP-4 catalyst in Air in THF

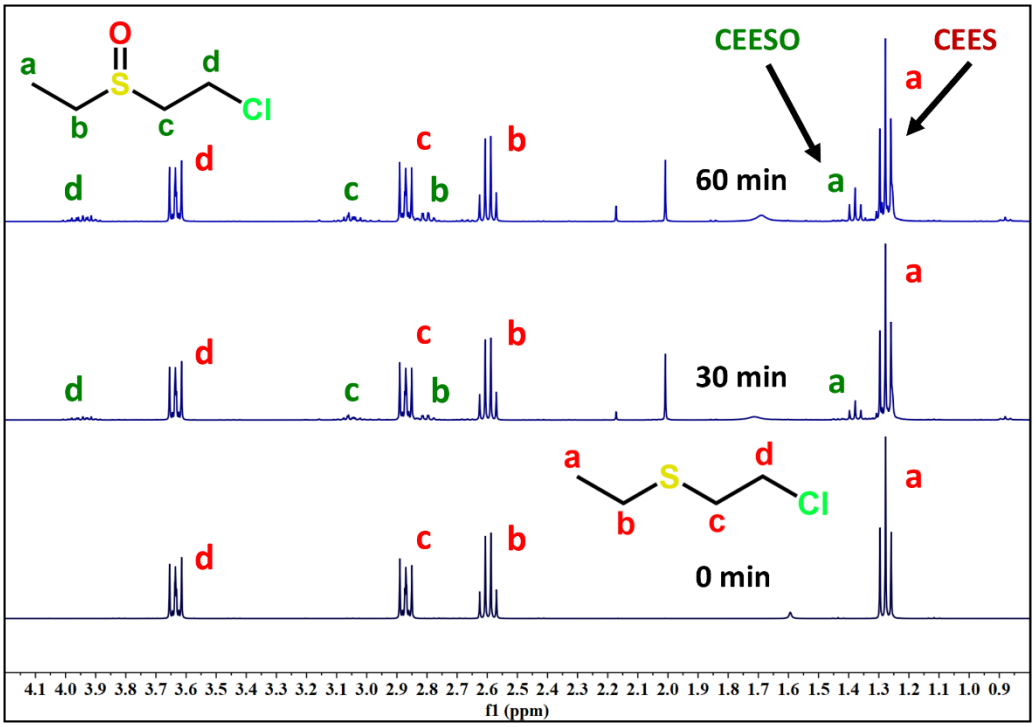

Appendix A14: ^{1}H NMR spectra before and after photooxidation reaction of CEES by IPPOP-4 catalyst in Air in $CHCl_3$

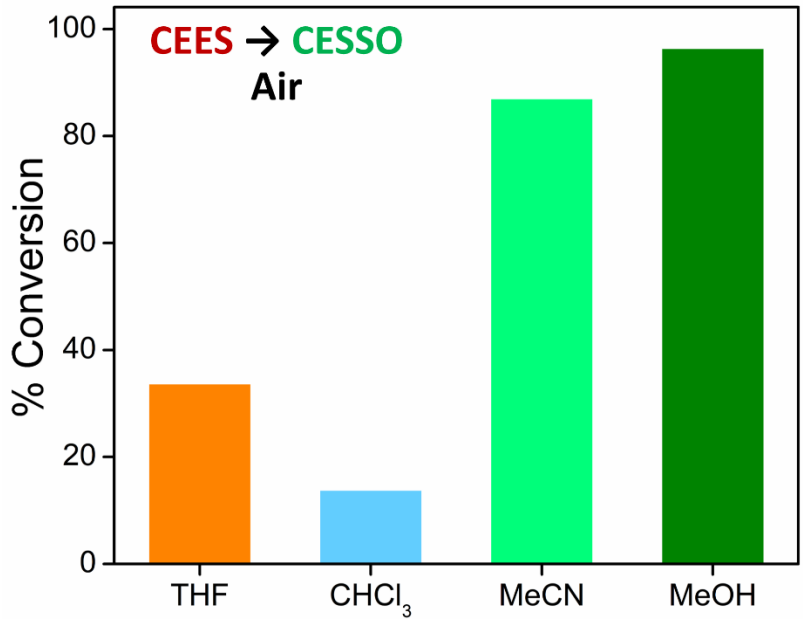

Appendix A15: % Conversion of CEES to CEESO in different solvent systems in Air

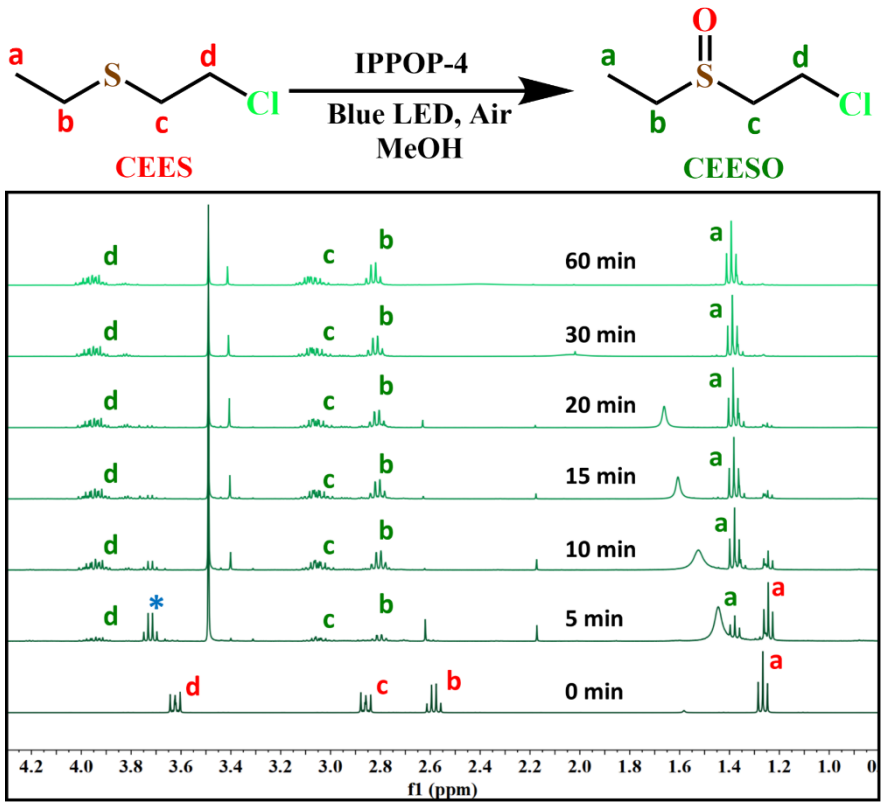

Appendix A16: Time dependent ^{1}H NMR of photocatalytic degradation of CEES by IPPOP-4 in MeOH in air (0.8-4.3 ppm)

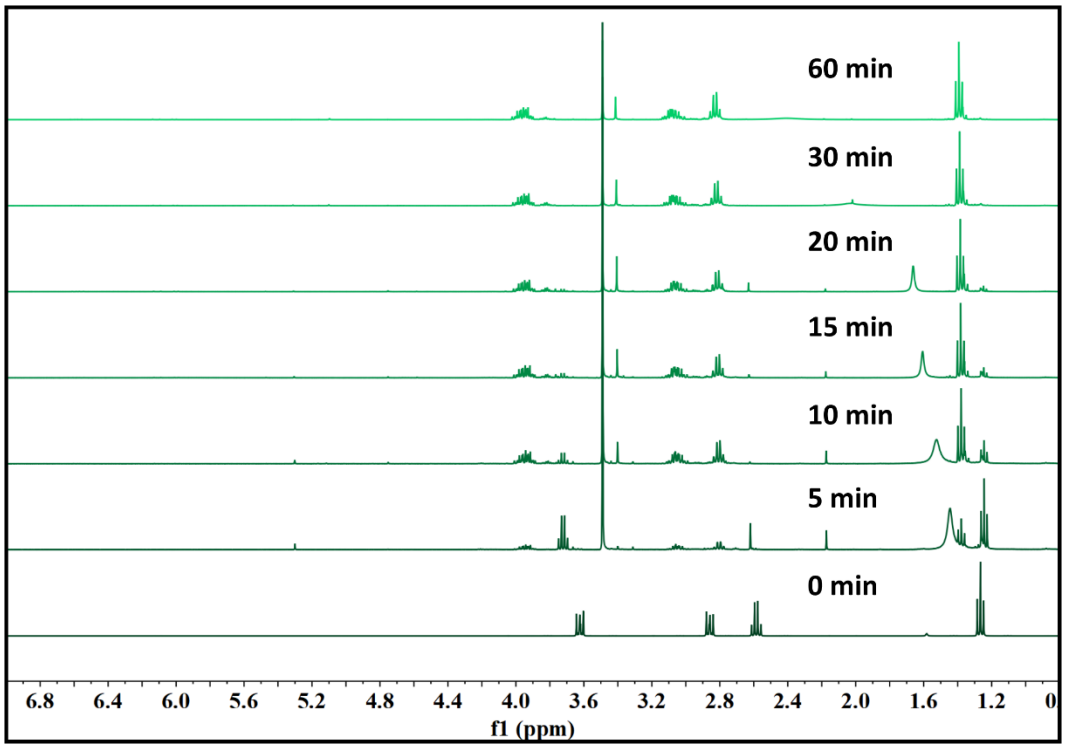

Appendix A17: Time dependent ^{1}H NMR of photocatalytic degradation of CEES by IPPOP-4 in MeOH in air (0.8-7 ppm)

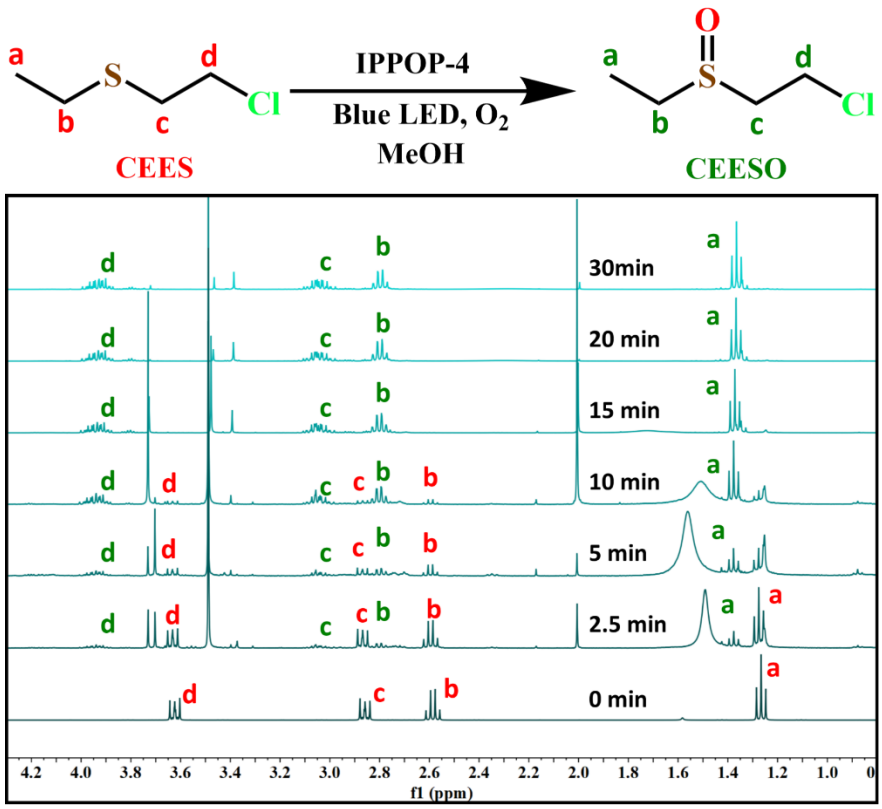

Appendix A18: Time dependent ^{1}H NMR of photocatalytic degradation of CEES by IPPOP-4 in MeOH in O_2 (0.8-4.3 ppm)

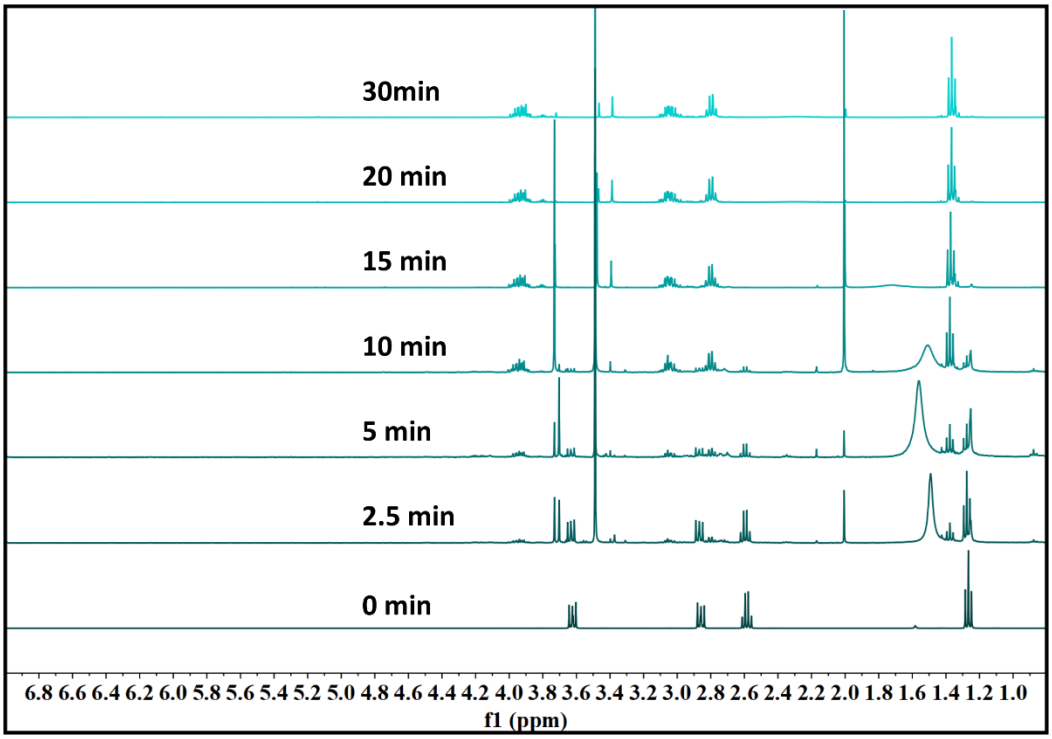

Appendix A19: Time dependent ^{1}H NMR of photocatalytic degradation of CEES by IPPOP-4 in MeOH in O_2 (0.8-7 ppm)

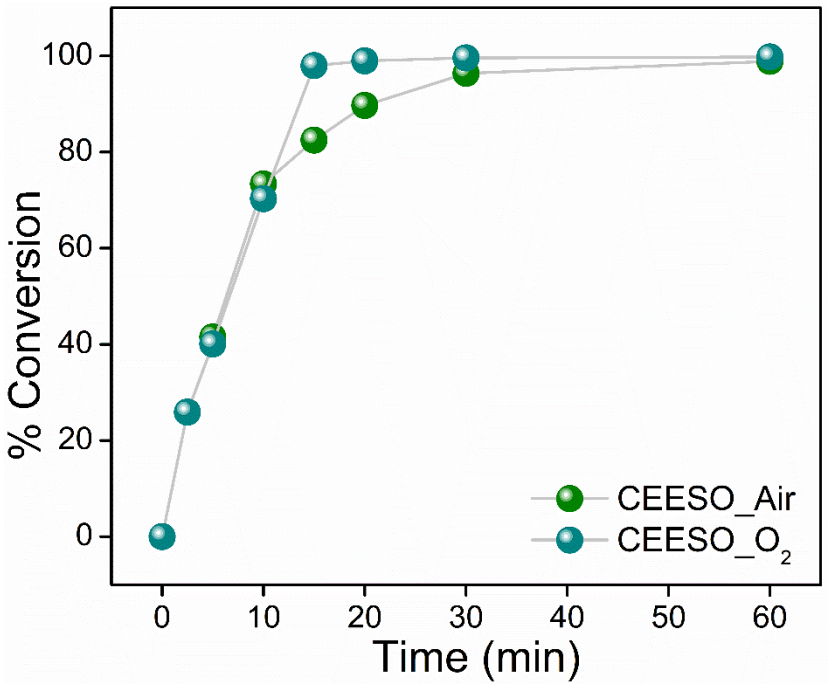

Appendix A20: % Conversion comparison of photocatalytic degradation of CEES by IPPOP-4 in MeOH in Air and O_2

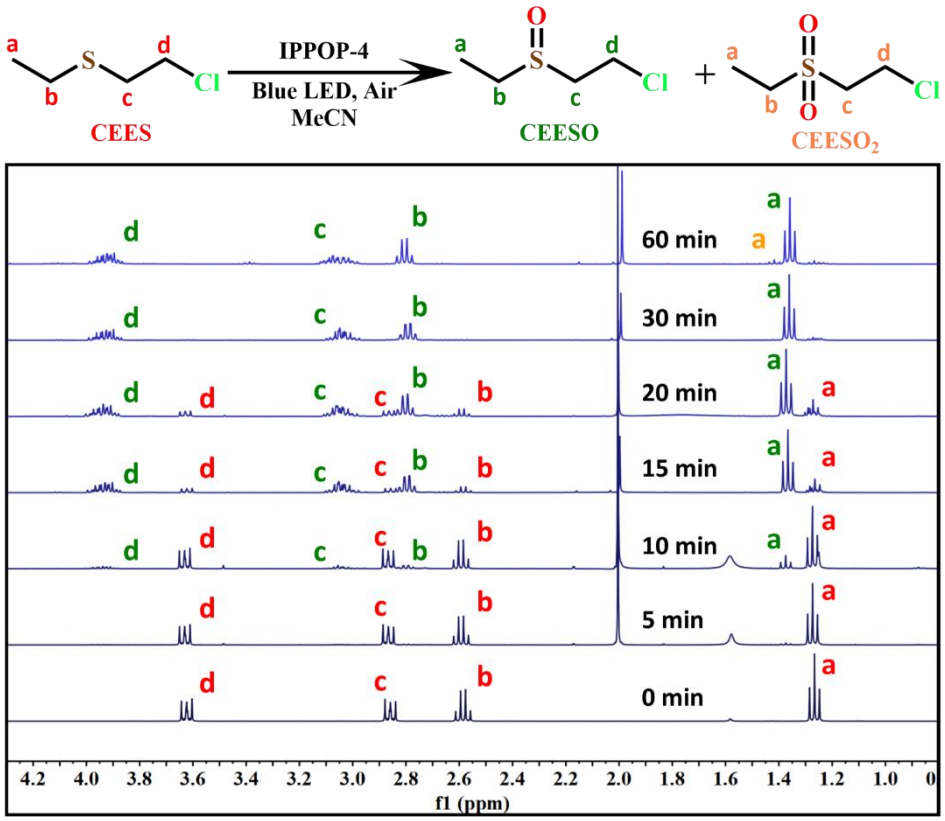

Appendix A21: Time dependent ^{1}H NMR of photocatalytic degradation of CEES by IPPOP-4 in MeCN in air (0.8-4.3 ppm)

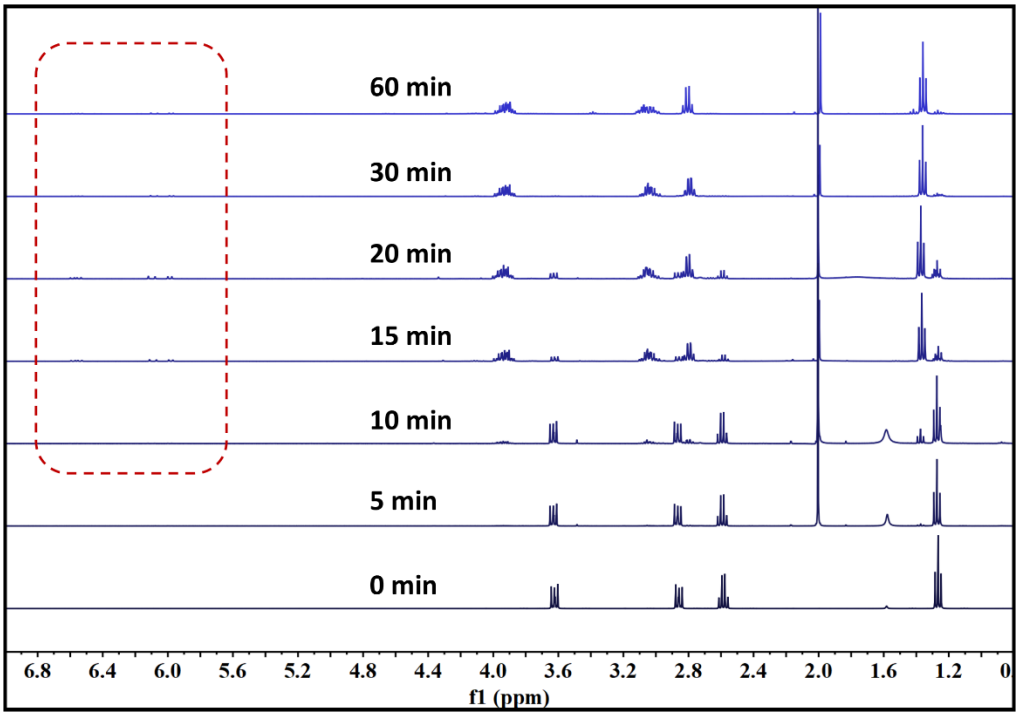

Appendix A22: Time dependent ^{1}H NMR of photocatalytic degradation of CEES by IPPOP-4 in MeCN in air (0.8-7 ppm)

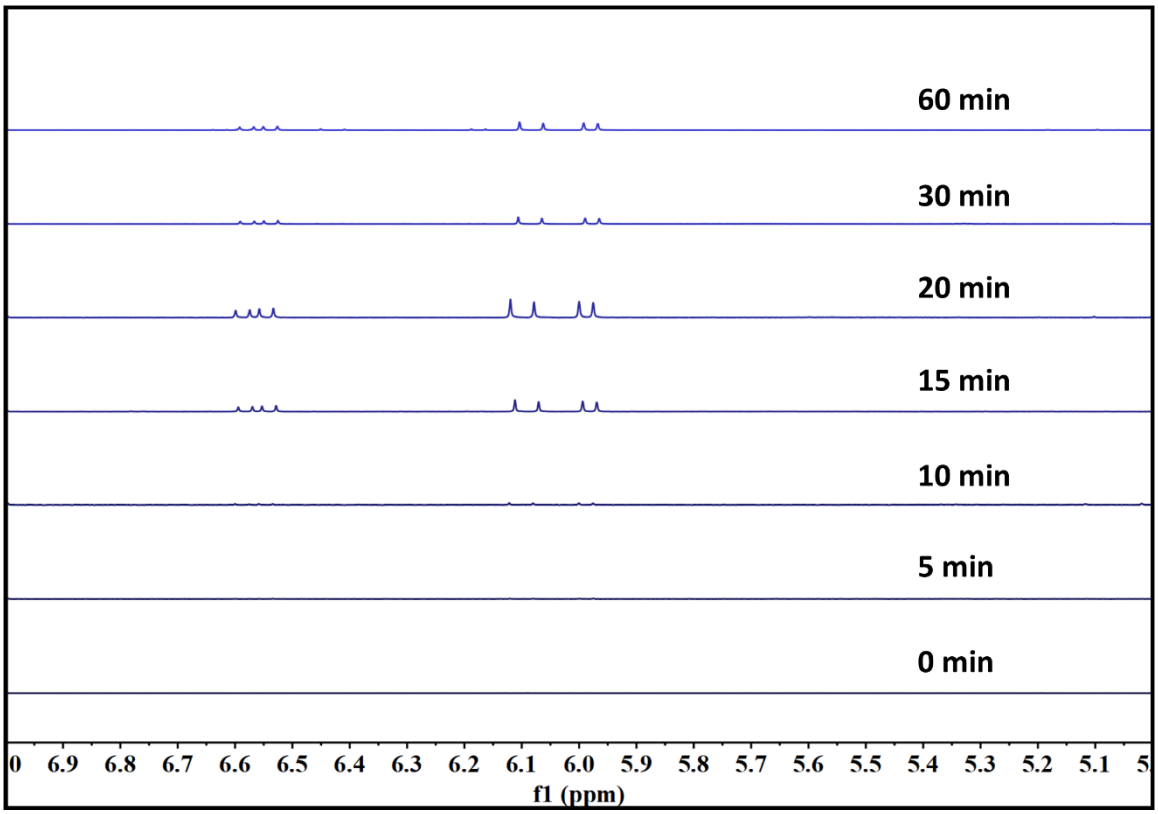

Appendix A23: Time dependent ^{1}H NMR of photocatalytic degradation of CEES by IPPOP-4 in MeCN in air (5-7 ppm)

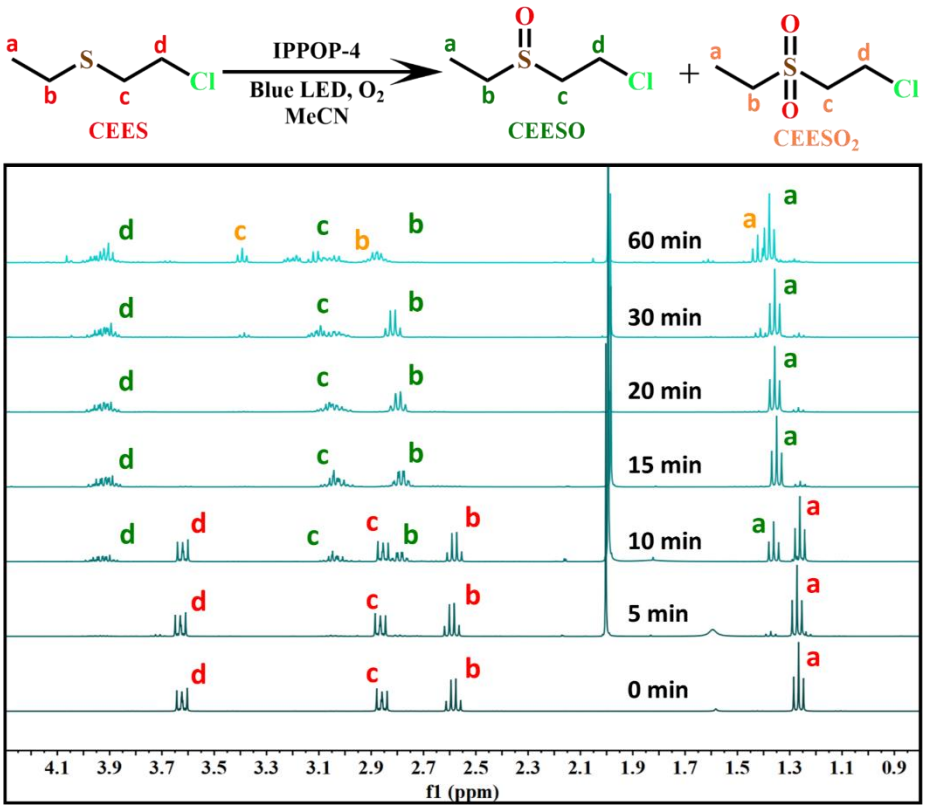

Appendix A24: Time dependent ^{1}H NMR of photocatalytic degradation of CEES by IPPOP-4 in MeCN in O_2 (0.8-4.3 ppm)

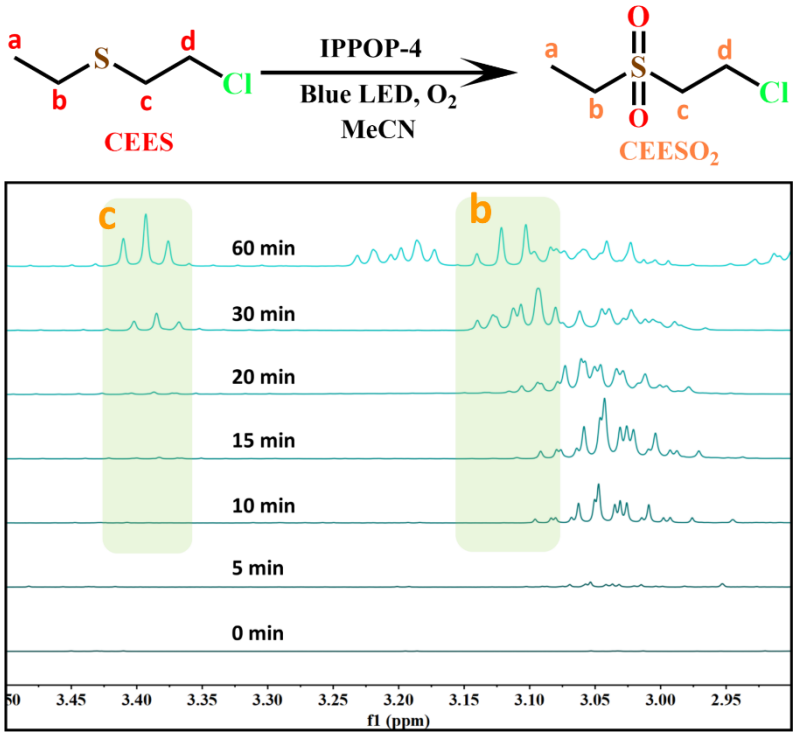

Appendix A25: Time dependent ^{1}H NMR of photocatalytic degradation of CEES by IPPOP-4 in MeCN in O_2 (2.9-3.5 ppm)

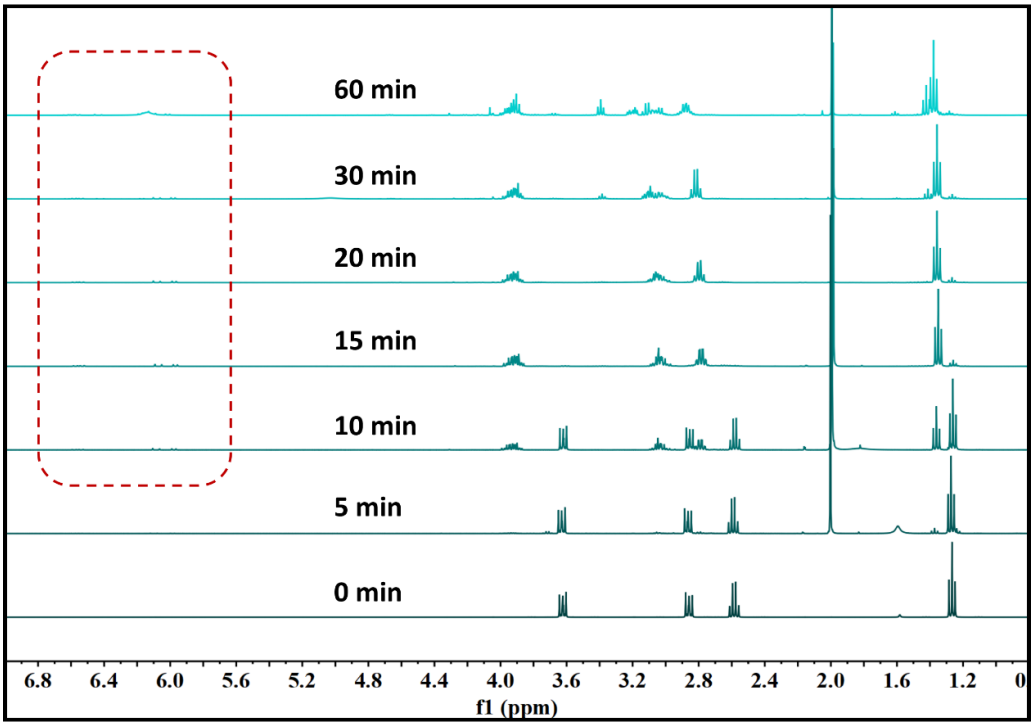

Appendix A26: Time dependent ^{1}H NMR of photocatalytic degradation of CEES by IPPOP-4 in MeCN in O_2 (0.8-7 ppm)

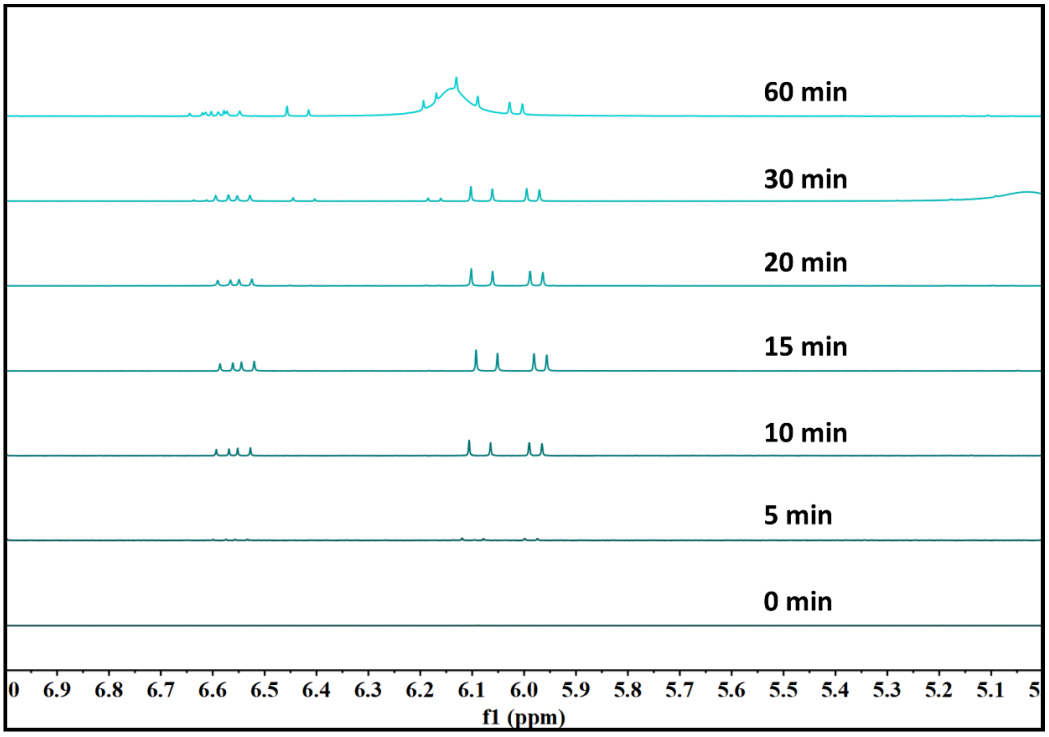

Appendix A27: Time dependent ^{1}H NMR of photocatalytic degradation of CEES by IPPOP-4 in MeCN in O_2 (5-7 ppm)

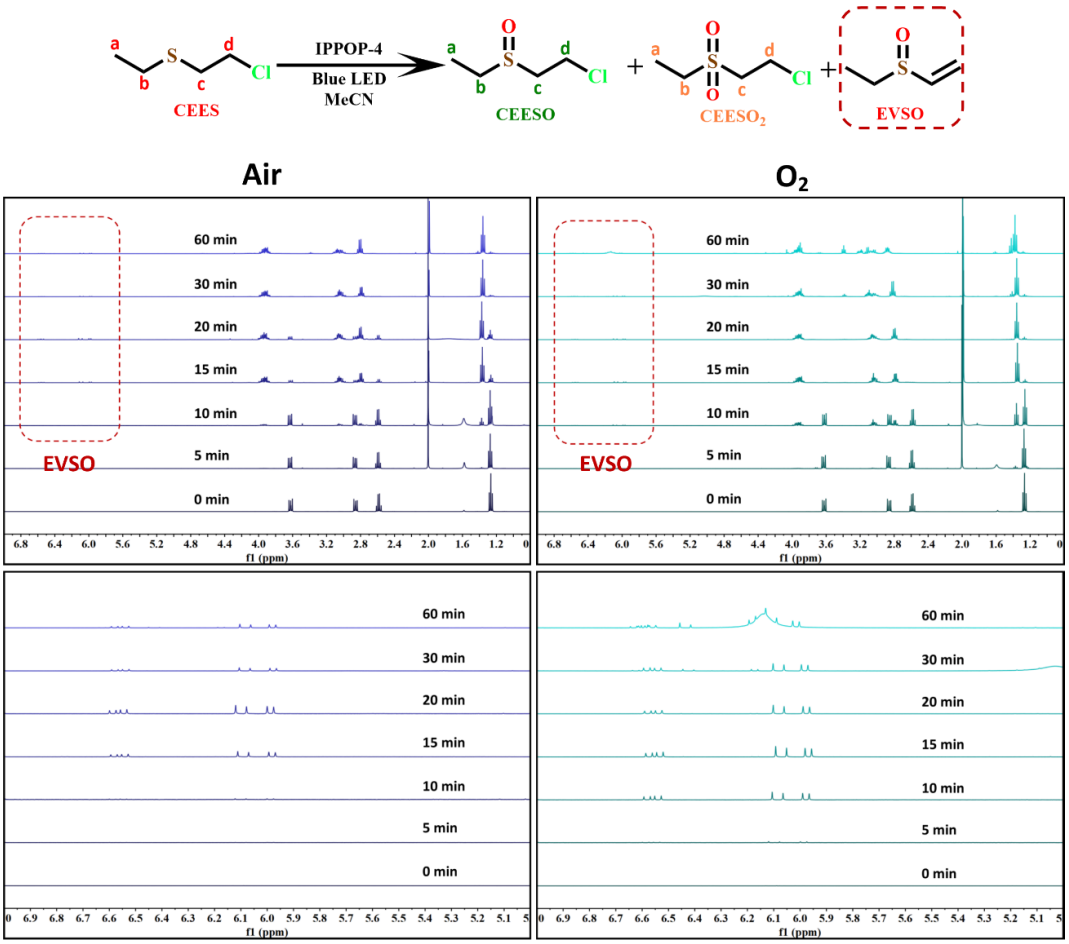

Appendix A28: Time dependent ^{1}H NMR of photocatalytic degradation of CEES by IPPOP-4 in MeCN (5-7 ppm). The peaks in the region 5.8 ppm to 6.8 ppm is evidence of formation of EVSO in air (left top and bottom) and O_2 (right top and bottom)

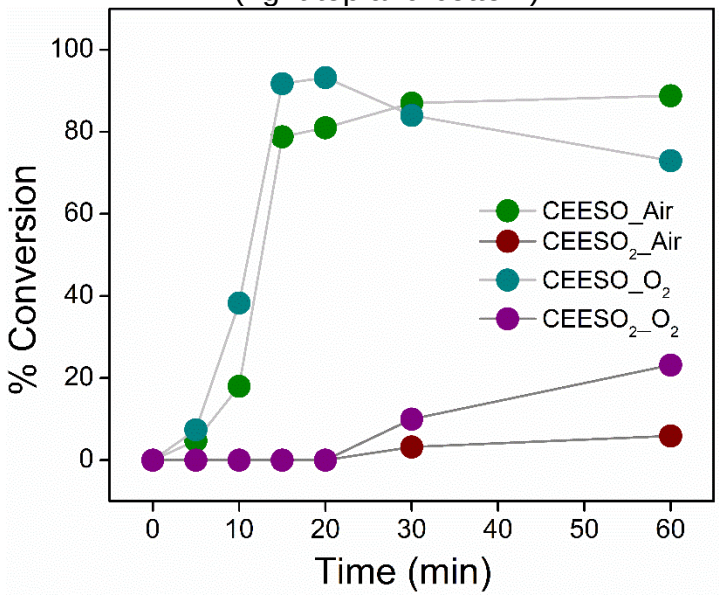

Appendix A29: CEES oxidation kinetics in MeCN in different environment

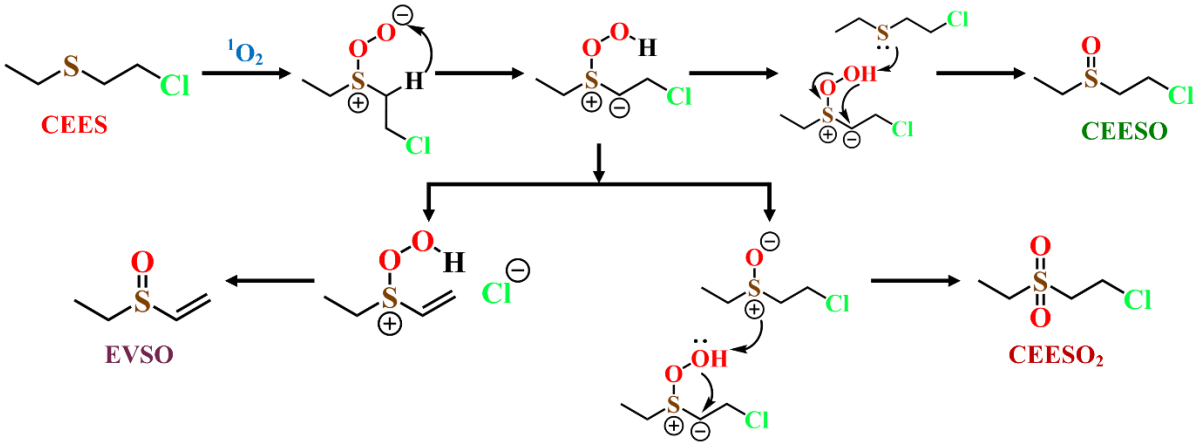

A

Appendix A30: Plausible mechanism of CEES degradation in MeCN

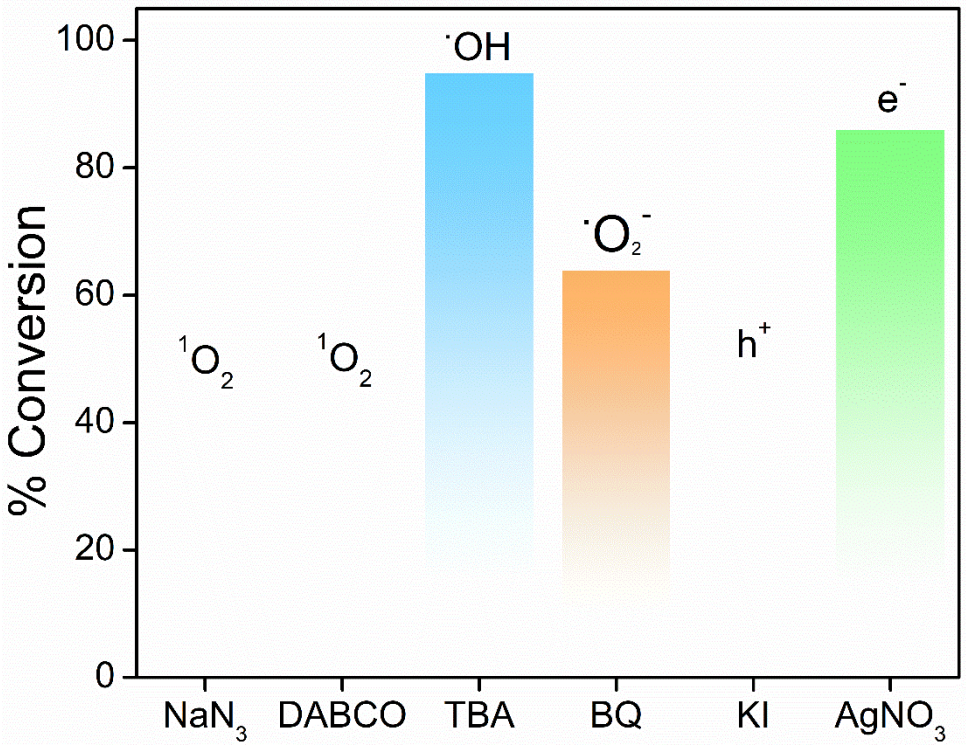

Appendix A31: Scavenger test for different reactive species for CEES oxidation

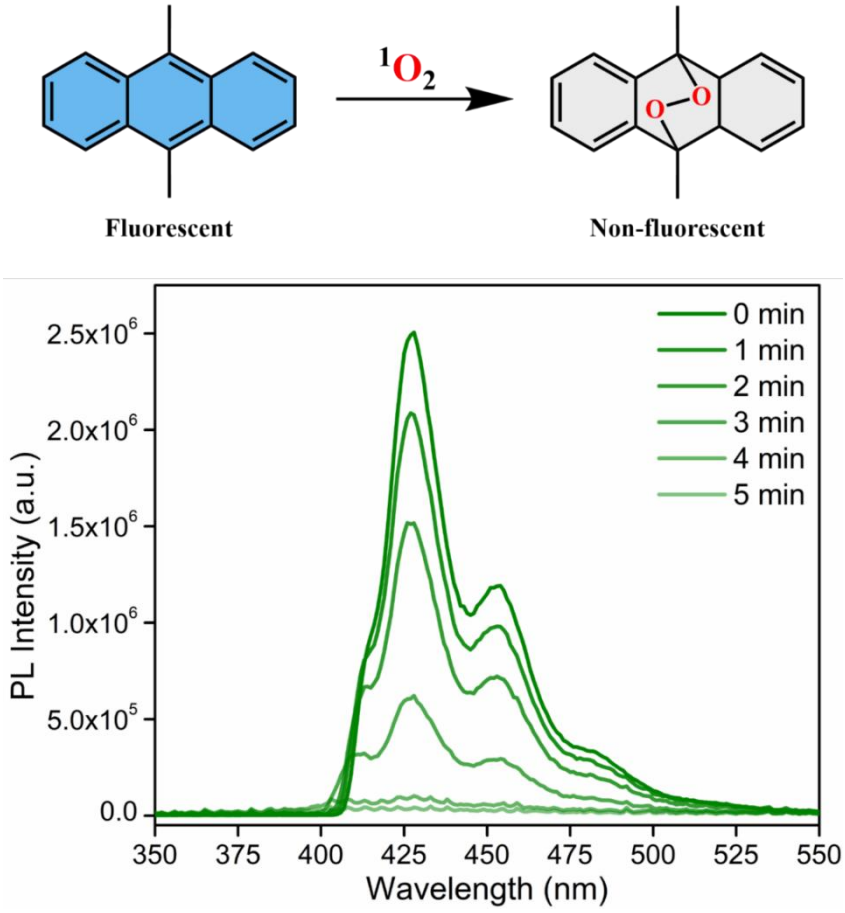

Appendix A32: Emission spectrum of DMA in the presence of IPPOP-4 in MeOH

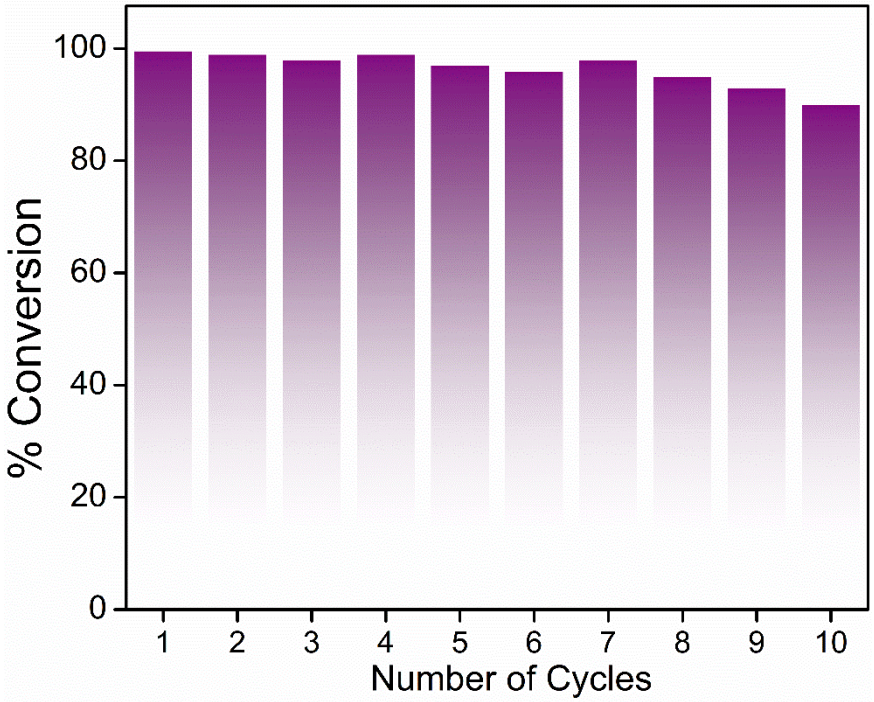

Appendix A33: Recyclability of CEES degradation by IPPOP-4

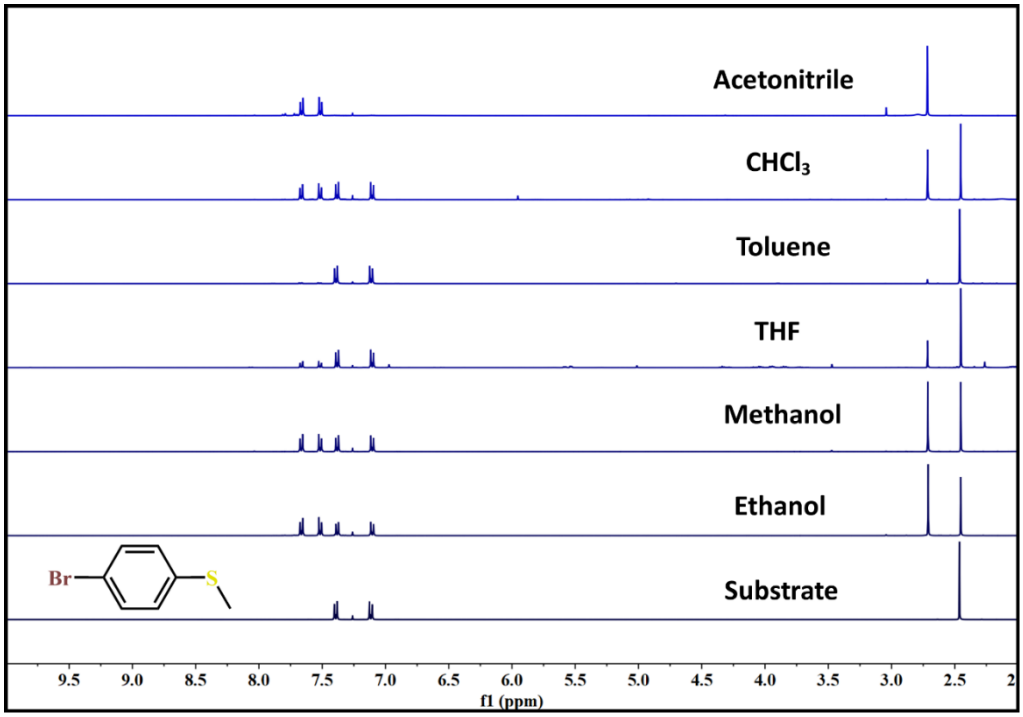

Appendix A34: ^{1}H NMR of photocatalytic 4-bromothioanisole oxidation in different organic solvent

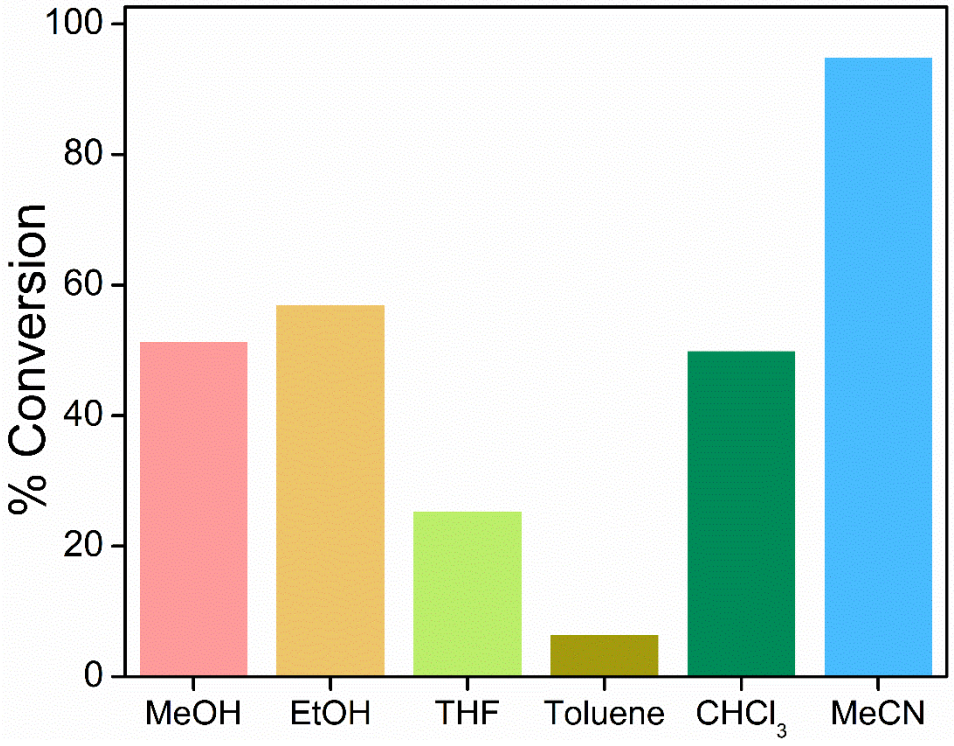

Appendix A35: % Conversion of photocatalytic 4-bromothioanisole oxidation in different organic solvent

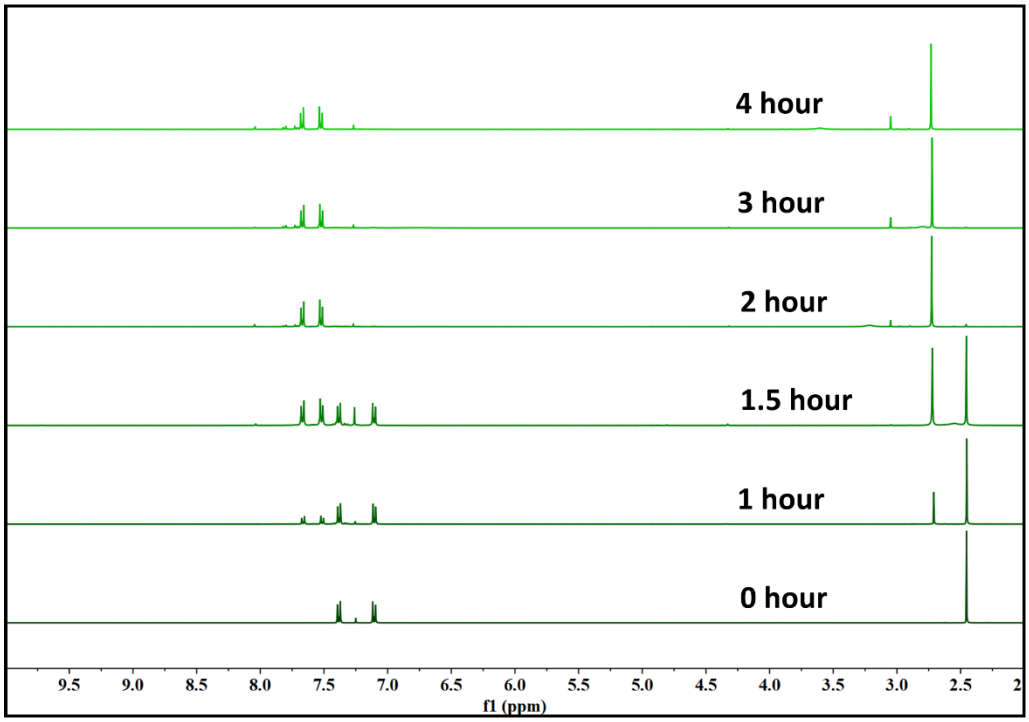

Appendix A36: ^{1}H NMR kinetics of photocatalytic 4-bromothioanisole oxidation in MeCN

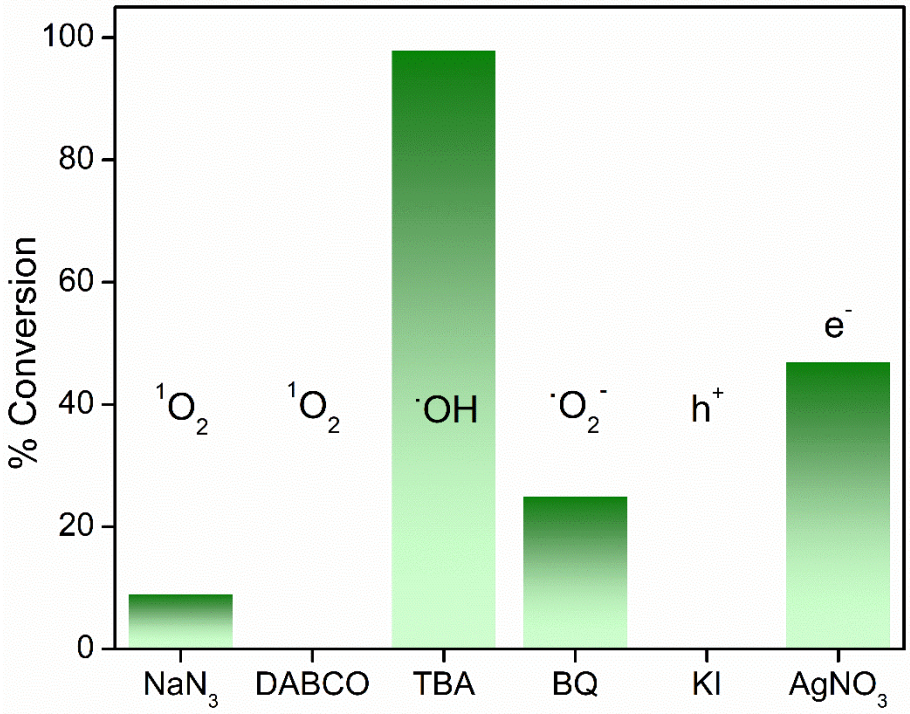

Appendix A37: % Conversion of photocatalytic 4-bromothioanisole oxidation in presence of different scavenger in MeCN

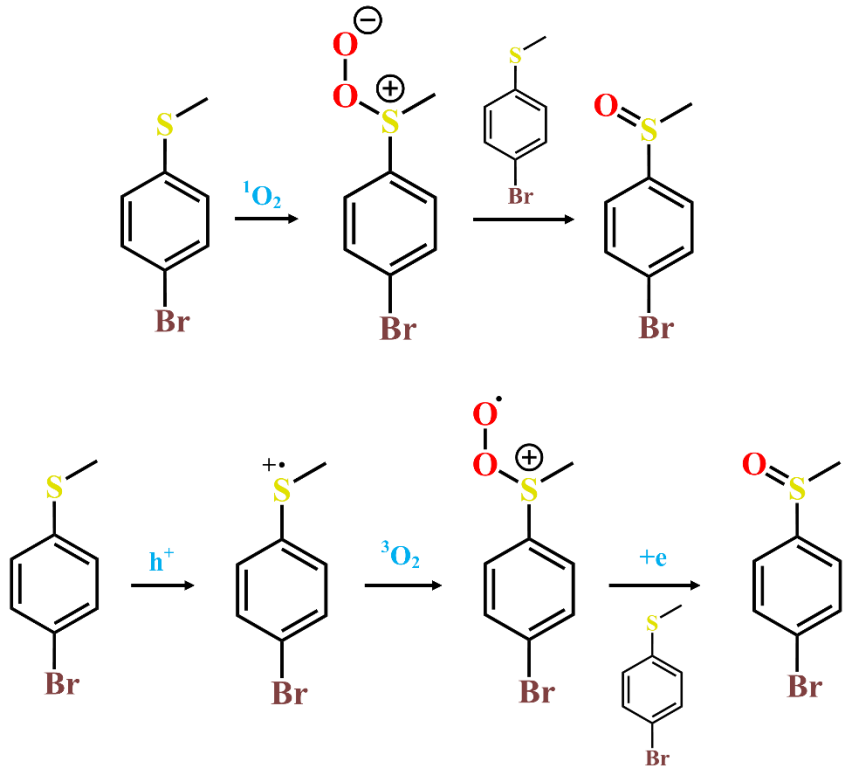

Appendix A38: Plausible Mechanism of photocatalytic 4-bromothioanisole oxidation in MeCN

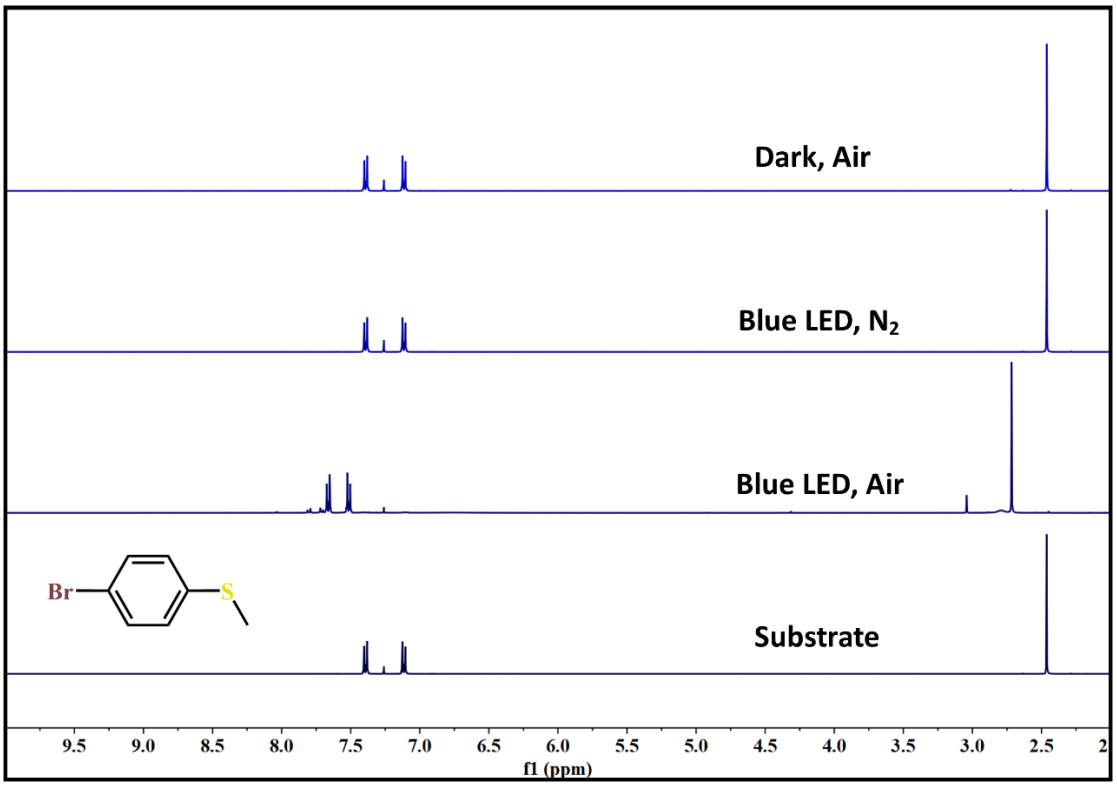

Appendix A39: ^{1}H NMR control experiment of photocatalytic 4-bromothioanisole oxidation in MeCN

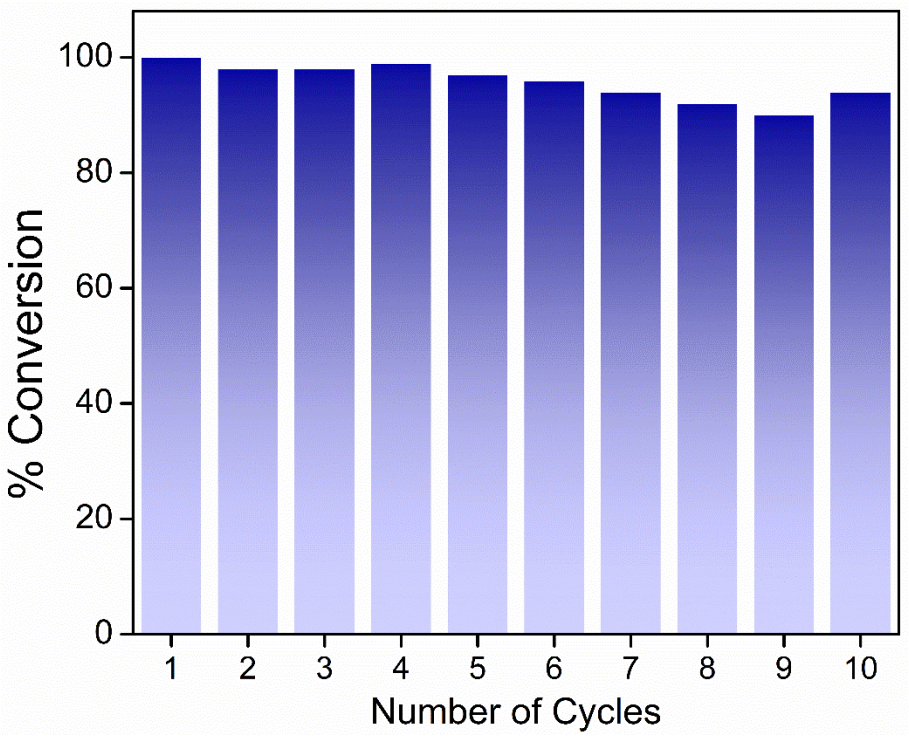

Appendix A40: Recyclability of photocatalytic 4-bromothioanisole oxidation in MeCN

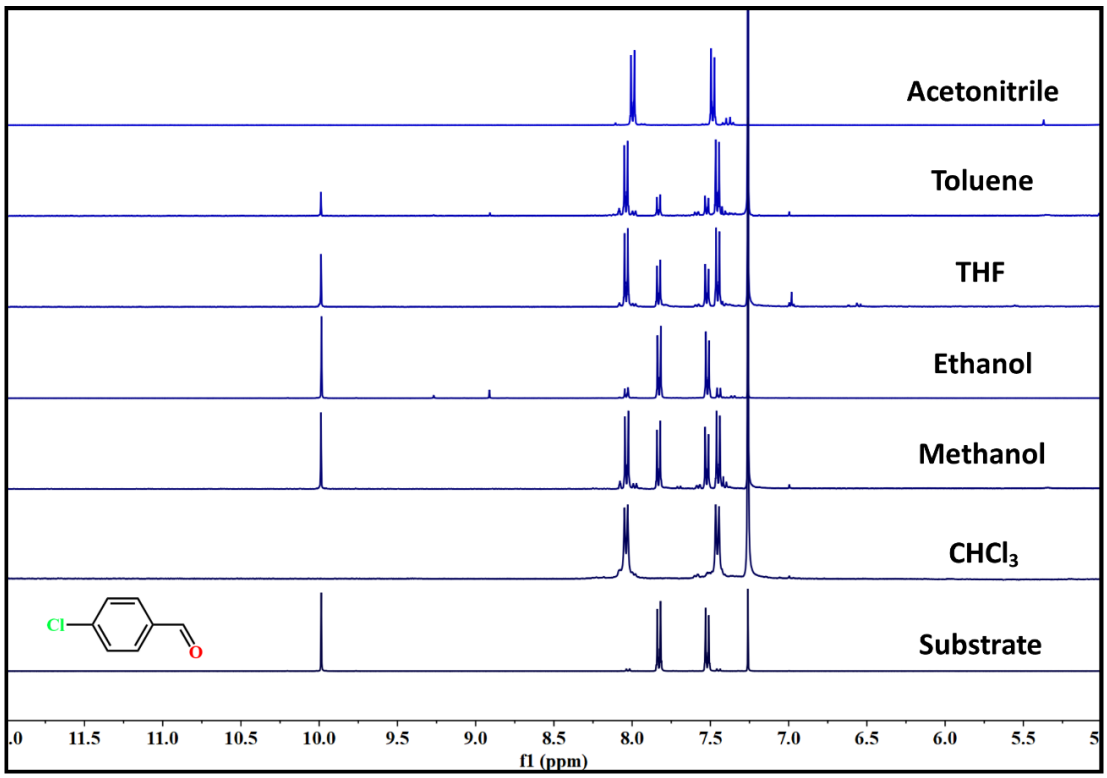

Appendix A41: ^{1}H NMR of photocatalytic 4-chlorobenzaldehyde oxidation in different organic solvent

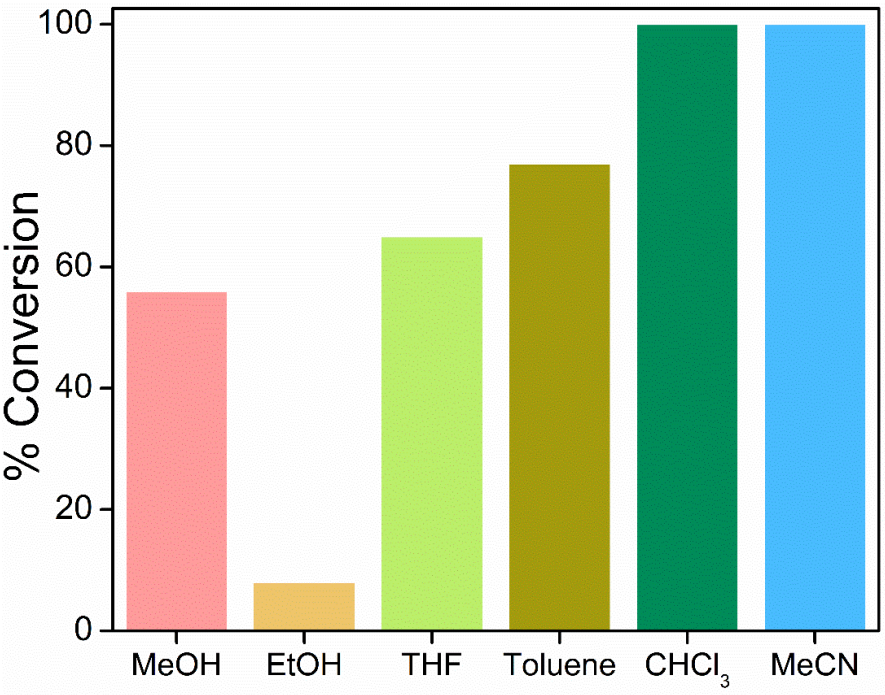

Appendix A42: % Conversion of photocatalytic 4-chlorobenzaldehyde oxidation in different organic solvent

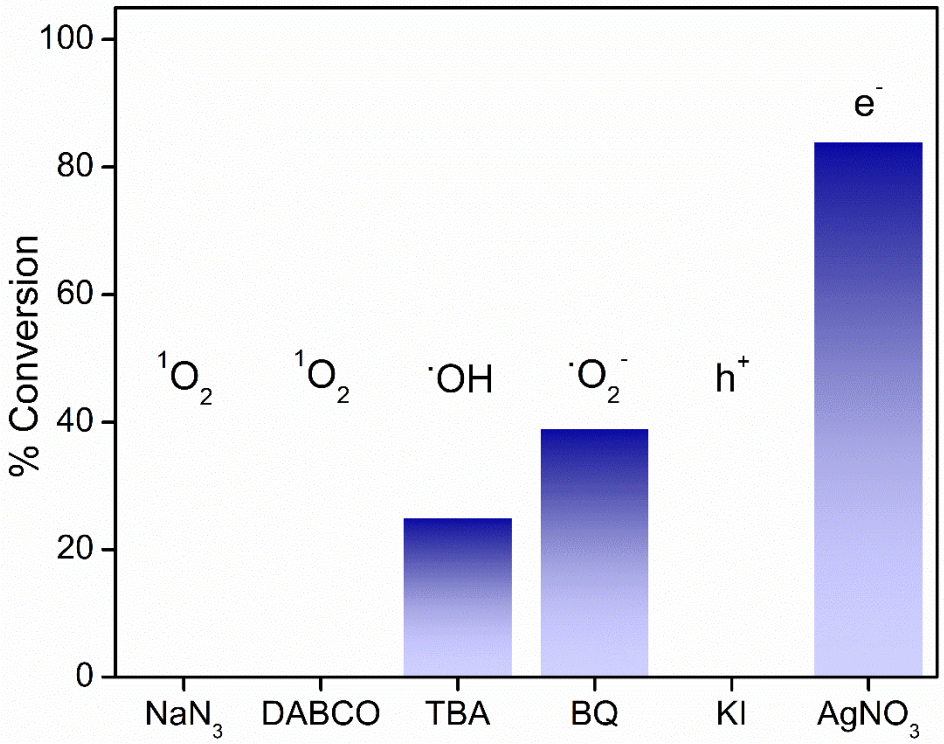

Appendix A43: % Conversion of photocatalytic 4-chlorobenzaldehyde oxidation in presence of different scavenger in MeCN

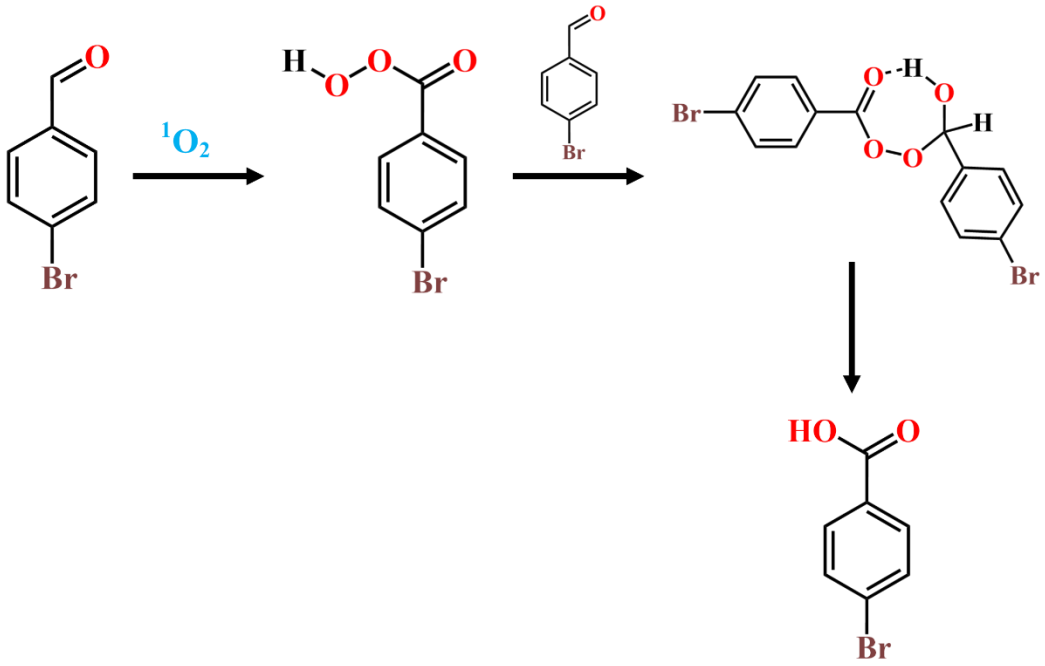

Appendix A44: Plausible Mechanism of photocatalytic 4-chlorobenzaldehyde oxidation in MeCN

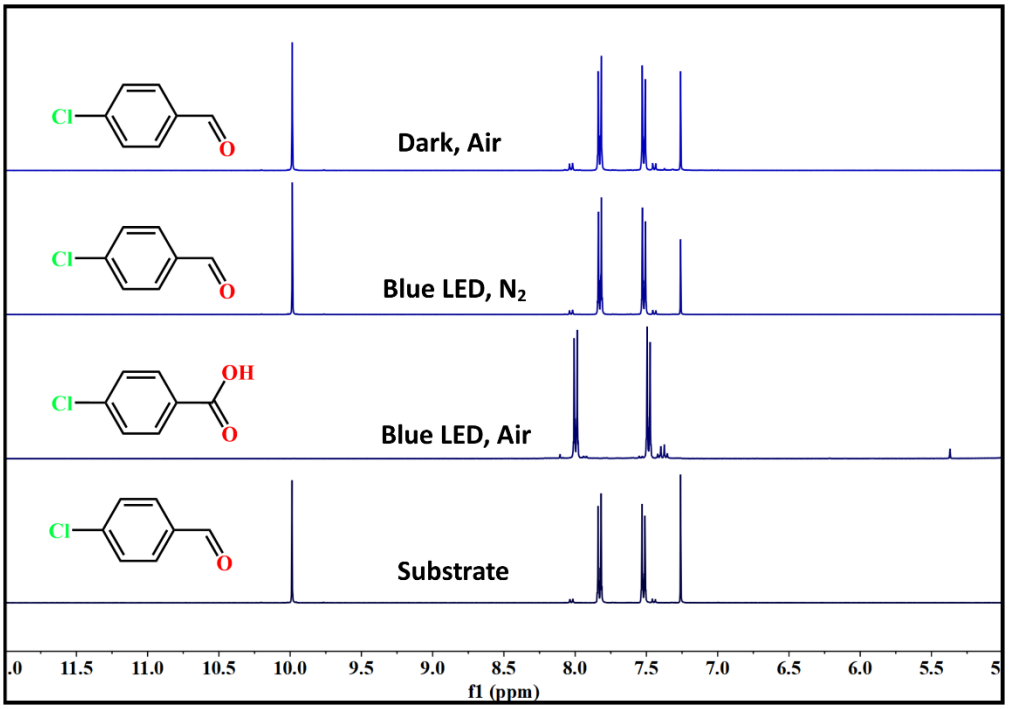

Appendix A45: ^{1}H NMR control experiment of photocatalytic 4-chlorobenzaldehyde oxidation in MeCN

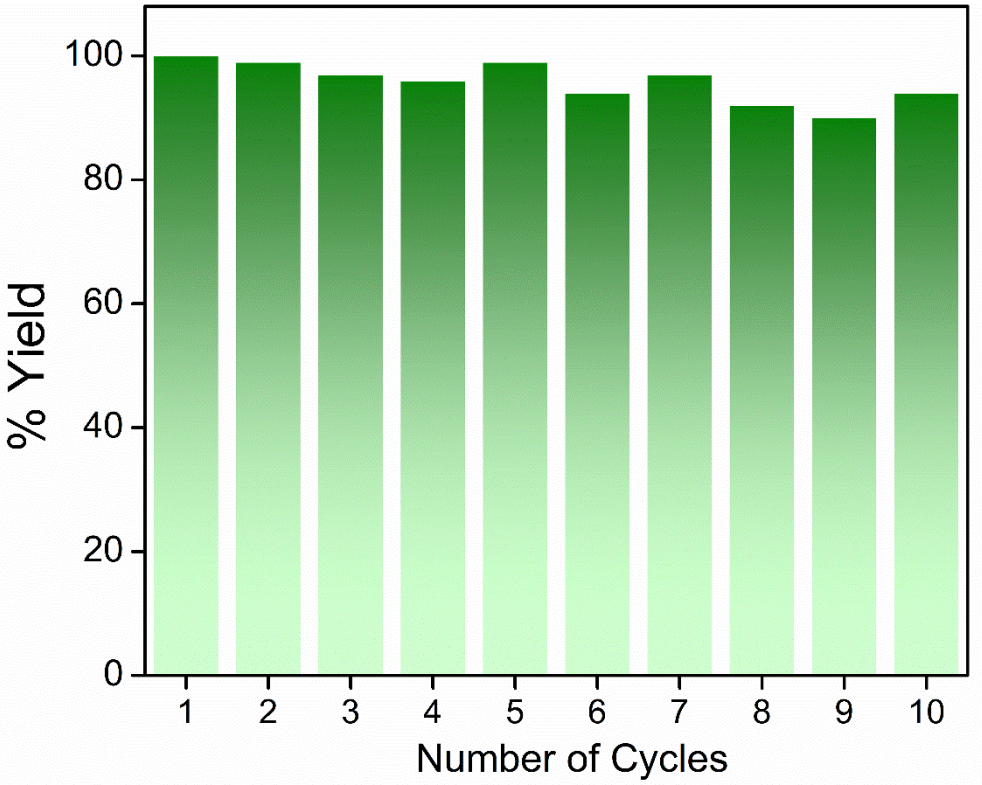

Appendix A46: Recyclability of photocatalytic 4-chlorobenzaldehyde oxidation in MeCN

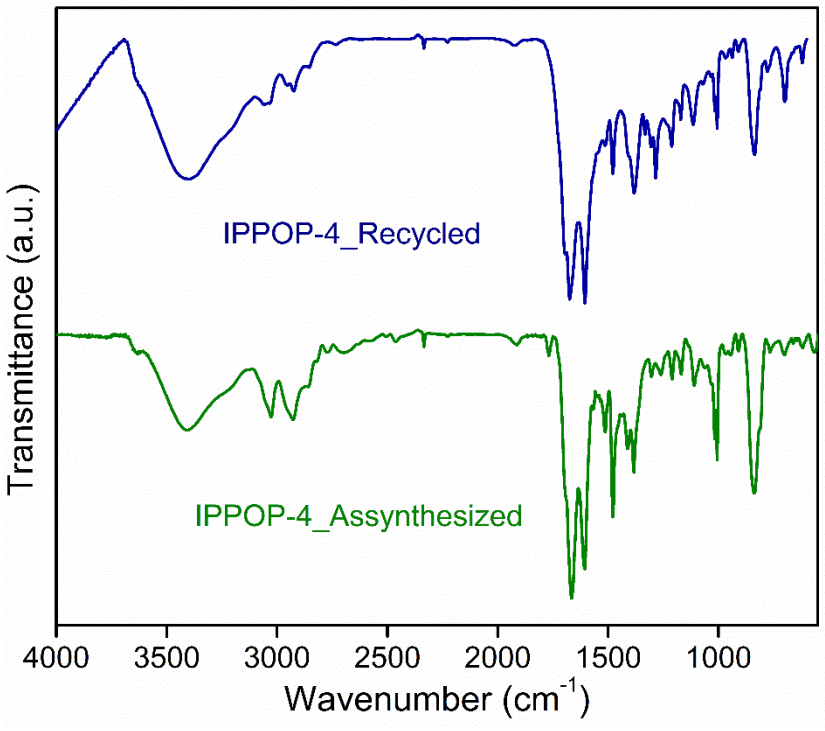

Appendix A47: FT-IR Spectra of IPPOP-4 before and after Catalysis

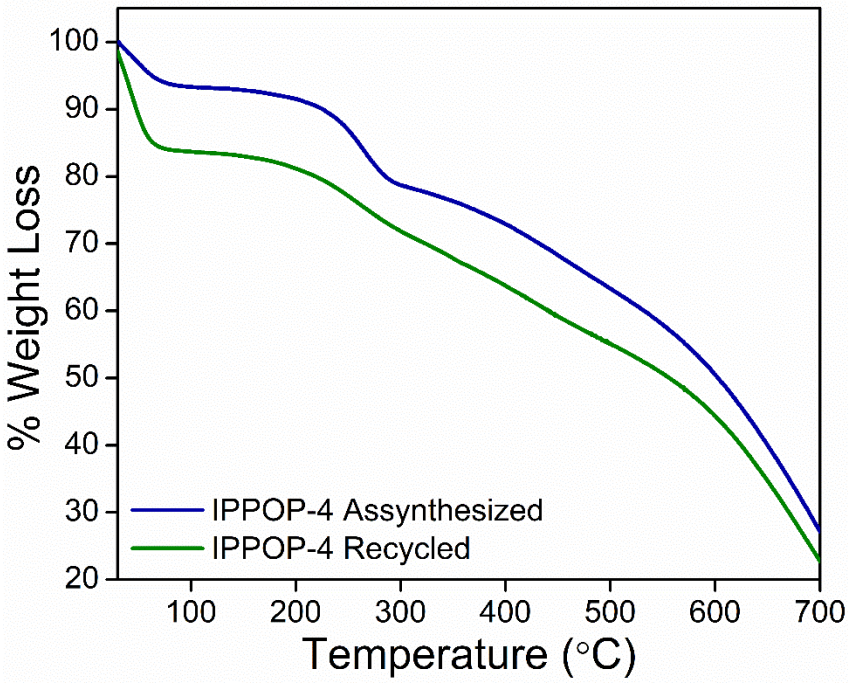

Appendix A48: TGA Spectra of IPPOP-4 before and after Catalysis

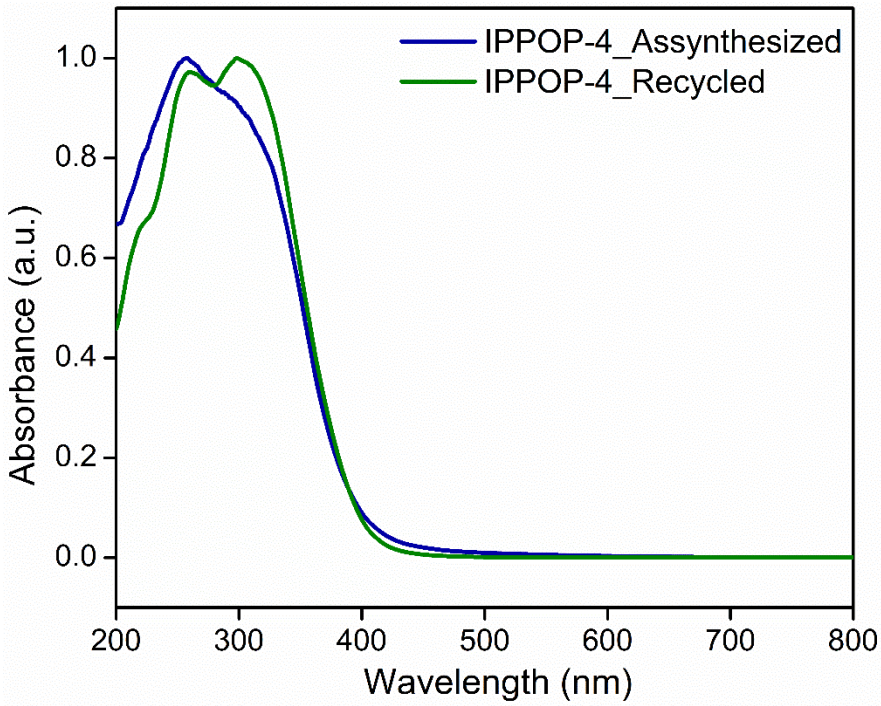

Appendix A49: Solid State UV-Vis Spectra of IPPOP-4 before and after Catalysis

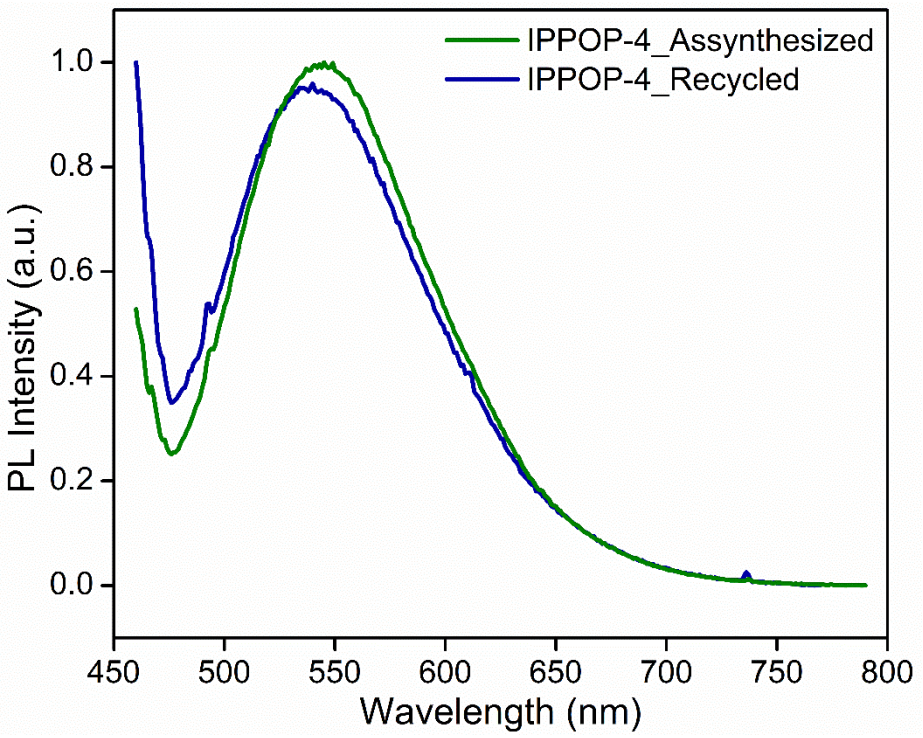

Appendix A50: Solid State PL Spectra of IPPOP-4 before and after Catalysis

5.2. ^{1}H NMR Spectra of Photocatalytic Sulfide Oxidation:

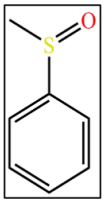

(methylsulfinyl)benzene:
^{1}H-NMR (400 MHz, $CDCl_3$, 25°C, TMS), δ (in ppm): 7.65 (m, 2H, J = 8 Hz, ArH), 7.52 (m, 3H, J = 8 Hz, ArH), 2.73 (s, 3H, Ali-H)

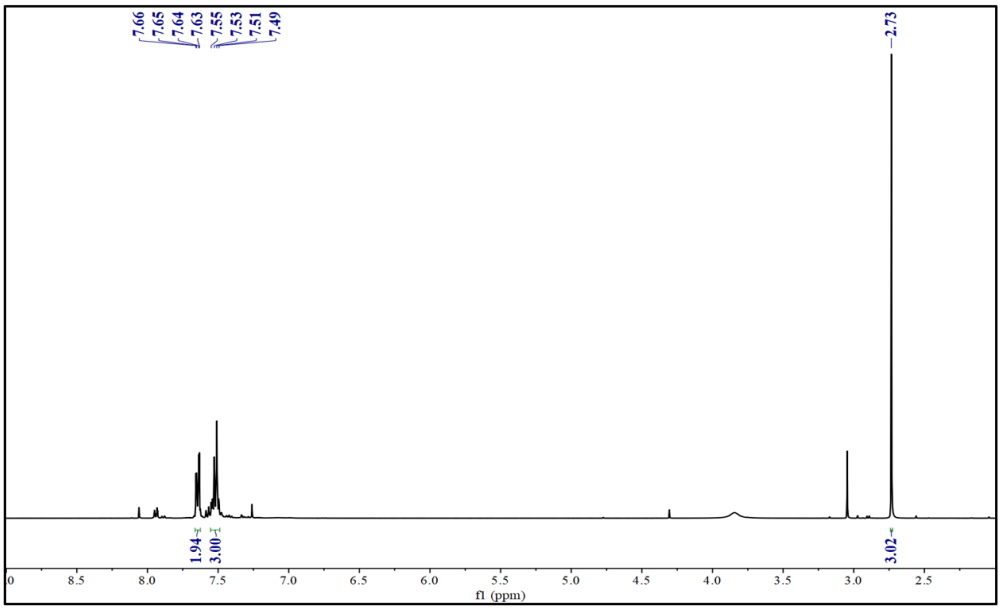

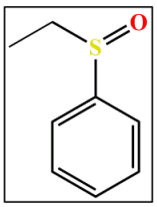

(ethylsulfinyl)benzene:
^{1}H-NMR (400 MHz, $CDCl_3$, 25°C, TMS),
δ (in ppm): 7.60 (d, 2H, J = 8 Hz, ArH), 7.51 (d, 2H, J = 8 Hz, ArH), 2.92 (m, 2H, J = 8 Hz, Ali-H), 1.18 (m, 3H, J = 8 Hz, Ali-H)

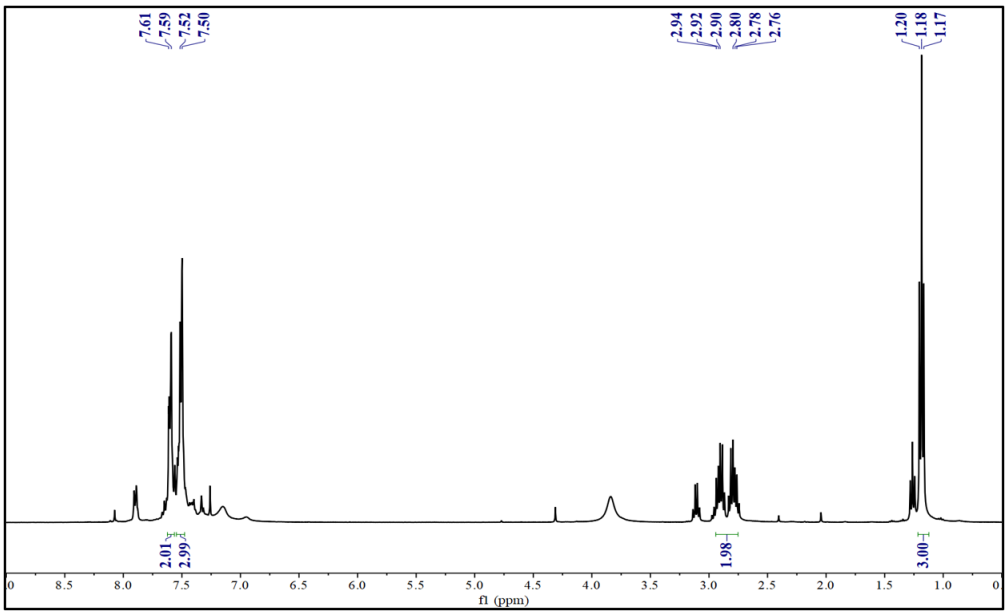

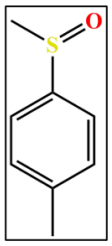

1-methyl-4-(methylsulfinyl)benzene:
^{1}H-NMR (400 MHz, $CDCl_3$, 25°C, TMS),
δ (in ppm): 7.53 (d, 2H, J = 8 Hz, ArH), 7.32 (d, 2H, J = 8 Hz, ArH), 2.71 (s, 3H, Ali-H), 2.40 (s, 3H, Ali-H)

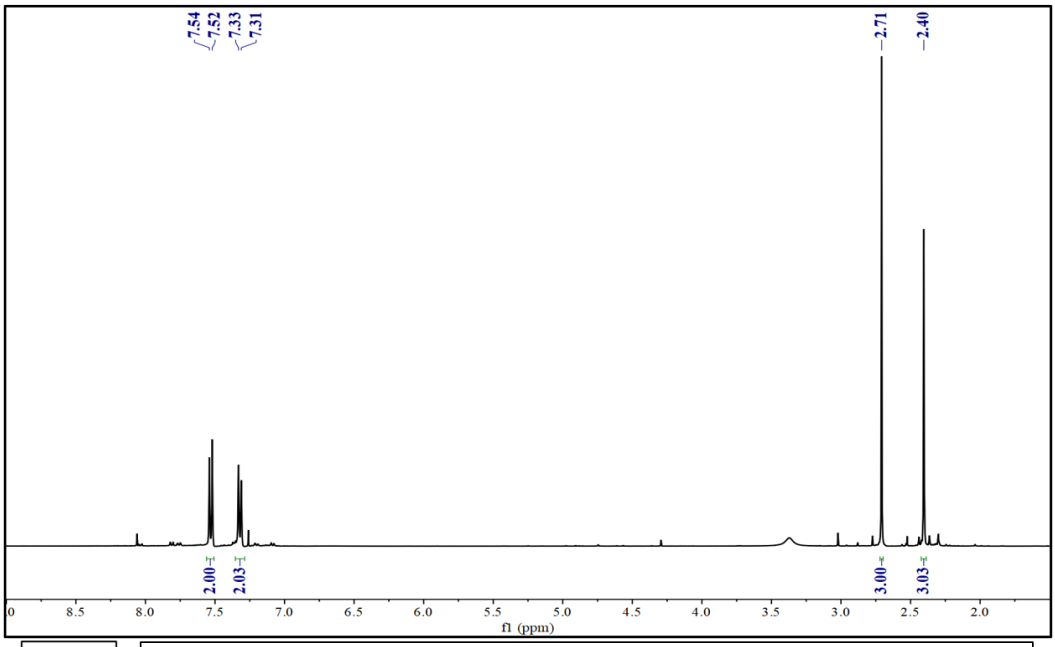

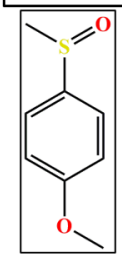

1-methoxy-4-(methylsulfinyl)benzene:
^{1}H-NMR (400 MHz, $CDCl_3$, 25°C, TMS),
δ (in ppm): 7.59 (d, 2H, J = 8 Hz, ArH), 7.01 (d, 2H, J = 8 Hz, ArH), 3.84 (s, 3H, Ali-H), 2.70 (s, 3H, Ali-H)

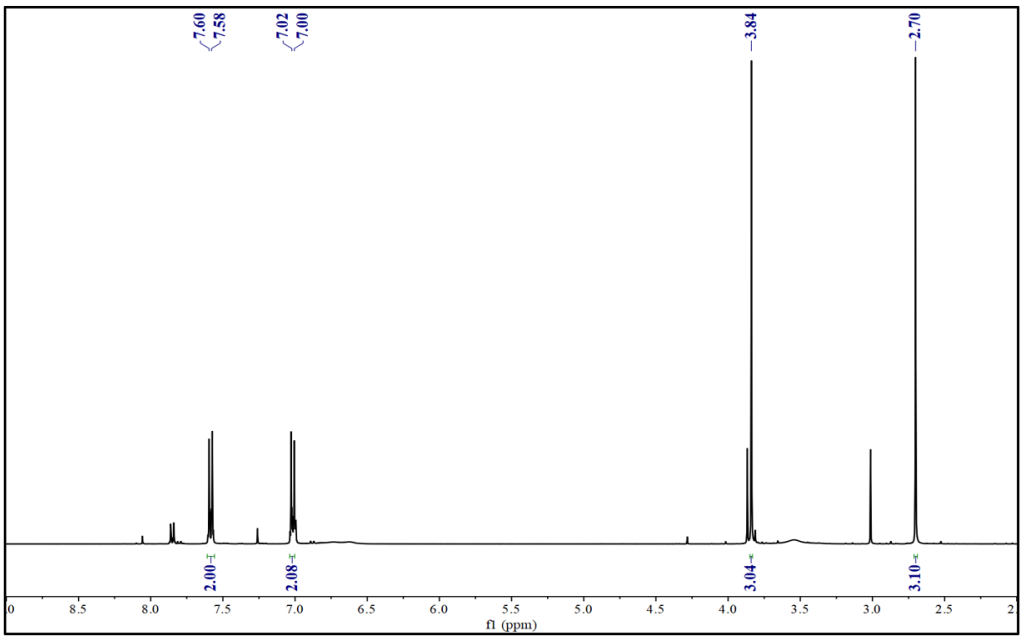

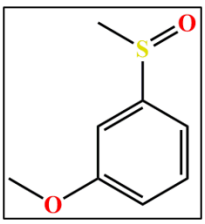

1-methoxy-3-(methylsulfinyl)benzene:
^{1}H-NMR (400 MHz, $CDCl_3$, 25°C, TMS), δ (in ppm): 7.42 (m, 1H, J = 8 Hz, ArH), 7.26 (m, 1H, J = 8 Hz, ArH), 7.14 (m, 1H, J= 8 Hz, ArH), 7.02 (m, 1H, J= 8 Hz, ArH), 3.87 (s, 3H, Ali-H), 2.74 (s, 3H, Ali-H)

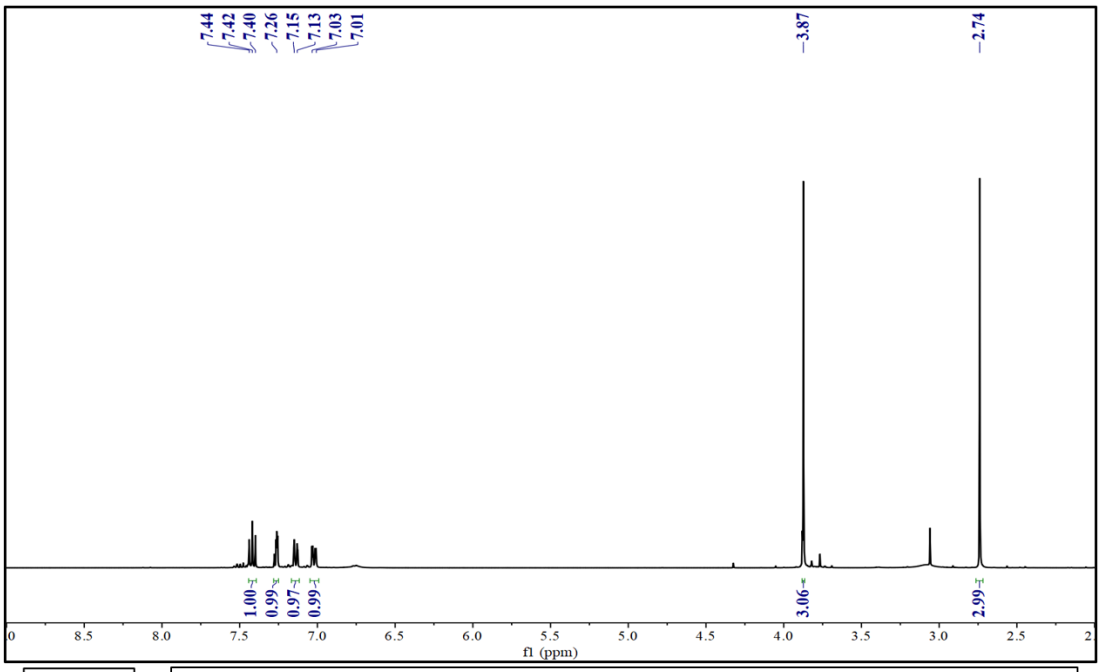

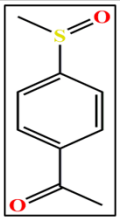

1-(4-(methylsulfinyl)phenyl)ethan-1-one:
^{1}H-NMR (400 MHz, $CDCl_3$, 25°C, TMS),
δ (in ppm): 8.09 (d, 2H, J = 8 Hz, ArH), 7.74 (d, 2H, J = 8 Hz, ArH), 2.76 (s, 3H, Ali-H), 2.64 (s, 3H, Ali-H)

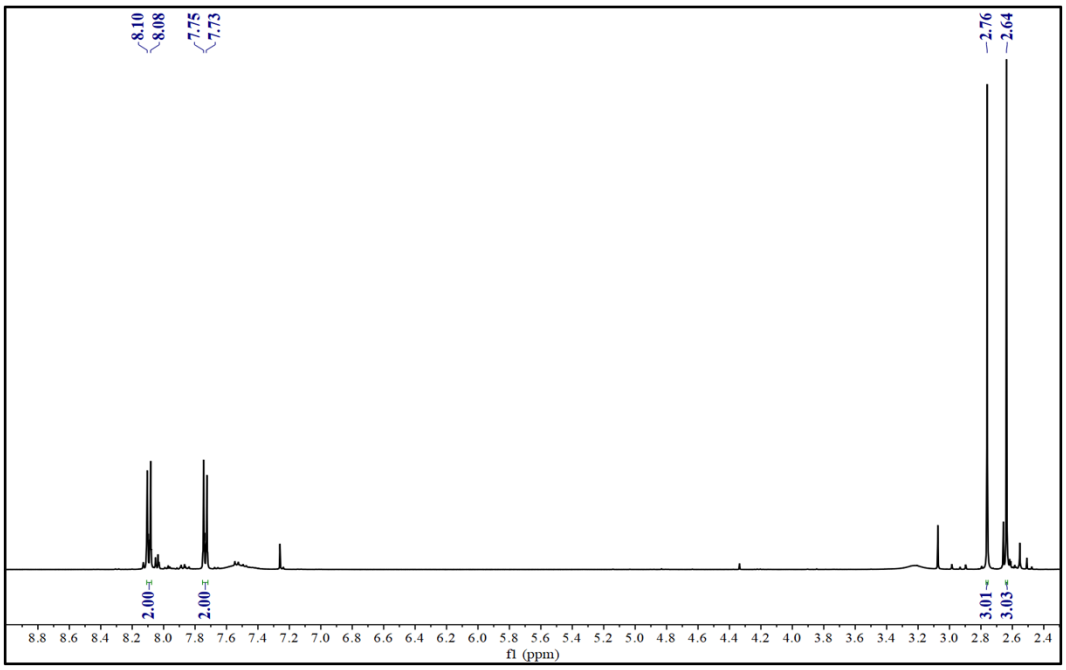

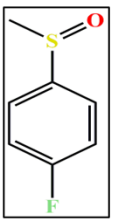

1-fluoro-4-(methylsulfinyl)benzene :
^{1}H-NMR (400 MHz, $CDCl_3$, 25°C, TMS),
δ (in ppm): 7.65 (d, 2H, J = 8 Hz, ArH), 7.22 (d, 2H, J = 8 Hz, ArH), 2.72 (s, 3H, Ali-H)

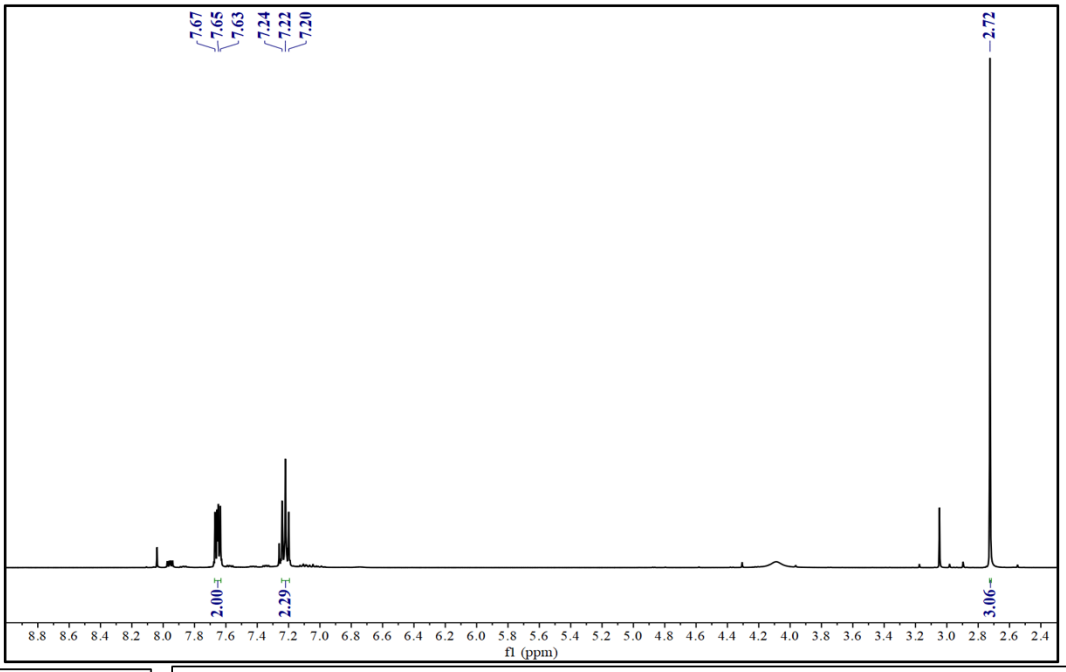

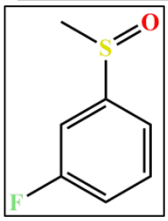

1-fluoro-3-(methylsulfinyl)benzene:
^{1}H-NMR (400 MHz, $CDCl_3$, 25°C, TMS),
δ (in ppm): 7.51 (m, 1H, J = 8 Hz, ArH), 7.40 (m, 2H, J = 8 Hz, ArH), 7.19 (m, 1H, J = 8 Hz , ArH), 2.75 (s, 1H, Ali-H)

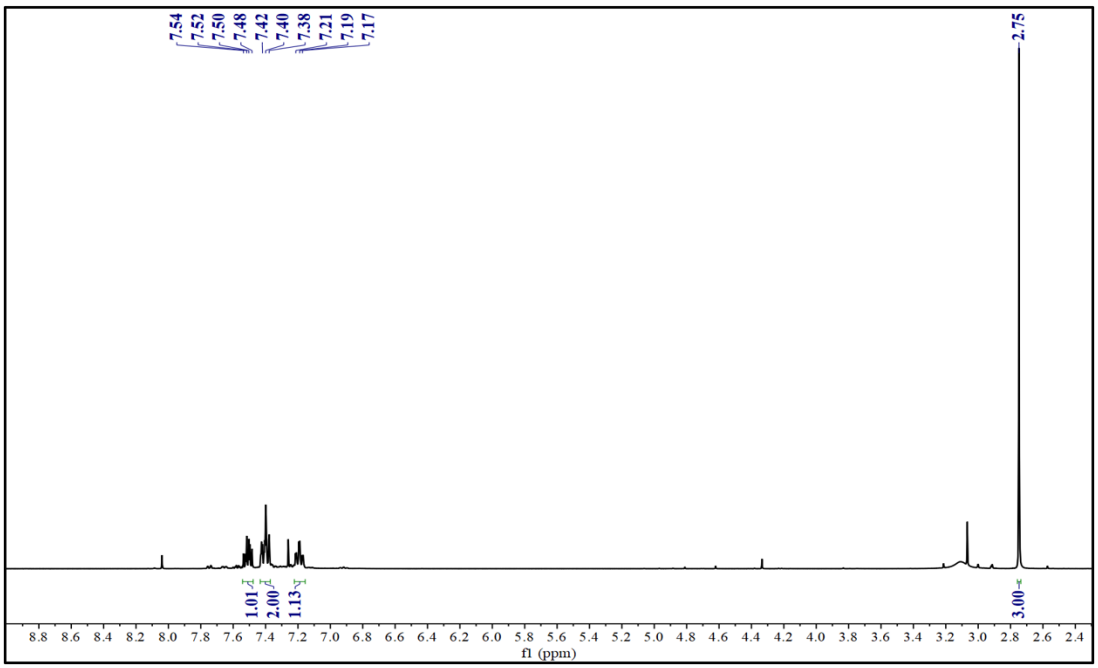

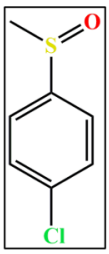

1-chloro-4-(methylsulfinyl)benzene:
^{1}H-NMR (400 MHz, $CDCl_3$, 25°C, TMS),
δ (in ppm): 7.59 (d, 2H, J = 8 Hz, ArH), 7.50 (d, 2H, J = 8 Hz, ArH), 2.72 (s, 3H, Ali-H)

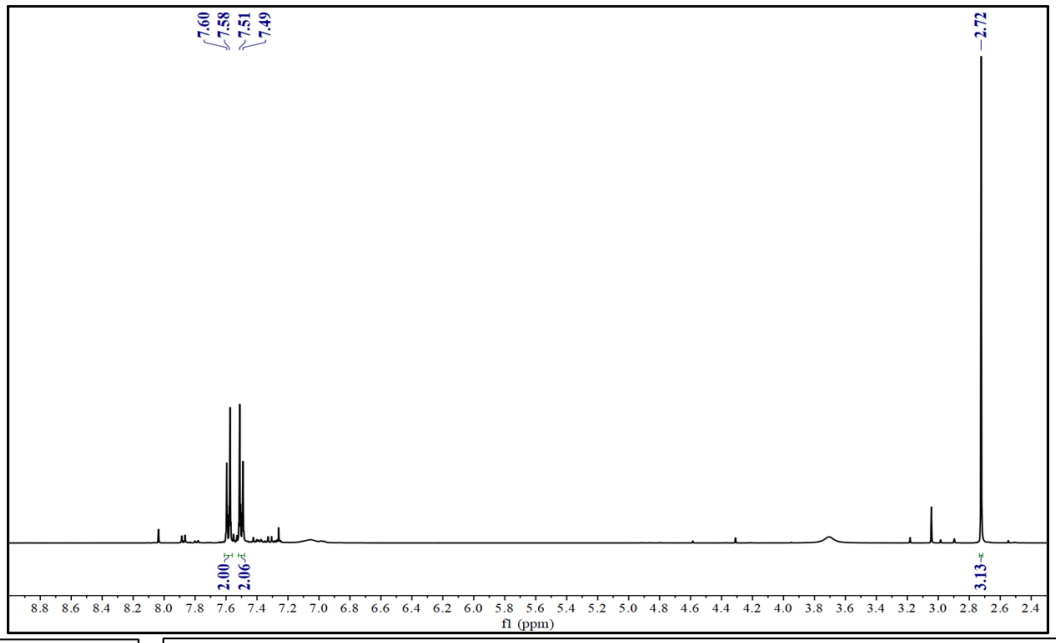

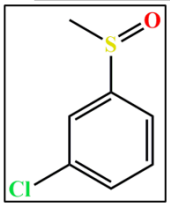

1-chloro-3-(methylsulfinyl)benzene:
^{1}H-NMR (400 MHz, $CDCl_3$, 25°C, TMS), δ (in ppm): 7.66 (s, 1H, ArH), 7.47 (m, 3H, J = 8 Hz, ArH), 2.74 (s, 3H, Ali-H)

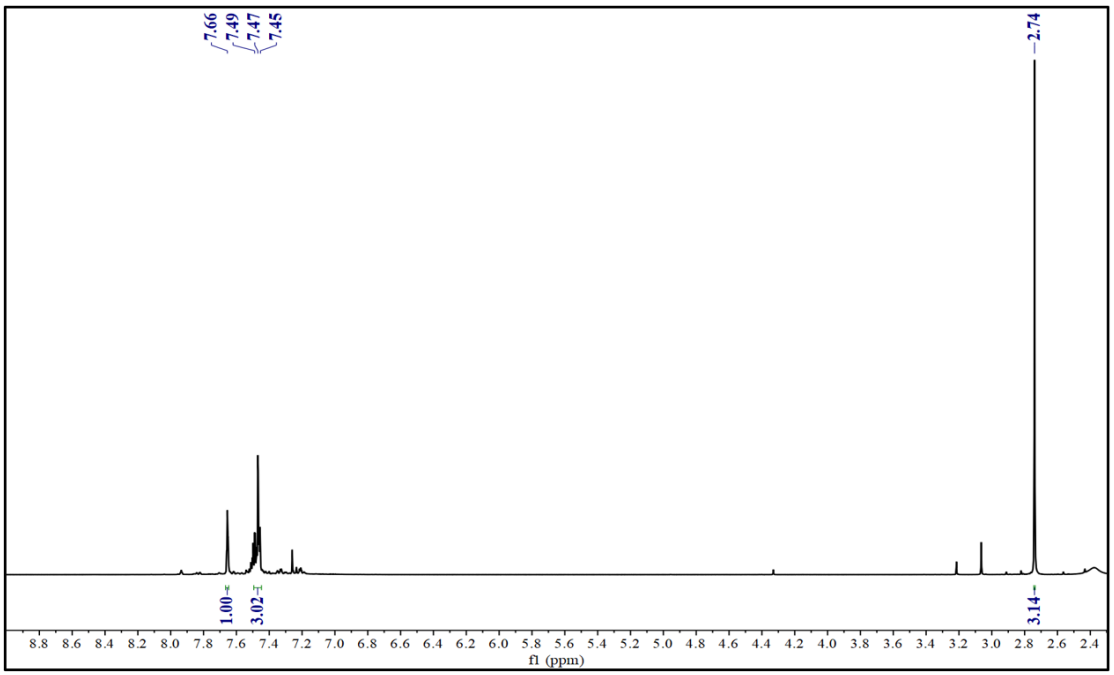

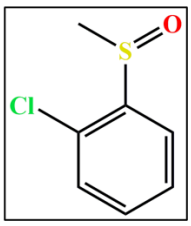

1-chloro-2-(methylsulfinyl)benzene :
^{1}H-NMR (400 MHz, $CDCl_3$, 25°C, TMS),
δ (in ppm): 7.96 (d, 1H, J = 8 Hz, ArH), 7.55 (m, 1H, J = 8 Hz, ArH), 7.46 (m, 1H, J = 8 Hz, ArH), 7.41 (m, 1H, J = 8 Hz, ArH), 2.85 (s, 1H, Ali-H)

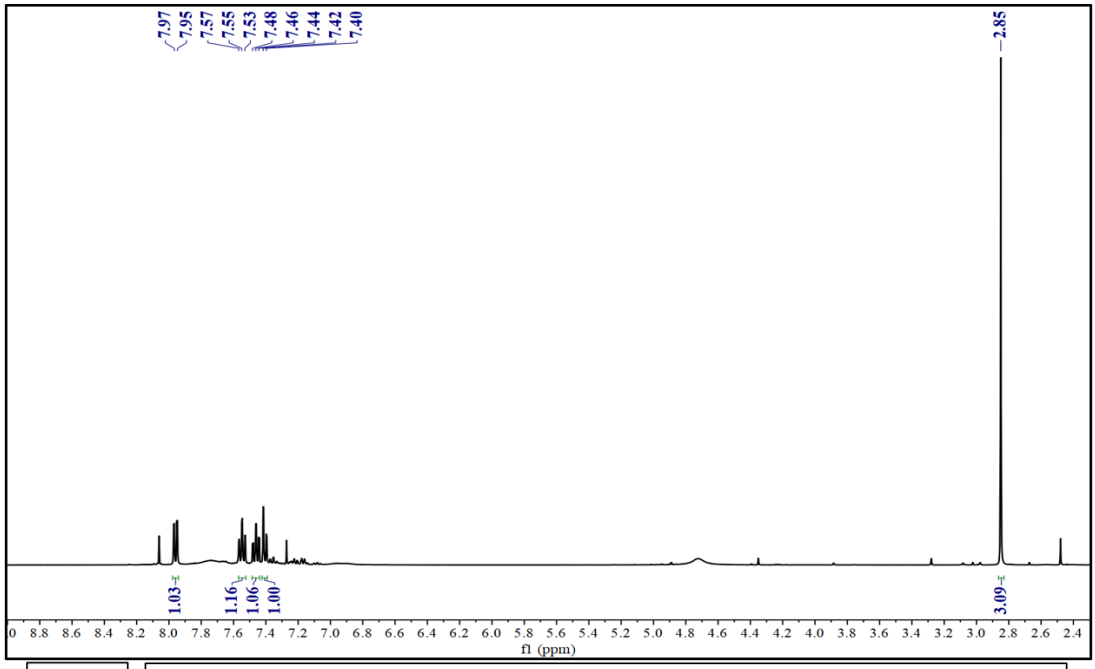

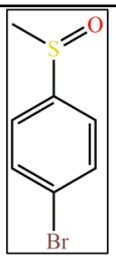

1-bromo-4-(methylsulfinyl)benzene:
^{1}H-NMR (400 MHz, $CDCl_3$, 25°C, TMS),
δ (in ppm): 7.66 (d, 2H, J = 8 Hz, ArH), 7.51 (d, 2H, J = 8 Hz, ArH), 2.72 (s, 3H, Ali-H)

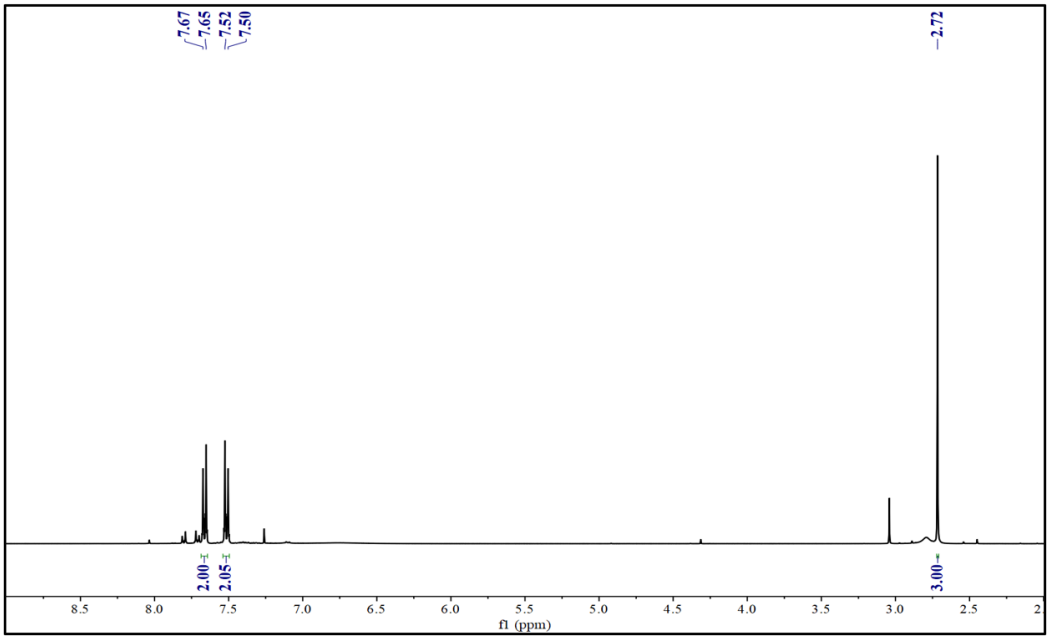

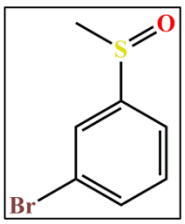

1-bromo-3-(methylsulfinyl)benzene :
^{1}H-NMR (400 MHz, $CDCl_3$, 25°C, TMS),
δ (in ppm): 7.80 (m, 1H, J = 8 Hz, ArH), 7.62 (m, 1H, J = 8 Hz, ArH), 7.54 (m, 1H, J = 8 Hz, ArH), 7.39 (m, 1H, J = 8 Hz , ArH), 2.74 (s, 3H, Ali-H)

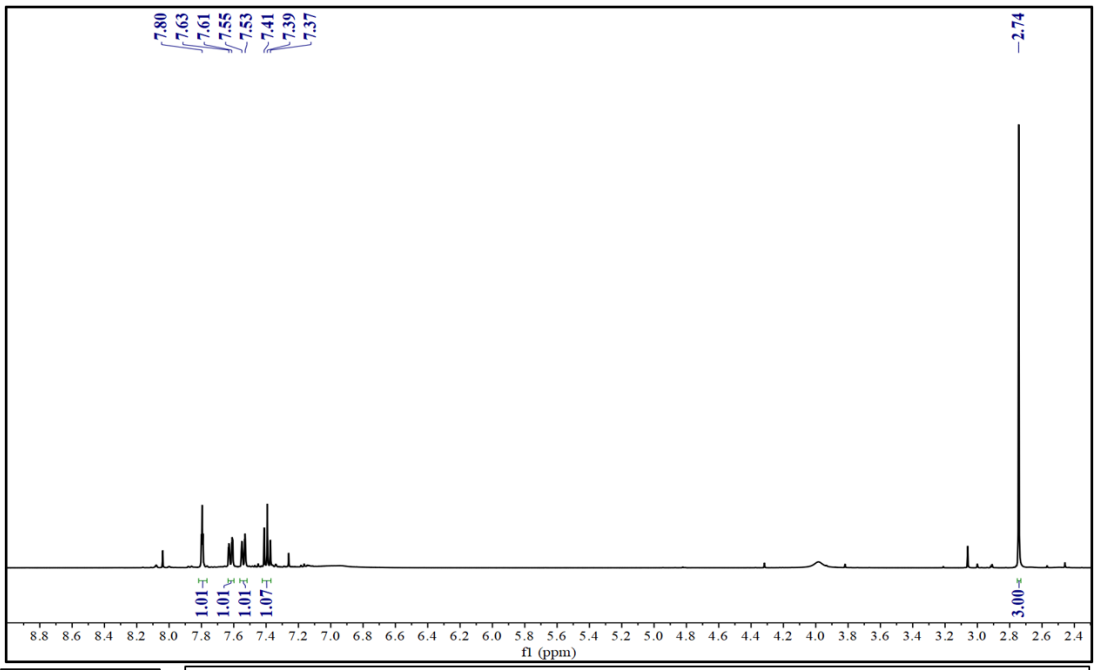

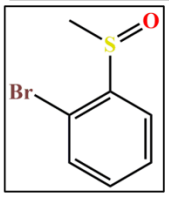

1-bromo-2-(methylsulfinyl)benzene:
^{1}H-NMR (400 MHz, $CDCl_3$, 25°C, TMS), δ (in ppm): 7.94 (d, 1H, J = 8 Hz, ArH), 7.59 (m, 1H, J = 8 Hz, ArH), 7.56 (m, 1H, J= 8 Hz, ArH), 7.37 (m, 1H, J= 8 Hz, ArH) 2.82 (s, 3H, Ali-H)

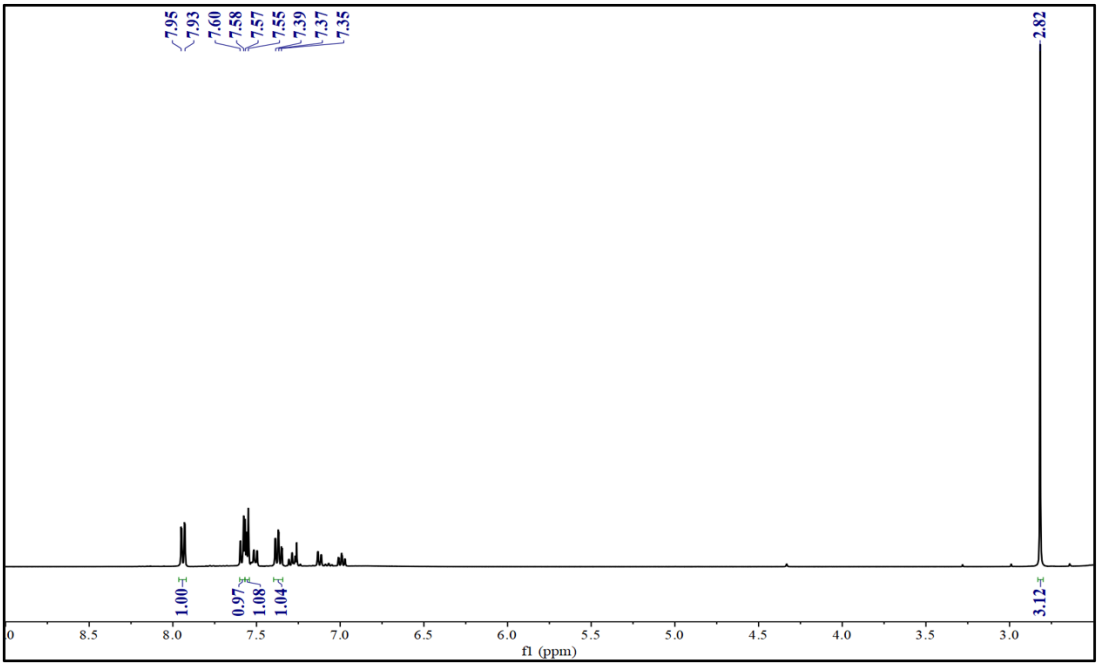

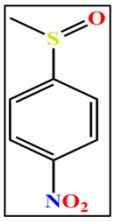

1-(methylsulfinyl)-4-nitrobenzene:
^{1}H-NMR (400 MHz, $CDCl_3$, 25°C, TMS),
δ (in ppm): 8.40 (d, 2H, J = 8 Hz, ArH), 7.84 (d, 2H, J = 8 Hz, ArH), 2.80 (s, 3H, Ali-H)

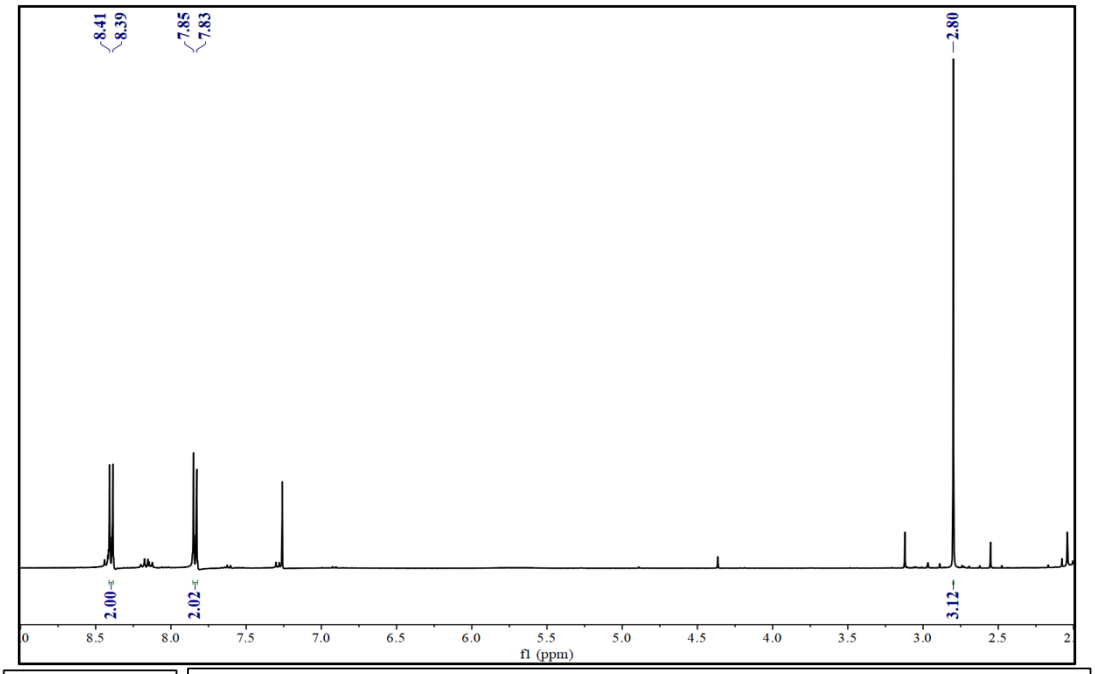

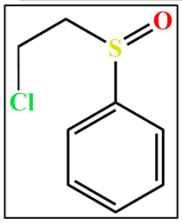

((2-chloroethyl)sulfinyl)benzene:
^{1}H-NMR (400 MHz, $CDCl_3$, 25°C, TMS),
δ (in ppm): 7.64 (m, 2H, J = 8 Hz, ArH), 7.54 (m, 2H, J = 8 Hz, ArH), 3.96 (m, 2H, J= 8 Hz, Ali-H), 3.66 (m, 2H, J = 8 Hz, Ali-H) (s, 1H, Ali-H)

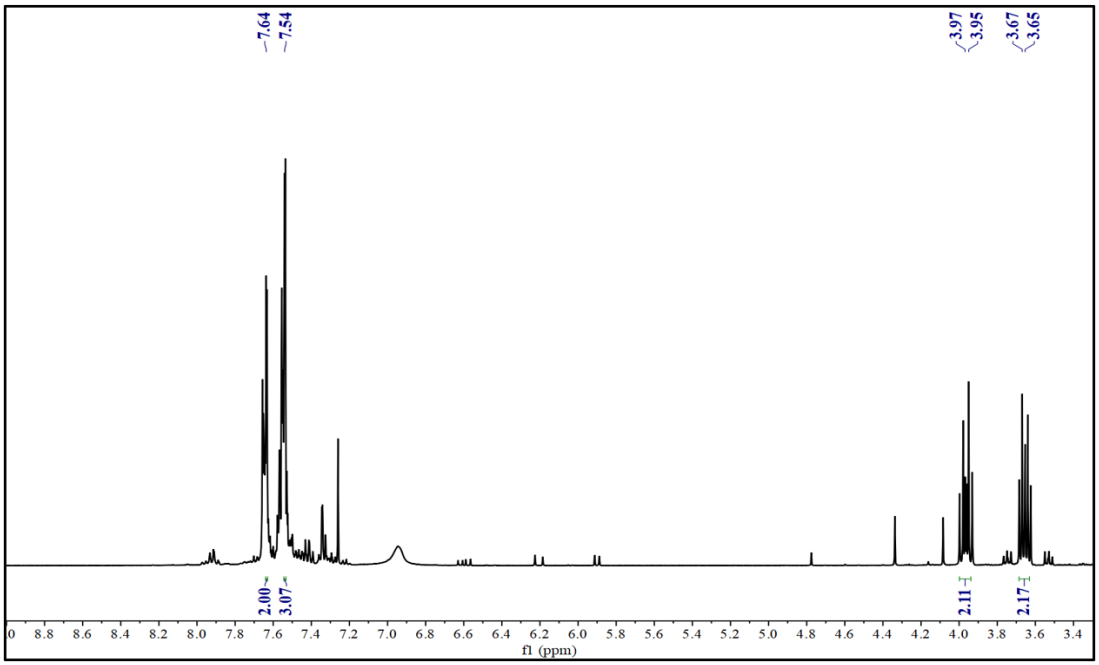

5.3. ^{1}H NMR Spectra of Photocatalytic Aldehyde Oxidation:

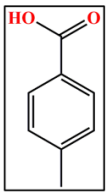

4-methylbenzoic acid : ^{1}H-NMR (400 MHz, $CDCl_3$, 25°C, TMS), δ (in ppm): 8.01 (d, 2H, J = 8 Hz, ArH), 7.28 (d, 2H, J = 8 Hz, ArH), 2.43 (s, 3H, Ali-H)

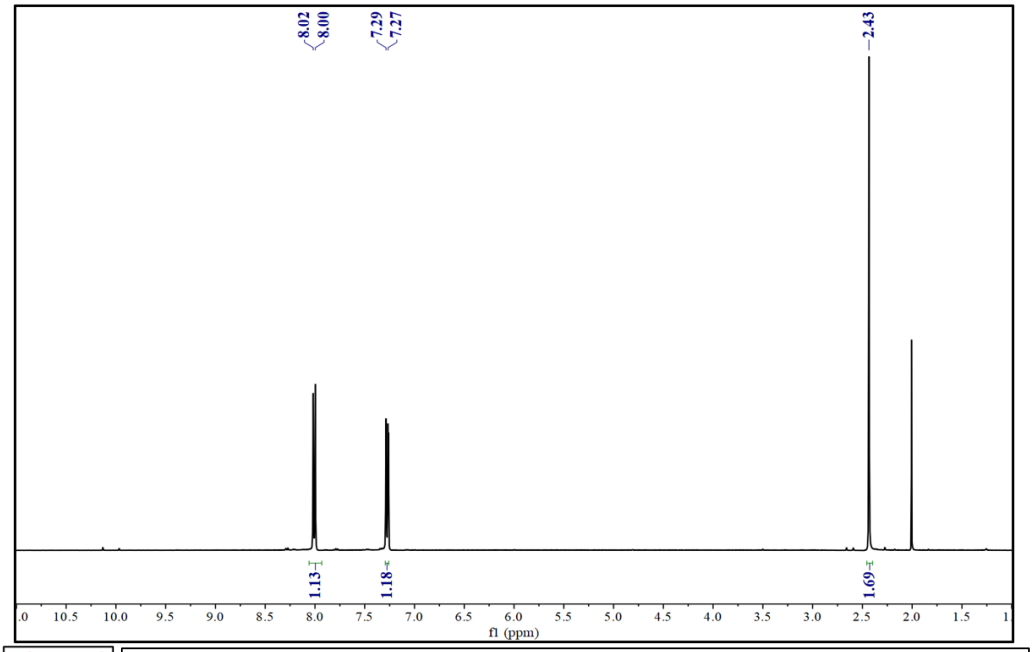

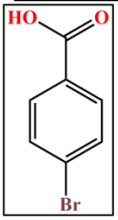

4-bromobenzoic acid : ^{1}H-NMR (400 MHz, $CDCl_3$, 25°C, TMS), δ (in ppm): 7.95 (d, 2H, J = 8 Hz, ArH), 7.63 (d, 2H, J = 8 Hz, ArH)

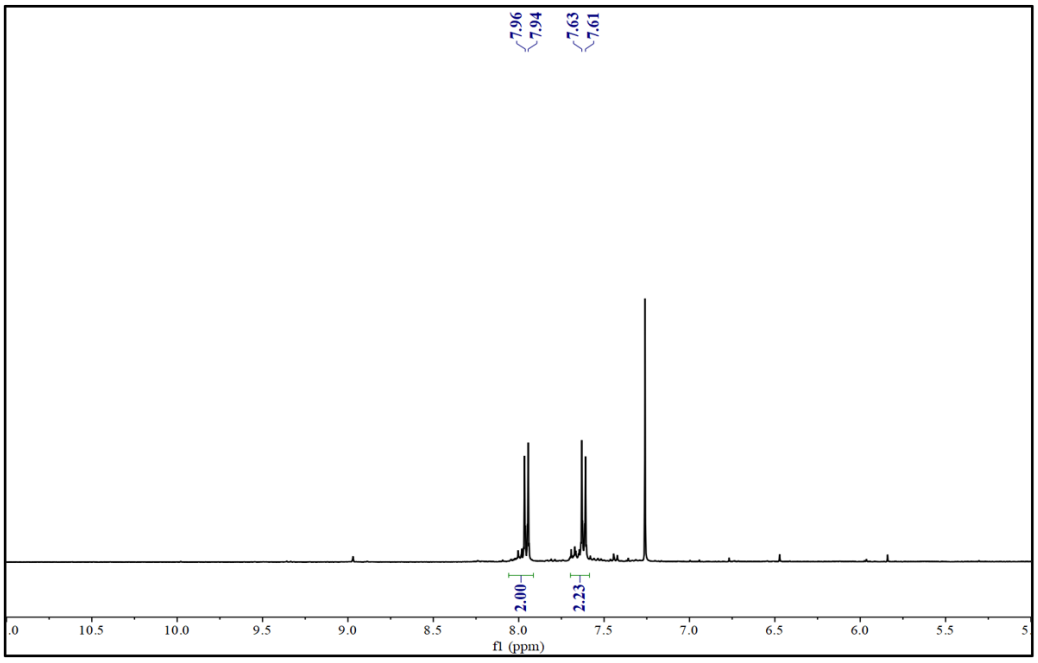

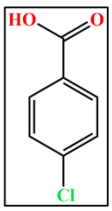

4-chlorobenzoic acid : ^{1}H-NMR (400 MHz, MeOD-d^{4}, 25°C, TMS), δ (in ppm): 8.00 (d, 2H, J = 8 Hz, ArH), 7.48 (d, 2H, J = 8 Hz, ArH)

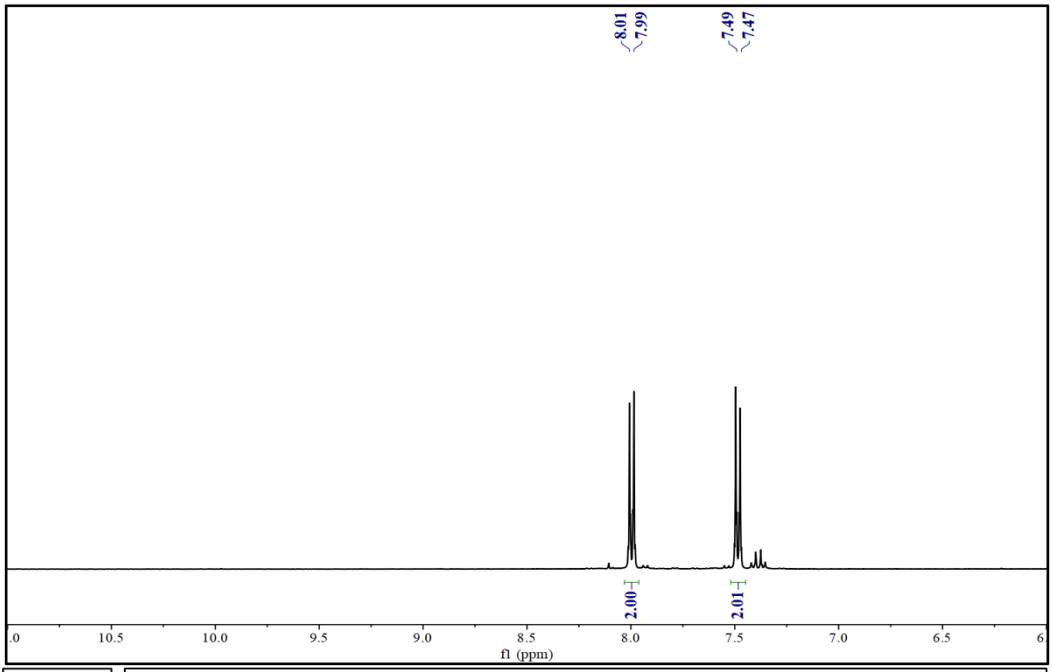

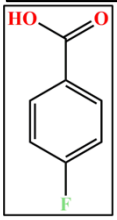

4-fluorobenzoic acid : ^{1}H-NMR (400 MHz, MeOD-d^{4}, 25°C, TMS), δ (in ppm): 7.99 (d, 2H, J = 8 Hz, ArH), 7.00 (d, 2H, J = 8 Hz, ArH)

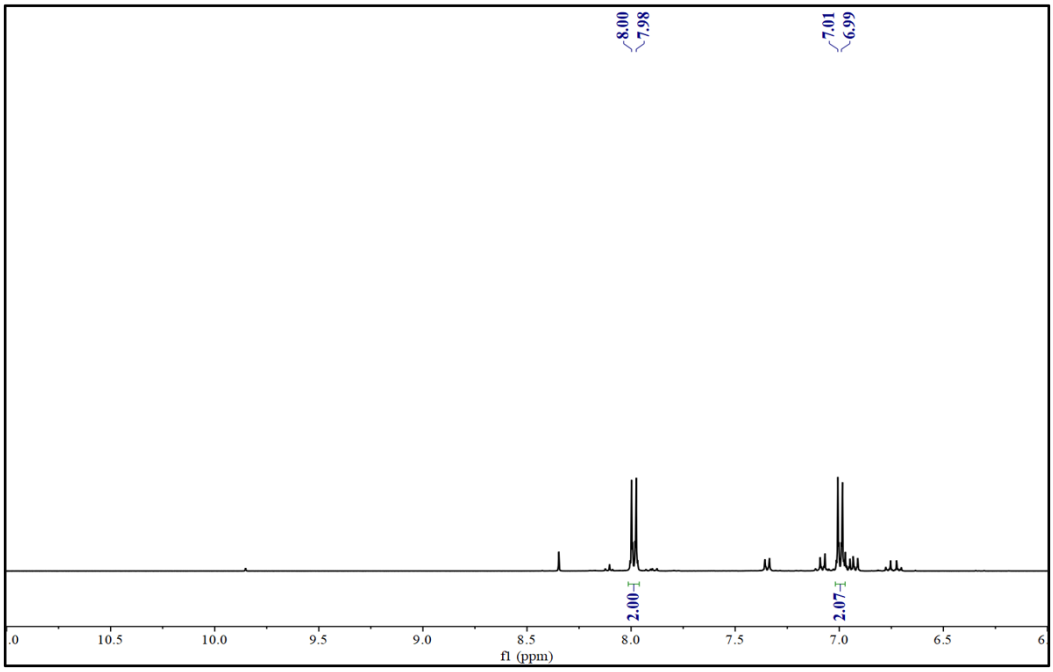

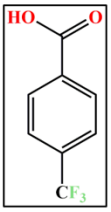

4-(trifluoromethyl)benzoic acid : ^{1}H-NMR (400 MHz, MeOD-d^{4}, 25°C, TMS), δ (in ppm): 8.23 (d, 2H, J = 8 Hz, ArH), 7.86 (d, 2H, J = 8 Hz, ArH)

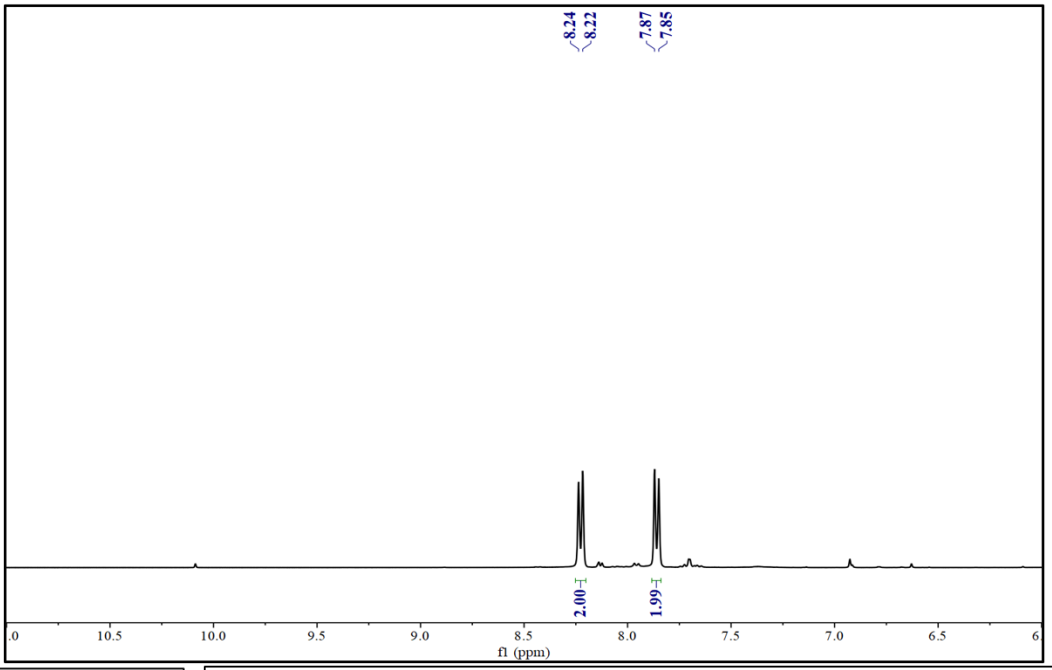

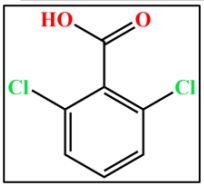

2,6-dichlorobenzoic acid : ^{1}H-NMR (400 MHz, MeOD-d^{4}, 25°C, TMS), δ (in ppm): 7.42 (m, 2H, J = 8 Hz, ArH), 7.38 (m, 1H, J = 8 Hz, ArH)

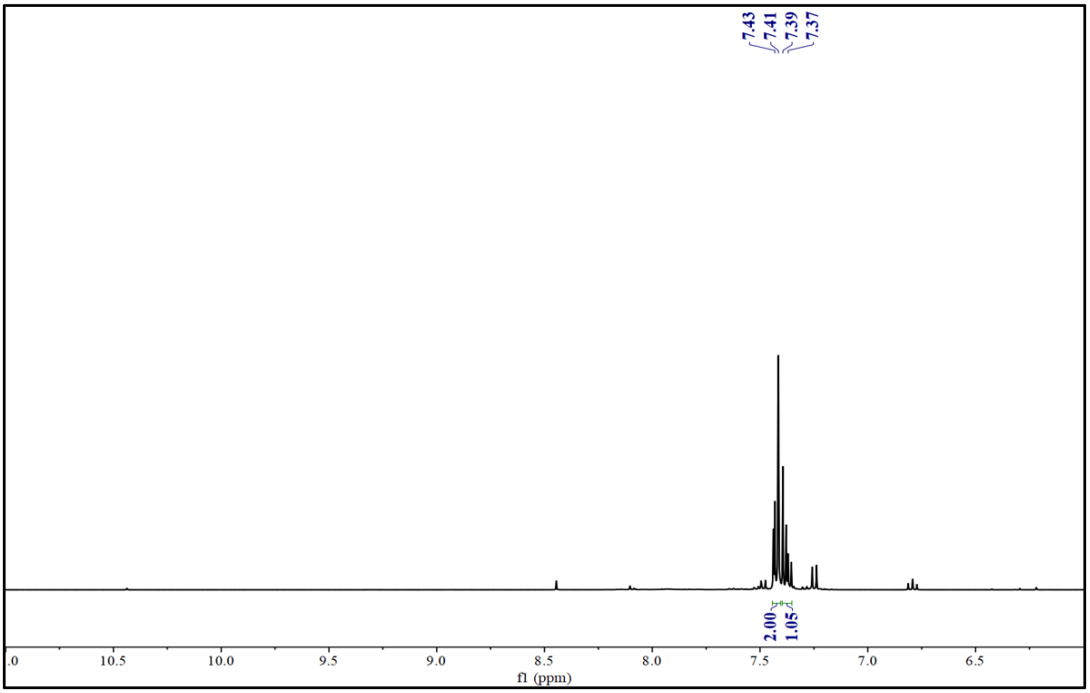

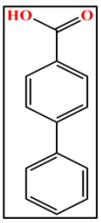

[1,1'-biphenyl]-4-carboxylic acid : ^{1}H-NMR (400 MHz, MeOD-d^4, 25°C, TMS), δ (in ppm): 7.63 (d, 2H, J = 8 Hz, ArH), 7.51 (m, 2H, J = 8 Hz, ArH), 7.46 (m, 2H, J= 8 Hz, ArH), 7.43 (m, 3H, J= 8Hz, ArH)

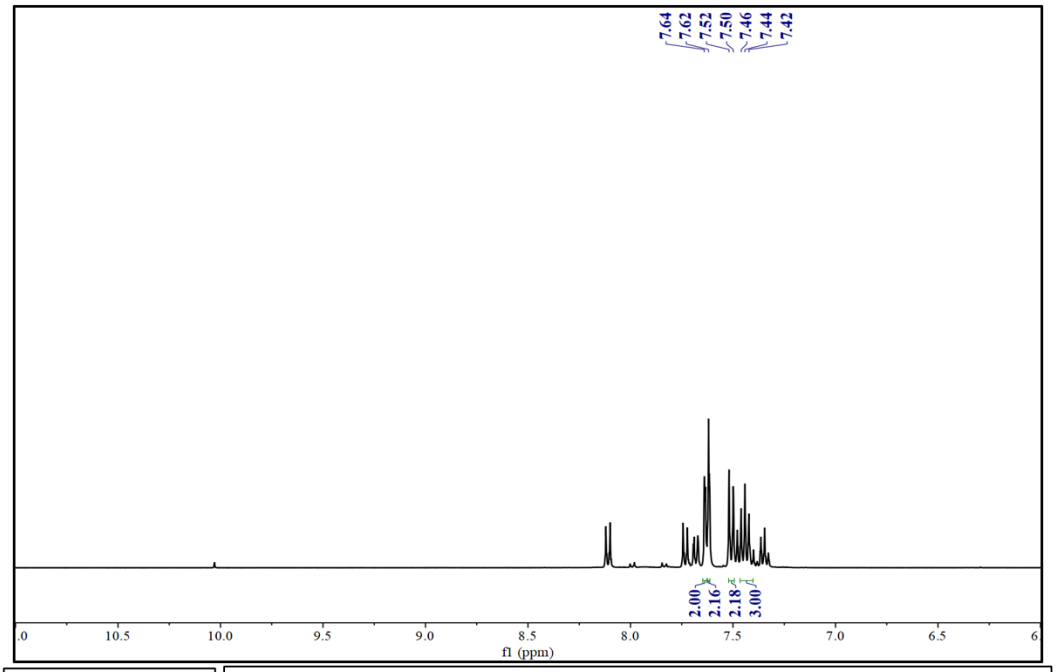

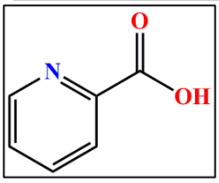

Pyridine-2-carboxylic acid : ^{1}H-NMR (400 MHz, MeOD-d^4, 25°C, TMS), δ (in ppm): 8.70 (d, 1H, J = 8 Hz, ArH), 8.22 (d, 1H, J = 8 Hz, ArH), 8.09 (m, 1H, J= 8 Hz, ArH), 7.70 (m, 1H, J= 8 Hz, ArH)

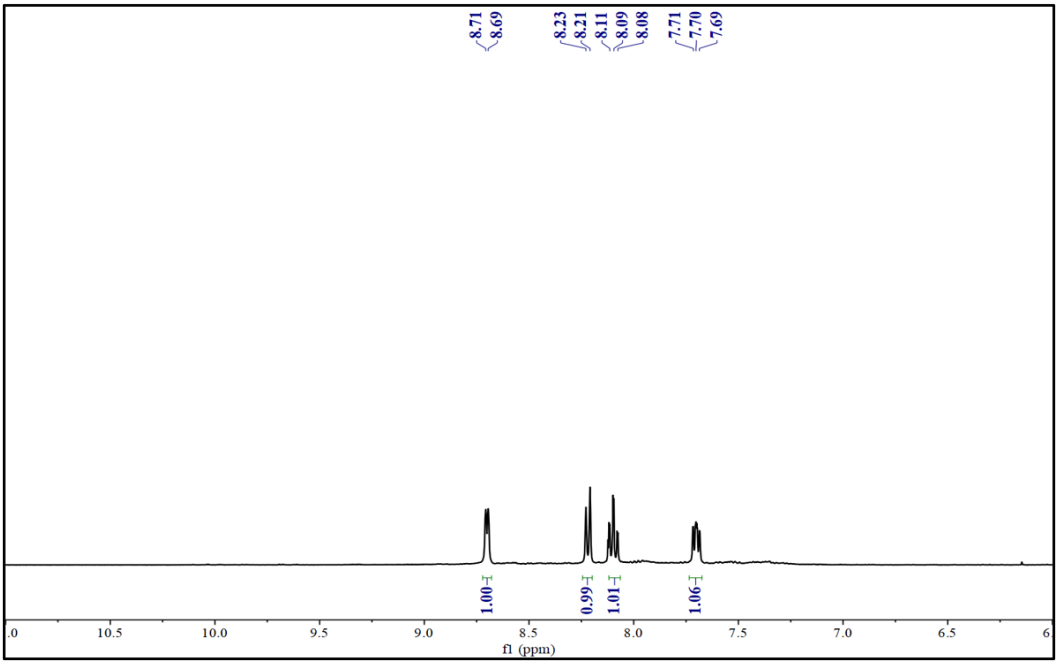

REFERENCES

1. K. Ganesan, S. K. Raza, R. Vijayaraghavan. J Pharm Bioallied Sci. 2010 Jul;2(3):166-78.
2. a) Y. J. Jang, K. Kim, O. G. Tsay, D. A. Atwood, D. G. Churchill, Chem. Rev. 2015, 115, PR1–PR76; b) T. Islamoglu, Z. Chen, M. C. Wasson, C. T. Buru, K. O. Kirlikovali, U. Afrin, M. R. Mian, O. K. Farha, Chem. Rev. 2020, 120, 8130–8160; c) K. Kehe, L. Szinicz. Toxicology 2005, 214, 198−209; d) K. G. Davis, G. Aspera. Ann. Emerg. Med. 2001, 37, 653−656; e) E. Tahmasbpour, S. Reza Emami, M. Ghanei, Y. Panahi. Inhal. Toxicol. 2015, 27, 659−672.
3. H. Li, R. Muir, N. R. McFarlane, R. J. Soilleux, X. Yu, I. P. Thompson, S. A. Jackman; Biodegradation 2013, 24, 125– 135, DOI: 10.1007/s10532-012-9564-7.
4. G. W. Wagner, O. B. Koper, E. Lucas, S. Decker, K. J. Klabunde; J. Phys. Chem. B 2000, 104, 5118– 5123, DOI: 10.1021/jp000101j.
5. a) H. Kim, J. Shin, D. W. Kang, Y. Kim, J. H. Kim, M. Kang, J. H. Choe, S. Park, J. S. Kim, and C. S. Hong. Cell Reports Physical Science 3, 100888, May 18, 2022. b) J. H. Kim, H. Yun, D. W. Kang, J. Shin, M. Kang, N. Singh, J. E. Jeong, C. S. Hong, and J. S. Kim. Matter 4, 3774–3785.
6. a) Y. Liu, A.J. Howarth, J.T. Hupp, and O.K. Farha; Angew. Chem. Int. Ed. 54, 9001–9005. https://doi.org/ 10.1002/anie.201503741. b) A. Atilgan, M.M. Cetin, J. Yu, Y. Beldjoudi, J. Liu, C.L. Stern, F.M. Cetin, T. Islamoglu, O.K. Farha, P. J. Deria; J. Am. Chem. Soc. 142, 18554–18564. https://doi.org/10.1021/jacs.0c07784.
7. M.C. DeRosa, and R.J. Crutchley; Coordination Chemistry Reviews 233-234 (2002) 351-371.
8. a) A. Atilgan, T. Islamoglu, A. J. Howarth, J. T. Hupp, and O. K. Farha. ACS Appl. Mater. Interfaces 2017, 9, 29, 24555–24560; b) A. J. Howarth, C. T. Buru, Y. Liu, A. M. Ploskonka, K. J. Hartlieb, M. McEntee, J. J. Mahle, J. H. Buchanan, E. M. Durke, S. S. Al-Juaid, J. F. Stoddart, J. B. DeCoste, J. T. Hupp, O. K. Farha. Chem. Eur. J. 2017, 23, 214–218; c) M. Cao, R. Pang, Q.Y. Wang, Z. Han, Z.Y. Wang, X.Y. Dong, S.F. Li, S.Q. Zang, and T.C.W. Mak. J. Am. Chem. Soc. 2019, 141, 14505–14509; d) Y. Beldjoudi, A. Atilgan, J.A. Weber, I. Roy, R.M. Young, J. Yu, P. Deria, A.E. Enciso, M.R. Wasielewski, J.T. Hupp, and J.F. Stoddart. Adv. Mater. 2020, 32, 2001592.

9. M. M. Wu, J. Su, D. Luo, B. C. Cai, Z. L. Zheng, D. S. Bin, Y. Y. Li, X. P. Zhou. Small, 2023, 19, 2301050.
10. A. Atilgan, T. Islamoglu, A. J. Howarth, J. T. Hupp, and O. K. Farha. ACS Appl. Mater. Interfaces 2017, 9, 29, 24555–24560.
11. a) L. Zhang, C. Sun, S. J. Xiao, Q. G. Tan, G. P. Yang, J. Q. Fan, Y. T. Luo, R. P. Liang, and J. D. Qiu. ACS Appl. Nano Mater. 2023, 6, 18, 17083–17091; b) Q. Y. Wang, J. Liu, M. Cao, J. H. Hu, R. Pang, S. Wang, M. Asad, Y. L. Wei, and S. Q. Zang, Angew. Chem. Int. Ed. 2022, 61, e202207130; c) X. Shena and B. Yan. J. Mater. Chem. A, 2024,12, 6455-6464.
12. a) B. Wang, J. Li, H. Huang, B. Liang, Y. Zhang, L. Chen, K. Tan, Z. Chai, S. Wang, J. T Wright, R. W. Meulenberg, S. Ma. ACS Cent. Sci. 2024, 10, 2, 426–438; b) A. Sen, S. Dutta, G. K. Dam, P. Samanta, S. Let, S. Sharma, M. M. Shirolkar, and S. K. Ghosh. Chem. Eur. J. 2021, 27, 13442-13449; c) S. Let, S. Dutta, P. Samanta, S. Sharma, and S. K. Ghosh. ACS Appl. Mater. Interfaces, 2021, 43, 51474-51484; d) Q. Sun, B. Aguila, Y. Song, and S. Ma, Acc. Chem. Res. 2020, 53, 4, 812–821; e) W. Mandal, S. Fajal, P. Samanta, S. Dutta, M. M. Shirolkar, Y. D. More, and S. K. Ghosh ACS Appl. Polym. Mater. 2022, 4, 11, 8633-8644.S
13. a) P. Zhang, S. Wang, S. Ma, F. S. Xiao, and Q. Sun. Chem. Commun. 2020, 56, 10631-10641; b) S. Let, G. K. Dam, P. Samanta, S. Fajal, S. Dutta, and S. K. Ghosh. J. Org. Chem. 2022, 87, 24, 16655-16664; c) S. Let, G. K. Dam, S. Fajal, and S. K. Ghosh. Chem. Sci. 2023, 14, 10591-10601; d) S. Kramer, N. R. Bennedsen, and S. Kegnæs, ACS Catal. 2018, 8, 8, 6961–6982; e) G. K. Dam, S. Let, V. Jaiswal, and S. K. Ghosh. ACS Sustainable Chem. Eng. 2024, 12, 8, 3000-3011.
14. a) A. Abid, S. Razzaque, I. Hussain, and B. Tan. Macromolecules, 2021, 54, 12, 5848-5855; b) Y. Cui, Z. Xu, H. Y. Li, D. J. Young, Z. G. Ren, and H. X. Li. ACS Appl. Polym. Mater. 2020, 2, 11, 4512-4520; c) B. Zhang, J. Yan, G. Li, and Z. Wang. Polym. Chem. 2019, 10, 3371-3379; d) Y. Liu, S. Wang, X. Meng, Y. Ye, X. Song, and Z. Liang. Mater. Chem. Front. 2021, 5, 5319-5327; e) M. G. Mohamed, T. C. Chen, and S. W. Kuo. Macromolecules, 2021, 54, 12, 5866-5877.
15. a) M. G. Mohamed, X. Zhang, T. H. Mansoure, A. F. M. El-Mahdy, C. F. Huang, M. Danko, Z. Xin, and S. W. Kuo. Polymer 2020, 205, 122857; b) M. M. Samy,

M. G. Mohamed, A. F. M. El-Mahdy, T. H. Mansoure, K. C. W. Wu, and S. W. Kuo. ACS Appl. Mater. Interfaces 2021, 13, 51906-51916; c) J. Li, Z. Cheng, M. Zhu, A. Thomas, and Y. Liao. ACS Appl. Energy Mater. 2018, 1, 11. 6535-6540; d) S. Bandyopadhyay, C. Singh, P. Jash, M. W. Hussain, A. Paul, and A. Patra. Chem. Commun. 2018, 54, 6796-6799; e) A. F. M. El-Mahdy, Y. H. Hung, T. H. Mansoure, H. H. Yu, T. Chen, and S. W. Kuo. Chem. Asian J. 2019, 14, 1429-1435.

16. a) J. Shin, D. W. Kang, J. H. Lim, J. M. An, Y. Kim, J. H. Kim, M. S. Ji, S. Park, D. Kim, J. Y. Lee, J. S. Kim & C. S. Hong. https://doi.org/10.1038/s41467-023-37156-x b) S. Subramanian, J. Oppenheim, D. Kim, T. S. Nguyen, W.M.H. Silo, B. Kim, W. A. Goddard III, and C. T. Yavuz. Chem 5, 3232–3242, December 12, 2019.
17. a) Y. Liu, C. T. Buru, A. J. Howarth, J. J. Mahle, J. H. Buchanan, J. B. DeCoste, J. T. Hupp, O. K. Farha, J. Mater. Chem. A 2016, 4, 13809–13813; b) C. F. Pereira, Y. Liu, A. Howarth, F. Figueira, J. Rocha, J. T. Hupp, O. K. Farha, J. P. C. Tomé, F. A. Almeida Paz, ACS Appl. Nano Mater. 2019, 2, 465–469; c) Y. Zhi, Z. Yao, W. Jiang, H. Xia, Z. Shi, Y. Mu, X. Liu, ACS Appl. Mater. Interfaces 2019, 11, 37578–37585; d) L. Ma, Y. Liu, Y. Liu, S. Jiang, P. Li, Y. Hao, P. Shao, A. Yin, X. Feng, B. Wang, Angew. Chem. Int. Ed. 2019, 58, 4221–4226; Angew. Chem. 2019, 131, 4265–4270; e) D. A. Giannakoudakis, T. J. Bandosz, ACS Appl. Mater. Interfaces 2020, 12, 14678–14689; f) Y. Hao, B. M. Liu, T. F. Bennett, C. G. Monsour, M. Selke, Y. Liu, J. Phys. Chem. C 2021, 125, 7392–7400; g) S. Goswami, C. E. Miller, J. L. Logsdon, C. T. Buru, Y. L. Wu, D. N. Bowman, T. Islamoglu, A. M. Asiri, C. J. Cramer, M. R. Wasielewski, J. T. Hupp, O. K. Farha, ACS Appl. Mater. Interfaces 2017, 9, 19535–19540; h) C. T. Buru, M. C. Wasson, O. K. Farha, ACS Appl. Nano Mater. 2020, 3, 658–664; i) Z. H. Long, D. Luo, K. Wu, Z. Y. Chen, M. M. Wu, X. P. Zhou, D. Li, ACS Appl. Mater. Interfaces 2021, 13, 37102–37110; j) C. T. Buru, P. Li, B. L. Mehdi, A. Dohnalkova, A. E. Platero-Prats, N. D. Browning, K. W. Chapman, J. T. Hupp, O. K. Farha, Chem. Mater. 2017, 29, 5174–5181; k) C. T. Buru, M. B. Majewski, A. J. Howarth, R. H. Lavroff, C. W. Kung, A. W. Peters, S. Goswami, O. K. Farha, ACS Appl. Mater. Interfaces 2018, 10, 23802–23806; l) R. Gil-San-Millan, E. Lopez-Maya, M. Hall, N. M. Padial, G. W. Peterson, J. B. DeCoste, L. M. Rodriguez-Albelo, J. E. Oltra, E. Barea, J. A. R.

Navarro, ACS Appl. Mater. Interfaces 2017, 9, 23967–23973; m) A. Atilgan, T. Islamoglu, A. J. Howarth, J. T. Hupp, O. K. Farha, ACS Appl. Mater. Interfaces 2017, 9, 24555–24560; n) V. Quezada-Novoa, H. M. Titi, A. A. Sarjeant, A. J. Howarth, Chem. Mater. 2021, 33, 4163–4169; l) D. T. Lee, J. D. Jamir, G. W. Peterson, G. N. Parsons, Matter 2020, 2, 404–415.

18. a) G. Sipos, E. E. Drinkel, R. Dorta. Chem. Soc. Rev. 2015, 44, 3834−3860.; b) E. Wojaczyńska, J. Wojaczyński. Chem. Rev. 2010, 110, 4303−4356.; c) G. L. Smith, J. E. Eyley, X. Han, X. Zhang, J. Li, N. M. Jacques, H. G. W. Godfrey, S. P. Argent, L. J. McCormick McPherson, S. J. Teat, Y. Cheng, M. D. Frogley, G. Cinque, S. J. Day, C. C. Tang, T. L. Easun, S. Rudić, A. J. Ramirez-Cuesta, S. Yang, M. Schröder, Nat. Mater. 2019, 18, 1358−1365.
19. M. R. Tchalala, P. M. Bhatt, K. N. Chappanda, S. R. Tavares, K. Adil, Y. Belmabkhout, A. Shkurenko, A. Cadiau, N. Heymans, G. D. Weireld, G. Maurin, K. N. Salama, M. Eddaoudi. Nat. Commun. 2019, 10, 1328, DOI: 10.1038/s41467-019-09157-2.
20. a) S. Caron, R. W. Dugger, S. G. Ruggeri, J. A. Ragan and D. H. B. Ripin, Chem. Rev., 2006, 106, 2943–2989.; b) Y. Nosaka and A. Y. Nosaka, Chem. Rev., 2017, 117, 11302– 11336; c) A. Dhakshinamoorthy, Z. Li and H. Garcia, Chem. Soc. Rev., 2018, 47, 8134–8172; d) L. Jiao, Y. Wang, H. L. Jiang and Q. Xu, Adv. Mater., 2018, 30, 1703663; e) J. Liu, L. Chen, H. Cui, J. Zhang, L. Zhang and C. Y. Su, Chem. Soc. Rev., 2014, 43, 6011–6061.
21. a) J. R. McNesby and C. A. Heller Jr., Chem. Rev., 1954, 54, 325–346; (b) S. A. Maslov and E. A. Blyumberg, Russ. Chem. Rev., 1976, 45, 155–167. (c) D. C. Cook, R. H. Jones, H. Kabir, D. J. Lythgoe, I. M. McFarlane, C. Pemberton, A. A. Thatcher, D. M. Thompson and J. B. Walton, Org. Process Res. Dev., 1998, 2, 157–168.
22. F. P. Byrne, S. Jin, G. Paggiola, T. H. M. Petchey, J. H. Clark, T. J. Farmer, A. J. Hunt, C. R. McElroy and J. Sherwood. Tools and techniques for solvent selection: green solvent selection guides. Sustain Chem Process (2016) 4:7, 10.1186/s40508-016-0051-z.